論文 / 著書情報
Article / Book Information

題目(和文)	
Title(English)	Radio Propagation Prediction Models for Site-Specific Characteristics of Urban Microcell Environment above 6 GHz for Fifth Generation Mobile Communication System
著者(和文)	猪又稔
Author(English)	Minoru Inomata
出典(和文)	学位:博士(工学), 学位授与機関:東京工業大学, 報告番号:甲第11348号, 授与年月日:2019年12月31日, 学位の種別:課程博士, 審査員:山下 幸彦,髙田 潤一,秋田 大輔,齋藤 健太郎,阪口 啓,青柳 貴洋
Citation(English)	Degree:Doctor (Engineering), Conferring organization: Tokyo Institute of Technology, Report number:甲第11348号, Conferred date:2019/12/31, Degree Type:Course doctor, Examiner:,,,,,
学位種別(和文)	博士論文
Type(English)	Doctoral Thesis

Doctoral Dissertation

Radio Propagation Prediction Models for Site-Specific Characteristics of Urban Microcell Environment above 6 GHz for Fifth Generation Mobile Communication System

December 2019

Graduate Major in Global Engineering for Development,
Environment and Society
Department of Transdisciplinary Science and Engineering
School of Environment and Society
Tokyo Institute of Technology
Minoru INOMATA

Contents

Chapeter 1. Introduction 1
1.1. Research Background 1
1.2. Propagation Characteristics for Cell Deployment 2
1.3. Conventional Model Issues 5
1.4. Objective 9
1.5. Outline of the Dissertation 11
Chapeter 2. Predictions of Outdoor Path Loss Characteristics considering Building Shapes 14
2.1 Introduction 14
2.2 Measurement Campaign 14
2.3 Outdoor Path Loss Characteristics for High Frequency Bands 16
2.4 Analysis of Dominant Path for Urban Microcell Environment 21
2.5 Path Loss Modeling 25
2.6 Summary of Chapter 2 29
Chapeter 3. Predictions of Penetration Loss Characteristics through the Building Windows 30
3.1 Introduction 30
3.2 Measurement Campaign 30
3.3 Building Penetration Loss for High Frequency Bands 34
3.4 Analysis of Dominant Path at Building Penetration 38
3.4.1 Analysis of the dominant path at building penetration 38
3.4.2 Analysis of Frequency and 3D Incident Angle Dependency 42
3.5 Building Penetration Loss Modeling 44
3.6 Performance of Proposed Building Penetration Loss Model 46
3.7 Summary of Chapter 3 50
Chapeter 4. Predictions of Channel Characteristics considering Buildings Surface Irregularity 51
4.1 Introduction 51
4.2 Conventional Prediction Method 52
4.2.1 Procedure 52
4.2.2 Conventional Map Database 56
4.3 Proposed Prediction Method 57
4.3.1 Hybrid Method with Point Cloud Data 57
4.3.2 Structure Model Based on Point Cloud Data 59
4.4 Measurement Campaign 60
4.4.1 Measurement Method 61
4.4.2 Acquisition of Point Cloud Data 63

4.5 Performance of Proposed Prediction Method 64
4.5.1 Measurement Results 64
4.5.2 Prediction of Specular Reflection and Diffraction with RT Method 65
4.5.3 Diffuse Scattering Prediction with ER Model 66
4.5.4 Comparison between Proposed Method and Measurements 67
5.6 Summary of Chapter 4 77
Chapeter 5. Predictions of Dynamic Channel Characteristics due to Vehicles 78
5.1 Introduction 78
5.2 Measurement Campaign 79
5.3 Investigation of Dynamic Channel Characteristics for NLOS Environment 80
5.4 Prediction of specular reflection from vehicles in NLOS environment 87
5.4.1 Procedure 87
5.4.2 Vehicle Model with Rectangular Smooth Screen 89
5.5 Performance of Proposed Method 89
5.6 Summary of Chapter 5 92
Chapeter 6. Conclusions 93
Reference 96
Appendix 104
Acknowledgements 108

List of Abbreviations

3D	three dimensional
5G	fifth generation mobile communications systems
ABG	alpha beta gamma (path loss model)
BS	base stations
CAD	computer aided design
CW	continuous waves
CI	close in (reference-distance path loss model)
CIF	CI model with frequency-dependent path loss exponent
eMBB	enhanced Mobile BroadBand
ER	effective roughness
InH	Indoor Hotspot
IoT	Internet of Things
ITU-R	international telecommunication union radio communication sector
LOS	line of sight
MIMO	multiple input multiple output
mMTC	massive Machine Type Communications
MS	mobile station
NLOS	non-line of sight
OFDM	Orthogonal Frequency Division Multiplexing

QoS	quality of service
RMa	Rural Macro
RT	ray-tracing
Rx	receiver
Tx	transmitter
UMa	Urban Macro
UMi	Urban Micro
URLLC	Ultra-Reliable and Low Latency Communications

Chapeter 1. Introduction

1.1. Research Background

The amount of traffic in wireless communication systems has been rapidly increasing in recent years and it is assumed that it will increase about 700 fold over the current traffic amount from 2010 [1][2]. Because microwave bands below 6 GHz are suitable for a wireless access system and used currently in such systems, their frequency resources are very limited. Currently, the frequency bands, such as 700 MHz, 800 MHz, 1.5 GHz, 1.7 GHz, 2 GHz, and 3.5 GHz, are allocated to mobile communication systems and allocated bands are higher as the generation changes because the wider bandwidth can be used and obtained the high-speed, high-capacity communication in higher frequency bands. Therefore, one avenue of research being pursued to address higher traffic is applying frequency bands above 6 GHz to the fifth generation mobile communications systems (5G) [2] [3] [4]. Mobile telephone operators around the world are now working hard to introduce 5G services, and, in Japan, the frequency bands of 3.7 GHz and 4.5 GHz at low SHF band, 28 GHz at high SHF band will be used in 5G. With 5G, high frequency bands at high SHF band are expected to be used to secure wider bandwidth and realize the high speed and capacity of enhanced Mobile BroadBand (eMBB). Other technologies are also being studied to implement Ultra-Reliable and Low Latency Communications (URLLC), and massive Machine Type Communications (mMTC), which will accommodate large numbers of Internet of Things (IoT) terminals [4].

A mobile communication system employs a cellular system that covers a service area with multiple base stations (BSs) in order to make effective use of the limited number of frequency resources. The service area covered by one BS is referred to as a cell. Historically, the existing service areas have basically been covered with the same size macrocells. However, small cells using high frequency bands will be overlaid on macro cells in high traffic areas, as shown in Figure 1-1 [2]. Radio propagation in a mobile communication system is characterized by multipaths that are shielded, reflected, and scattered by surrounding objects. This can cause fading in the received power. In the 5G small cells using high frequency bands, since the new high-frequency bands have extremely short wavelengths, radio propagation is significantly affected by objects such as buildings and vehicles surrounding a mobile station (MS). Therefore, radio propagation characteristics need to be understood and predicted for cell deployment.

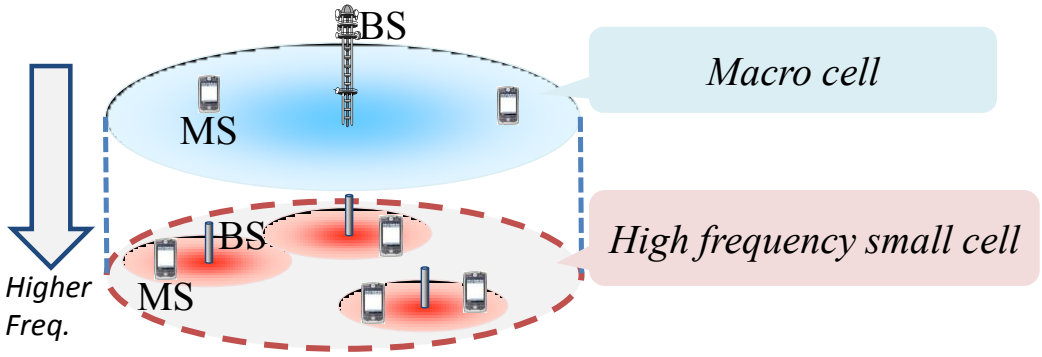

Figure 1-1 5G cell design

1.2. Propagation Characteristics for Cell Deployment

In order to optimize a service area, it is important to understand the fading characteristics of the propagation loss. Propagation loss fading can be divided into three types of fading based on a fading scale [6] [7]. Figure 1-2 shows the fading classification. The large-scale fading (path loss) is caused by attenuation resulting from an increase in the propagation distance between the BS and MS. The scale of the fading exceeds one hundred meters. The small-scale fading (shadowing) is caused by geographical variations such as the layout of buildings around a moving MS. Fast fading occurs due to the composition of the multipaths. The scale of the fading is several wavelengths.

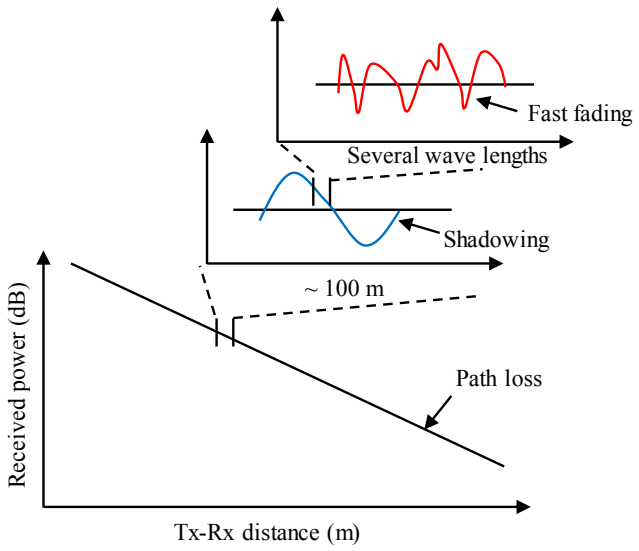

Figure 1-2 Fading classification

Path loss characteristics are important in designing the link budget (transmission power, BS antenna height, distance between BSs, required transmitter / receiver antenna gain), and must be predicted to understand the coverage. There are also multipaths between the BS and MS in the

mobile communication environment, and the BS performance depends on the multipath characteristics. Here, multipath characteristics are sometimes referred to as channel characteristics. Since each propagation path between the BS and MS has a different propagation distance, the arrival time for the path from the BS to the MS is different according to the propagation distance. Here, the arrival time of the path from the BS to the MS based on the shortest path is referred to as the propagation delay. In digital data transmission, since propagation delay causes inter-symbol interference, clarification of the propagation delay and modeling its characteristics is important to evaluate the mobile communication system performance. Since the angle distributions of departure and arrival characterize the spatial distribution of the received power fading, conventionally the modeling of those characteristics has been an important issue. 5G utilizes massive multiple input multiple output (MIMO). MIMO multiplexing improves the communication speed by simultaneously transmitting different data from multiple antennas. It is known that spatially distributing the received power fading affects the system performance in Massive MIMO transmission. Therefore, in evaluating the 5G system performance, modeling of the angle distribution for departing and arriving waves is important.

In the study of these predictions, modeling scenarios are classified because the propagation characteristics are affected by the structures and objects around the BS and the MS. The traditional modeling scenarios of Urban Macro (UMa), Urban Micro (UMi), Rural Macro (RMa), and Indoor Hotspot (InH) have previously been considered in ITU-R M.2135 for modeling of the radio propagation in bands below 6 GHz [7]. In 5G, since high-frequency-band small cells are newly installed in urban areas where high volume traffic occurs, it is necessary to understand the path loss and channel characteristics in a UMi environment for high-frequency bands. The cell radius in a UMi environment is typically less than several hundred meters and the BSs are mounted below building rooftop level. The MSs are deployed outdoors at ground level or indoors on all floors in a building.

Figure 1-3 shows the factors that affect the radio propagation characteristics outdoors [9]. In a UMi environment, in which basically radio waves transmitted from a BS propagate along the street, the propagation characteristics are significantly affected by moving objects, e.g., vehicles and people, and geometry-induced objects, e.g., buildings, on the street. In addition, in the UMi scenario, a significant number of the MSs are expected to be indoors. These indoor MSs increase the strain on the link budget since additional losses are associated with the penetration into buildings, which is referred to as building penetration loss. The characteristics of the building penetration loss and in particular its variation over the higher frequency range is of interest.

Figure 1-4 shows the future cell deployment using high frequency bands. In conventional cell deployment, the coverage is basically calculated using stochastic characteristics constructed by statistically processing measurement data obtained from field experiments. In addition, the

predictions are corrected based on the building distribution, and the building penetrating loss is uniformly attenuated. Also, ray tracing method with uniform building structure is used in low frequency band to estimate stochastic characteristic. On the other hand, in the cell deployment of high frequency bands, it is important to consider the path specific characteristics in the actual environments where BS is installed. Since there are various building shapes in actual environment, the path loss characteristics should be significant affected by the reflected paths from the buildings. Moreover, arriving waves from surface roughness of buildings and vehicles impact the propagation channel characteristics. In addition, since building wall transmission loss increases as the frequency increases, the penetration paths to building windows affect building penetration loss characteristics. Therefore, it is necessary to clarify specific the outdoor path loss characteristics, building penetration loss characteristics, and outdoor channel characteristics based on the detailed building structure and objects in a UMi environment for high frequency 5G cell deployment.

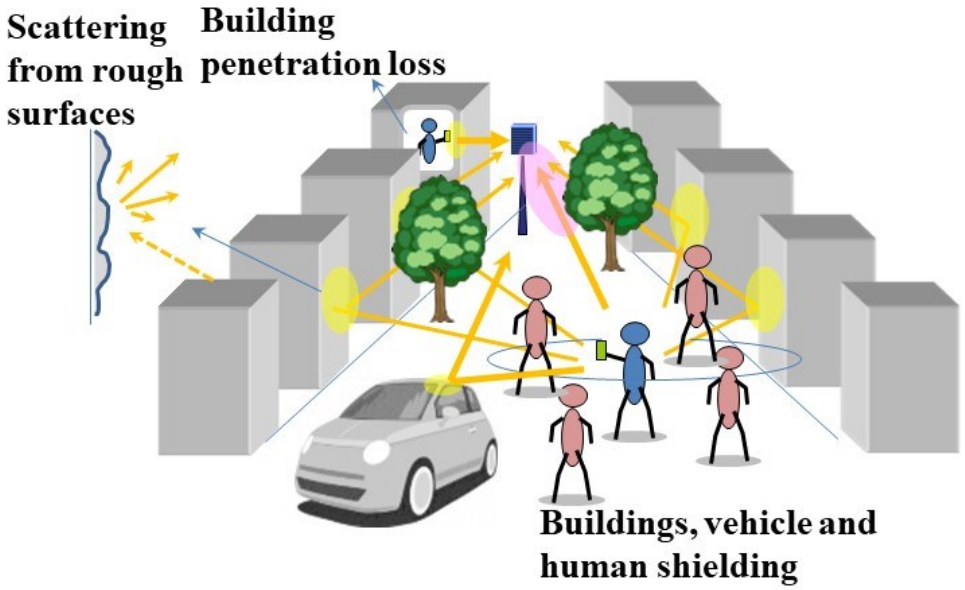

Figure 1-3 Factors affecting radio propagation characteristics

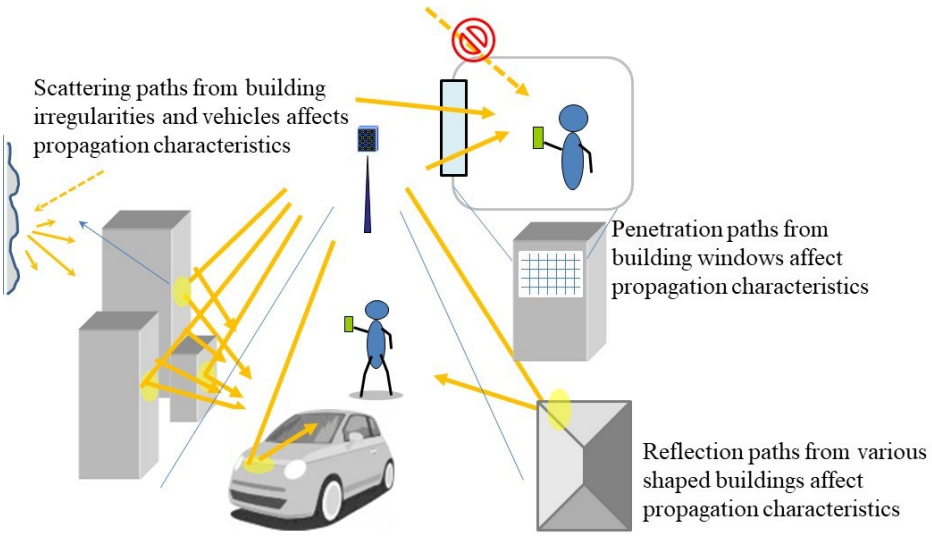

Figure 1-4 Future cell deployment using high frequency bands based on specific path

1.3. Conventional Model Issues

For the development of the new 5G systems to operate in high frequency bands, conventional propagation predictions are not addressed because the applicable frequency range of reference is up to 6 GHz [7] [9] [10]. There are many existing research efforts worldwide targeting 5G radio propagation measurements and characterization in high frequency bands. They include Mobile and wireless communications Enablers for the Twenty-twenty Information Society (METIS) [11] [12], 5G Channel Model Special Interest Group (5GCM SIG) [3], Millimetre-Wave Evolution for Backhaul and Access (MiWEBA) [13], NYU WIRELESS [14] [15] [16], International Telecommunication Union Radiocommunication Sector (ITU-R) [17], Third Generation Partnership Project (3GPP) [18], and Millimetre-Wave Based Mobile Radio Access Network for Fifth Generation Integrated Communications (mmMAGIC) [19] [20]. ITU-R and 3GPP models are constructed based on these group's investigations. METIS channel models are categorized into two types. The first type is map-based model using ray-tracing (RT) method which is deterministic radio propagation predictions based on a detailed simulation using a description of the propagation environments, e.g., obtained through conventional commercially available map databases and suitable formulations for physical propagation phenomena. On the other hand, there is the stochastic channel prediction based on geometry-based stochastic channel model (GSCM) which obtains spatial channel characteristics by spatially distributing clusters based on measurement channel parameters for evaluation of MIMO performance. 5GCM SIG, NYU WIRELESS and mmMAGIC also develop GSCM. MiWEBA provided the methodology of quasi-deterministic channel modeling. Under this approach, the channel propagation scenario is set, several stronger propagation paths are determined using RT method, and radio propagation over them is calculated based on the geometry

of the BS and MS position. For UMi scenario, the propagation is determined mostly by 4 deterministic-rays in the line of sight (LOS) environment, the one reflected from the nearest wall and the one reflected from the ground. The reflection is calculated by effective reflection coefficient. Also, random rays with lower power (reflected from far walls, vehicles, lampposts etc.) are described as random clusters. Both deterministic-ray and random-ray have intra-clusters that are exponentially distributed.

In the outdoor path loss models of 5GCM SIG, NYU WIRELESS, and mmMAGIC, reference [21] [22] report the measurement results in millimeter wave bands, the reference [23] [24] [25] [26] [27] proposed the 1m free space close-in (CI) reference distance model, the reference [28] [29] proposed the CI model with frequency-dependent path loss exponent (CIF) which is 2 optimization parameters, and the reference [30] [31] [32] proposed the alpha-beta-gamma (ABG) model, just like the Okumura-Hata model [33]. These models employ stochastic modeling approach, and these models cannot evaluate site-specific path loss characteristics. Also, in the cell deployment, it is necessary to evaluate the interference to the neighboring cells and to construct a prediction that considers a continuous environment from LOS to non-line of sight (NLOS). However, since these models are constructed using a path loss prediction based on measurement data in LOS and NLOS environments, the region between LOS and NLOS is discontinuous.

Deterministic radio propagation prediction methods described in [11] [12] [34] [35] [36] [37] [38] have been widely used to predict channel characteristics with reasonable computational time because memory and computing speed have dramatically improved. Now, even with inexpensive laptops, accurate path loss characteristics can be obtained without measurements. By using the RT method in which the BS and MS positions, frequency, and polarization characteristics of the BS and MS antennas are set, the results of the amplitude, propagation delay, departure and arrival angles, and polarization of each ray can be obtained. Moreover, channel characteristics can be understood by considering the system bandwidth and antenna characteristics of the BS and MS. In the reference [34] [35], using results of experimental measurements and RT simulations, the prediction is parameterized for indoor scenario, and the parameterization may not be valid for outdoor UMi environments. METIS map-based model [11] [12] and ITU-R P.1411 model [36] [37] [38] is characterized based on the results of RT method using Manhattan grid layout. Those models are basically constructed by multiple reflection waves from the wedge shape buildings which propagate along the street. Reference [12] reported comparison results between measurement path loss data and prediction results using map-based model, however, they showed that predicted path loss results are larger than measurement results. It is assumed that the path loss characteristics should be significant affected by the buildings shape. In the reference [39] and [40], the building shape at intersection significantly affects the path loss characteristics in NLOS and proposed the prediction method with round shaped building at the intersection. However, the predictions are smaller than measurement

results because of stronger specular reflection from round shaped building. Therefore, it is necessary to clarify what building shape should be considered based on measurements.

Building penetration loss models have been studied in [7] [9] [41] [42]. The conventional models in [7], [9] and [41] describe a building penetration model in low frequency bands below 6 GHz. Although the models can predict average transmission loss in windows, doors and walls, these models are applicable to high frequency bands was not clarified. Reference [42] described a building penetration loss model that takes the three dimensional (3D) incident angle characteristics into consideration in low frequency bands. However, the target scenario is indoor-to-outdoor-to-indoor and the scenario is considerably different from the target scenario in this dissertation. The models described in [43], [44], [45], [46], [47], and [48] are applicable in high frequency bands. The target of these models is to clarify various material losses which are regular glass, metal coated glass, concrete and brick at external walls. From the results that the material loss is increased as the frequency is increased, reference [48] developed building penetration loss model by linear regression based on frequency dependency. In the reference [49] and [50], the transmission loss due to the window material significantly affect building penetration loss characteristics. Therefore, the building penetration loss model was constructed by measurements results which are set of high penetration loss results for buildings constructed with IRR glass, and a set of lower loss results for different buildings where regular glass. Also, mmMAGIC [20] refined those models considering the indoor loss and 3D incident angle characteristics for massive MIMO. However, there can be quite some variation even if those factors are considered and it is assumed that the site-specific characteristics which are characterized by penetration paths to building windows from the surrounding building affect variation. Therefore, it is necessary to measure and clarify the effect of those penetration loss characteristics through the building windows.

In the channel predictions, RT method fails to represent properly diffuse scattering phenomena from the building surface irregularity. In high frequency bands, diffuse scattering waves due to scattering objects that have building irregularities such as the shape of buildings, windows, and balconies, significantly affect the propagation channel. It was reported that diffuse scattering contributes to the propagation characteristics because of building irregularities described in [51] [52] [53]. Therefore, the RT method must be extended so that it can properly handle diffuse scattering characteristics.

Scattering based on random rough surface is consisted of specular reflection component and diffuse scattering component. The GSCM model in 5GCM SIG and mmMAGIC calculate each random cluster which is consisted of about 20 rays that represent diffuse scattering component. However, since the clusters are parameterized by measurement channel data [54] [55] [56] [57], these models are assumed that the site-specific channel are ignored. The channel modelling should take into

account realistic modelling of specific paths as described in [58] [59]. Therefore, METIS developed map-based model to express the scattering [12]. The received power of diffuse scattering component is increased, while the received power of specular reflection is decreased as shown in [62] [63] [64] [65] [66] [67] [68]. From these results, map-based model uses the effective reflection coefficient which can express power reduction of specular reflection. The feasibility of the approach to the prediction is clarified in microcell environments [69] [70] [71]. On the other hand, according to [12] diffuse scattering from building irregularities is applied to an effective roughness (ER) model based on Gaussian surface roughness described in [72]. The ER model is one solution that accurately predicts diffuse scattering from various scattering objects. There have been several studies on the application of the ER model [12] [73] [74] [75] [76] [77]. In these applications, a hybrid method was described that employs RT and the ER model to evaluate channel characteristics considering diffuse scattering. In [73], an isolated building is digitized and input to an RT tool; however, it is not clear whether or not the digitized model considers the building irregularities. Therefore, although the model parameters are tuned by measurement results in front of a building, it is not clear whether or not the tuned parameters are appropriate for the diffuse scattering from building irregularities. In [74], [75], and [76], a hybrid method was described for urban environments for a low frequency band below 6 GHz. However, since the building model in an urban environment is generated by means of conventional commercially available map databases, the building irregularities are not considered. In [12], since the building model is constructed using a smooth surface, building irregularities cannot be considered. As the mentioned above, in the conventional method, the building irregularities are not measured, and prediction results are not suitable for site-specific channel characteristics in high-frequency bands in an actual urban environment for cell deployment.

In recent architecture and civil engineering research, a point cloud using laser scanner is accepted method to obtain detailed structure data from environments [78] [79]. A detailed structure model can be obtained with an accuracy of several millimeters using laser scanning. Therefore, in order to clarify the scattering from building irregularity, it is need to study how the point cloud data is applied to the radio propagation prediction method based on a hybrid of the RT method and ER model.

In UMi environment, shielding and scattering occurs due to moving objects such as human and vehicles. The effect of vehicles shielding reported in [80] and that of human is described in [81] [82]. In various group, the blockage model is represented by diffraction from the screen based on those measurement results. On the other hand, in the effect of the scattering from vehicles, METIS map-base model represented the received power of scattering which is expressed using the randomly installation sphere. Also, MiWEBA [83] utilized random rays with lower power than quasi-deterministic rays. However, these predictions represent stochastic characteristic and the comparison of channel predictions with measurements have not been enough studied. Therefore, it is not clarified whether these models can evaluate site-specific channel characteristics based on the

effect of vehicles in actual installation environments.

1.4. Objective

Table 1-1 shows the summarize described in sections 1.1 to 1.3 and the target area considered in this dissertation for UMi environment. As described in Sections 1.1 to 1.3, it is necessary to clarify the site-specific outdoor path loss characteristics, building penetration loss characteristics, and outdoor channel characteristics based on the dominant path considered detailed building structure and objects for high frequency cell deployment, however, those specific path characteristics have not been thoroughly studied. Therefore, the target of this dissertation is to clarify a path loss and channel characteristics based on detailed building structure and objects and to construct the prediction models condisdered those effects in UMi environment for high frequency 5G cell deployment. In order to clarify those characteristics in UMi environment, the subjects of this dissertation are to clarify dominant path from each building shape in actual site which significantly affect the outdoor path loss characteristics and construct the prediction, to clarify the specific building penetration loss characteristics which considered penetration paths to building windows and construct a building penetration loss prediction, to construct the channel prediction based on scattering from the building irregularities and reflection from vehicles in actual site.

Object	Attribute	Requirement	Model type	Improvement addressed in this dissertation	Comments	References
Path loss characteristics for the coverage evaluation	Outdoor path loss	Regression of measurements at Various building shape	Stochastic model		GSCM supports requirement	[3][11][12][14][15][16][17][18][19][20][21][22][23][24][25][26][27][28][29][30][31][32][33]
		Uniform wedge shape building	Ray tracing		ITU-R and Map-based model supports requirement	[11][12][17][18][34][35][36][37][38]
		Building shape in actual site	Ray tracing	✓	Target in this dissertation	
	Building penetration loss	Regression of measurements at various external wall and windows	Stochastic model		GSCM supports requirement	[3][17][18][19][20][43][44][45][46][47][48][49][50]
		Penetration paths through the building windows	Ray tracing	✓	Target in this dissertation	
Channel characteristics for system performance evaluation	Channel in LOS environment	Regression of measurements in various site	Stochastic model		GSCM supports requirement	[3][17][18][19][20][54][55][56][57]
		Effective reflection	Ray tracing		Quasi-Deterministic model and Map-based model support requirement, however, the accuracy is not clarified	[13][69][70][71]
		Scattering from smooth surface	Hybrid of ray tracing and ER model		Map-based model supports requirement, however, the accuracy is not clarified	[11][12][74][75][76][77]
		Scattering from building irregularities	Hybrid of ray tracing and ER model	✓	Target in this dissertation	
	Channel in NLOS environment	Randomly generate the scattering from vehicle	Stochastic model		Quasi-Deterministic model supports requirement, however, the accuracy is not clarified.	[13][83]
		Randomly generate the scattering from vehicle	Ray tracing		Map-based model supports requirement, however, the accuracy is not clarified.	[11][12]
		Generate scattering based on site-specific vehicle model	Ray tracing	✓	Target in this dissertation	

Table 1-1 Target area of this paper in a UMi environment

1.5. Outline of the Dissertation

This dissertation is constructed as shown in Figure 1-5 and 1-6. Chapter 2 describes the dominant paths from various building shapes and constructs outdoor path loss predictions based on dominant paths in a UMi environment for high-frequency bands. In this chapter, outdoor path loss characteristics obtained based on measurement results from 2.2 to 37.1 GHz are shown. Our use of RT to analyze how building shapes affect outdoor path loss characteristics at an intersection is presented. Based on the results, for less complexity, a model that covers the frequency range from microwave to millimeter-wave bands is proposed based on the dominant paths.

Chapter 3 shows the dominant path which penetrates to building window and the building penetration loss predictions in a UMi environment for high-frequency bands. In this chapter, it is first reported how measurements are conducted in the bands ranging from 0.8 to 37.0 GHz. We also measure the 3D incident angle and indoor loss characteristics. Second, it is clarify that the dominant paths affecting the path loss characteristics based on RT results. On the basis of the obtained results, the frequency and 3D incident angle characteristics of dominant paths is analyzed and the building penetration loss model using these results is developed.

Chapter 4 describes channel predictions in a UMi LOS environment for high-frequency bands. In this chapter, a radio propagation prediction method using point cloud data based on a hybrid of the RT method and ER model is proposed in a UMi environment for high-frequency bands. Since the parameters related to structure irregularities in the proposed prediction method can be obtained by point cloud data, the prediction method takes into consideration the diffuse scattering from the structure irregularities. First the prediction method process is reported. Then, it is verify that the prediction accuracy based on a comparison between measurements and prediction results using the proposed method. Based on the obtained results, it is clarified that the validity of the proposed method and statistical parameters that properly represent the specific channel characteristics considering diffuse scattering from structure irregularities in a UMi LOS environment for high-frequency bands.

Chapter 5 shows channel predictions considering scattering from vehicles in a UMi NLOS environment for high frequency bands. First the dynamic channel characteristics are investigated based on arriving waves from vehicles in high-frequency bands in a UMi NLOS environment and clarify the dominant paths based on the measured power delay angular profile using a 20-GHz band channel sounder. Furthermore, the proposed prediction method based on scattering from site-specific vehicle model is improved so that it can be applied to UMi NLOS environments.

Finally, in Chapter 6, remarks are presented to conclude the preceding chapters.

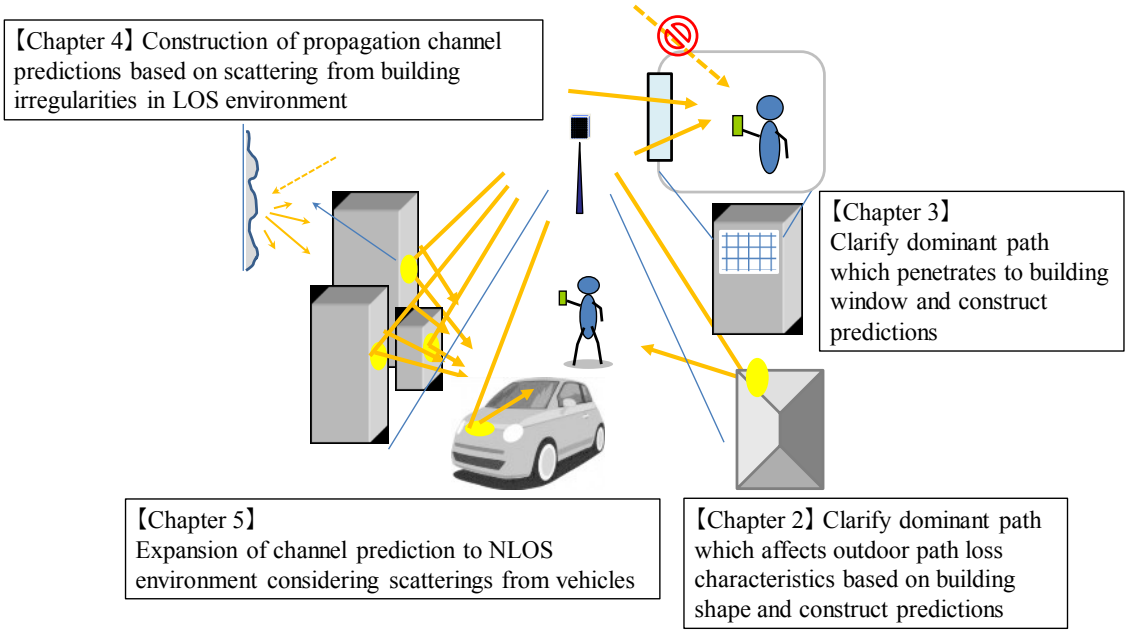

Figure 1-5 Subjects of this dissertation

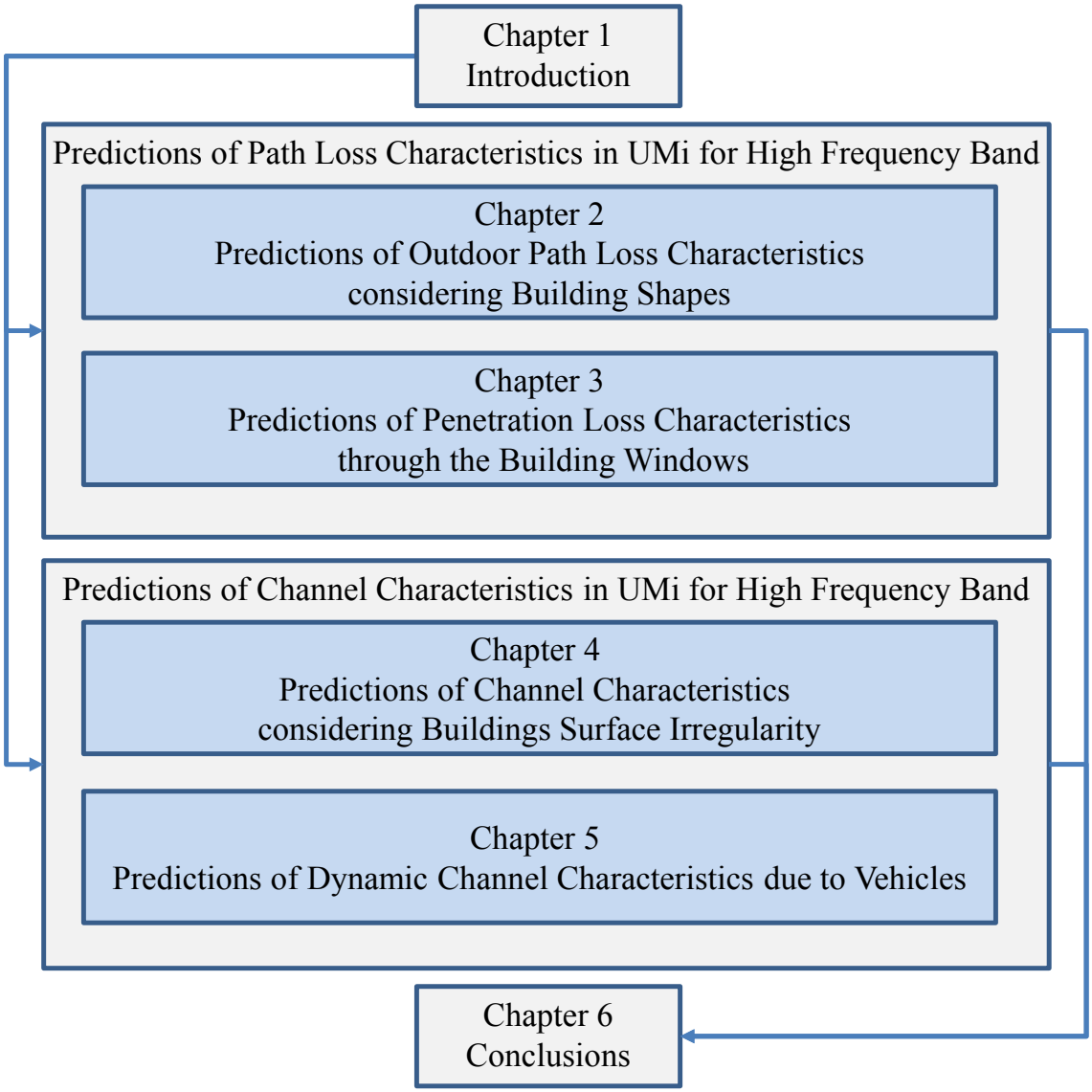

Figure 1-6 Dissertation Outlines

Chapeter 2.

Predictions of Outdoor Path Loss Characteristics considering Building Shapes

2.1 Introduction

In this section, the dominant path from each building shape in UMi is clarified and outdoor path loss predictions which can cover the frequency range from microwave to millimeter-wave bands based on the dominant path is presented. In UMi environment, basically, its radio waves which transmitted from BS propagate along the street. The conventional models [12] [36] are basically constructed by multiple reflection waves from the wedge shape buildings, however, since there are various building shapes in actual environment and the path loss characteristics should be significant affected by the buildings shape, it needs to be clarified whether the model is applicable to millimeter-wave bands based on the building shape.

Accordingly, this section describes path loss characteristics for the model obtained based on the measurement results from 2.2 to 37.1 GHz. It presents our use of ray tracing to analyze how building shapes affect path loss characteristics at an intersection. It also shows how it is clarified that the dominant paths that significantly affect the path loss by comparing calculation and measurement results. Based on these dominant paths, the outdoor path loss model from microwave band to millimeter wave band is constructed in UMi and the validity of proposed model is verified.

2.2 Measurement Campaign

The outdoor path loss characteristics were measured in an area nearby Tokyo Station, Tokyo, Japan. The streets in the area were surrounded by tall buildings (about ten stories or 40 m high). The road width is about 30m. Therefore, this environment is typical UMi scenario. The path loss measurements were taken in four NLOS routes, NLOS1, NLOS2, NLOS3 and NLOS4, as shown in Figure 2-1 Measurement route. The measurements were taken in four frequency bands: 2.2, 4.7, 26.4, and 37.1 GHz. Tx antennas were set at two different positions (Tx1 and Tx2), at 10-m height. The continuous waves (CW) is transmitted. An Rx antenna was fixed on the roof of a measurement car whose height was 2.5 m. The antenna radiation pattern was omni-directional. Table 2-1 summarizes these parameters. The distance to the intersection was about 192 m for NLOS 1 and 169 m for NLOS 2. The moving distance after the corner was 180 m for NLOS1, 925 m for NLOS2, 440m for NLOS3 and 913m for NLOS4. Figure 2-2 shows photographs of the measurement environment.

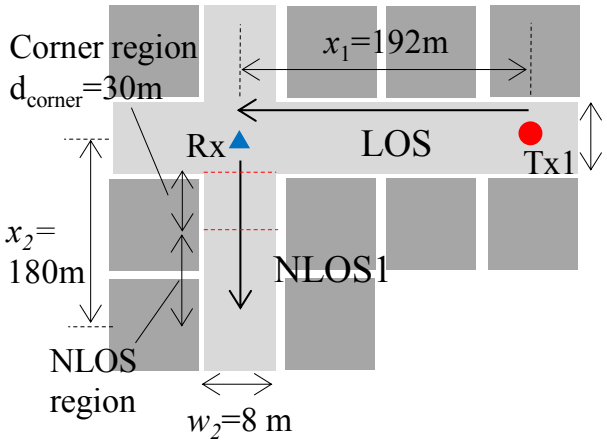

(a) Measurement route at NLOS1.

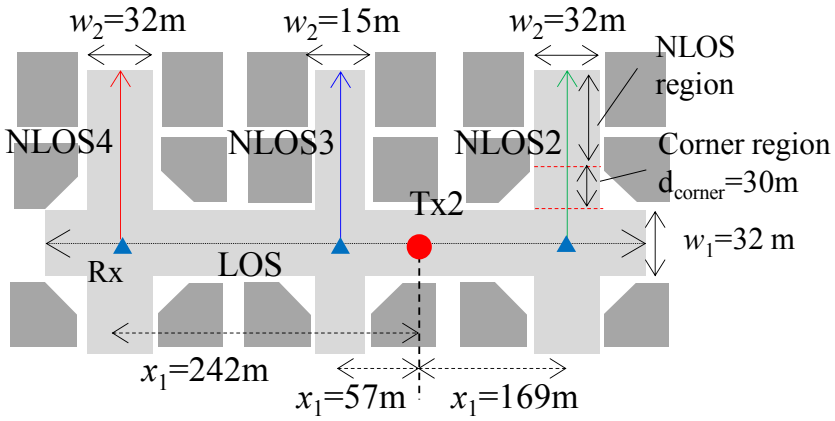

(b) Measurement route at NLOS2, 3 and 4

Reference:

Minoru Inomata, Motoharu Sasaki, Wataru Yamada, Takeshi Onizawa, Masashi Nakatsugawa, Nobutaka Omaki, Koshiro Kitao, Tetsuro Imai, Yukihiko Okumura, "Outdoor-to-Indoor Corridor Path Loss Model up to 40 GHz Band in Microcell Environments," *IEICE Trans. on Communication*, Vol.E100-B, No.2, pp.242-251, Feb. 2017.

Figure 2-1 Measurement route

(a) Photo from Tx1 at NLOS1.

(b) Photo from Tx2 at NLOS2, 3 and 4.

Reference:

Minoru Inomata, Motoharu Sasaki, Wataru Yamada, Yasushi Takatori, Koshiro Kitao, Tetsuro Imai, "Effects of Building Shapes on Path Loss up to 37 GHz Band in Street Microcell Environments," *2017 International Conference on Computational Electromagnetics (ICCEM),* Kumamoto, Japan, pp. 249-251, March.2017.

Figure 2-2 Photos of measurement environment

Table 2-1 Measurement parameters

Measured frequency (GHz)	2.2, 4.7, 26.4, and 37.1 (CW)
Tx/Rx Antenna radiation pattern	Omni-directional in horizontal plane
Antenna gain	Around 2 dBi for each antenna
Tx antenna height	10 m above ground
Rx antenna height	2.5 m above ground

2.3 Outdoor Path Loss Characteristics for High Frequency Bands

In this section, measurements are compared with the predictions of the conventional model in Recommendation ITU-R P.1411 [36]. This model addresses path loss for short range communication channels within a street microcell environment. The path loss L_{LOS} in the LOS street is obtained by using equations (2.1), (2.2), and (2.3).

$$L_{LOS} = L_{bp} + 6 + \begin{cases} 20\log_{10}\left(\frac{x_1}{R_{bp}}\right), & for\ x_1 \le R_{bp} \\ 40\log_{10}\left(\frac{x_1}{R_{bp}}\right), & for\ x_1 > R_{bp} \end{cases} \tag{2.1}$$

$$L_{bp} = \left|20\log_{10}\left(\frac{\lambda^2}{8\pi h_1 h_2}\right)\right| \tag{2.2}$$

$$R_{bp} = 4\frac{(h_{BS}-h_s)(h_{MS}-h_s)}{\lambda} \tag{2.3}$$

where x_1 is the distance from the Tx antenna to the Rx antenna, L_{bp} is a value for the basic transmission loss at the breakpoint and R_{bp} is the breakpoint distance, h_{BS} is the Tx antenna height, h_{MS} is the Rx antenna height, and h_s is the effective road height, and d_1 is the traveling distance calculated from equation (2.4).

$$d_1 = \sqrt{x_1^2 + (h_{BS} - h_{MS})^2} \tag{2.4}$$

The NLOS street includes two parts: the corner region L_C and the NLOS region L_{att}. The NLOS region lies beyond the corner region. The path loss in the NLOS street is obtained by using equations (2.5), (2.6), (2.7) and (2.8).

$$L_{NLOS} = L_{LOS} + L_c + L_{att} \tag{2.5}$$

$$L_c = \begin{cases} \frac{L_{corner}}{\log_{10}(1+d_{corner})}\log_{10}(x_2 - w_1/2), for\ w_1/2 + 1 < x_2 < w_1/2 + 1 + d_{corner} \\ L_{corner},\ for\ x_1 > w_1/2 + 1 + d_{corner} \end{cases} \tag{2.6}$$

$$L_{att} = \begin{cases} 10\beta\log_{10}\left(\frac{x_1+x_2}{x_1+w_1/2+d_{corner}}\right), for\ x_2 > w_1/2 + 1 + d_{corner} \\ 0,\ for\ x_2 \le w_1/2 + 1 + d_{corner} \end{cases} \tag{2.7}$$

$$d_2 = \sqrt{x_2^2 + (h_{BS} - h_{MS})^2} \tag{2.8}$$

where the corner loss L_{corner} is expressed as the additional attenuation over the distance d_{corner}. x_2 is the distance from the intersection to the Rx antenna and w_1 is the LOS street width. For an urban environment the recommended L_{corner} value is 20 dB and the recommended d_{corner} value is 30 m. The applicable frequency range of the conventional model is limited to up to 16 GHz in street microcell environments. Therefore, it is necessary to clarify whether the model is applicable to millimeter wave band based on building shielding.

To clarify this, measurements were taken at two different intersections for two differently shaped buildings. At the NLOS1 intersection, the building is wedge shaped as shown in Figure 2-3 (a). Figure 2-3 (b), (c) and (d) shows the shape of a building situated at the NLOS2, 3 and 4 intersection. It should be noted that buildings at large intersections do not often tend to be wedge shaped. Buildings shaped like that in Figure 2-3 (b), (c) and (d) can frequently be seen at intersections in modern capital cities; they are shaped this way for safety reasons. It refers to such buildings as “chamfered shaped buildings.” Figure 2-4 shows the comparison results between measurement results at NLOS1 and predictions with the conventional model and the comparison results for

NLOS2. From Figure 2-4 (a), it can be seen that the conventional model predictions are relatively accurate. A quantitative evaluation is given where median prediction errors are calculated. Prediction error is the median values of difference between prediction results and measurement results. The prediction error values are about -1.2 dB at 2.2 GHz, -1.5 dB at 4.7 GHz, -2.6 dB at 26.4 GHz, and -2.3 dB at 37.1 GHz. This shows that the conventional model can cover the frequency band up to 37 GHz for a wedge shaped building. On the other hand, Figure 2-4 (b) shows the prediction error becomes larger after the intersection. In this case, it can be seen that P.1411 model obtains the good fit with measured results for the LOS. Therefore, in wedge shaped building case, the dominant paths are multiple reflection waves which propagate along the street. However, the prediction error values for NLOS2 are about from -8.5 dB to -11.8 dB. This shows that the conventional model cannot effectively be applied to a chamfered shaped building in NLOS region in high frequency bands. It is therefore important to analyze the outdoor path loss characteristics in this region.

(a) Wedge shaped building at NLOS1.

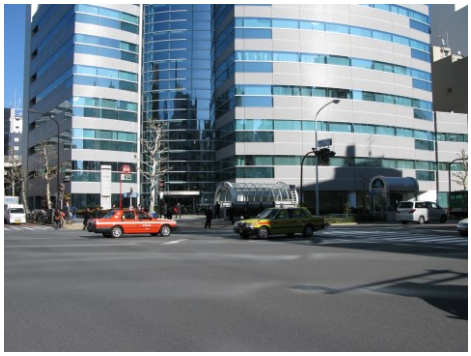

(b) Chamfered shaped building at NLOS2.

(c) Chamfered shaped building at NLOS3.

(d) Chamfered shaped building at NLOS4.

Reference:

Minoru Inomata, Motoharu Sasaki, Wataru Yamada, Yasushi Takatori, Koshiro Kitao, Tetsuro Imai, “Effects of Building Shapes on Path Loss up to 37 GHz Band in Street Microcell Environments,” *2017 International Conference on Computational Electromagnetics (ICCEM),* Kumamoto, Japan, pp. 249-251, March.2017.

Figure 2-3 Building shapes at intersections

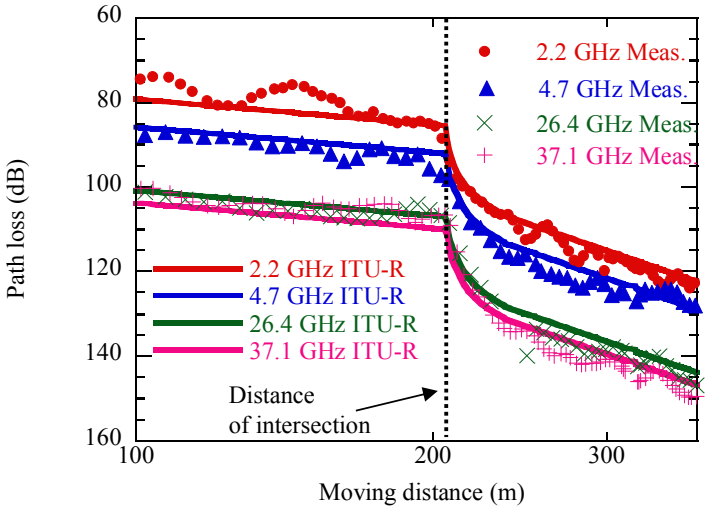

(a) Wedge shaped building at NLOS1.

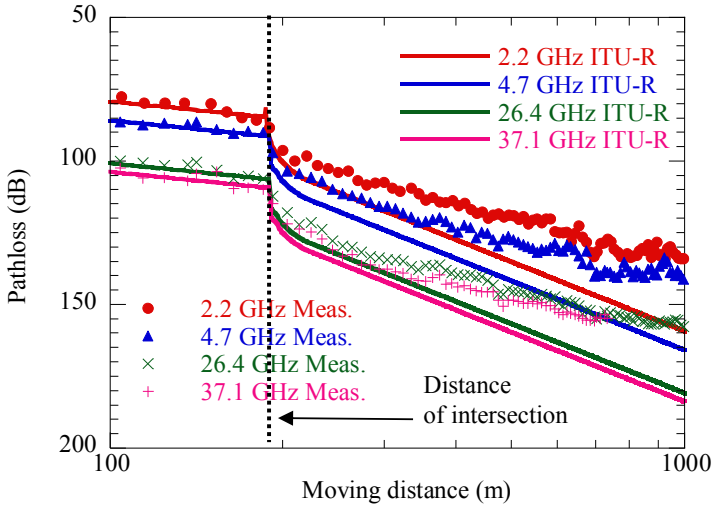

(b) Chamfered shaped building at NLOS2.

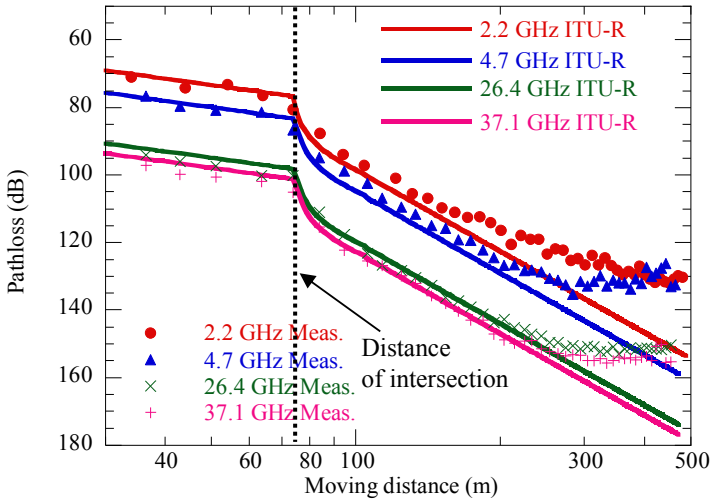

(c) Chamfered shaped building at NLOS3.

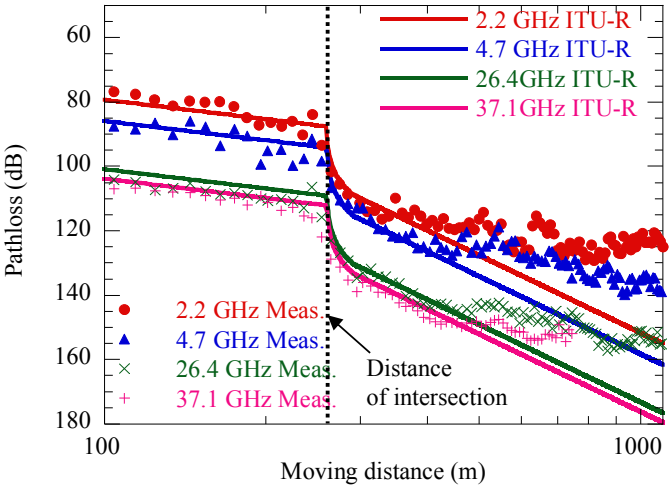

(d) Chamfered shaped building at NLOS4.

Reference:

Minoru Inomata, Motoharu Sasaki, Wataru Yamada, Yasushi Takatori, Koshiro Kitao, Tetsuro Imai, "Effects of Building Shapes on Path Loss up to 37 GHz Band in Street Microcell Environments," *2017 International Conference on Computational Electromagnetics (ICCEM),* Kumamoto, Japan, pp. 249-251, March.2017.

Figure 2-4 Comparison results

2.4 Analysis of Dominant Path for Urban Microcell Environment

In this section, analysis results of path loss characteristics obtained by ray tracing are described, and clarify the dominant paths in the NLOS street. In order to clarify the dominant paths, the shapes of four buildings were varied. Namely, ray tracing calculations were implemented for the following five cases:

- Case (1) Building 1 was chamfered shaped and buildings 2, 3, and 4 were wedge shaped.
- Case (2) Building 2 was chamfered shaped and buildings 1, 3, and 4 were wedge shaped.
- Case (3) Building 3 was chamfered shaped and buildings 1, 2, and 4 were wedge shaped.
- Case (4) Building 4 was chamfered shaped and buildings 1, 2, and 3 were wedge shaped.
- Case (5) Buildings 1-4 were chamfered shaped.

Figure 2-5 shows example of ray tracing simulation model for case (5). Since ray tracing calculates specular reflection from the surface for a chamfered shaped building however calculates diffraction for a wedge shaped building, smaller path loss is obtained for chamfered shaped buildings. It should be noted that case (5) is the nearest to the actual measurement environment. Each calculation took six reflections and one diffraction into account. The building walls and the ground are assumed to be made of concrete.

Figure 2-6 compares path loss measurement results with the ray racing calculation results obtained for each of the five cases. From Figure 2-6, it can be seen that the calculation results for case (5) which is the nearest to the actual building shape is similar to measurement results, however, for cases (1), (2), and (4) tend to be from 12.0 to 25.6 dB larger than the measurement results after the intersection point. On the other hand, for case (3) they are representative of the path loss characteristics, with estimated prediction error ranging from 4.1 to 7.0 dB. This indicates the paths of case (3) strongly contribute to the path loss power of case (5), which as previously noted is nearest to the actual measurement environment.

Figure 2-7 shows the dominant path in NLOS regions. For wedge shaped building cases, the path loss in NLOS regions is large because specular paths will be rare in such cases. As a result, the attenuation coefficient β becomes large in these regions. However, in chamfered shaped building cases, the calculation results clarify that specular reflection from the building strongly contributes the power. In particular, it is found that the paths of specular reflection from the chamfered shaped building in case (3) are dominant and that the attenuation coefficient β consequently becomes small in the NLOS region, therefore, it is need to consider those characteristic.

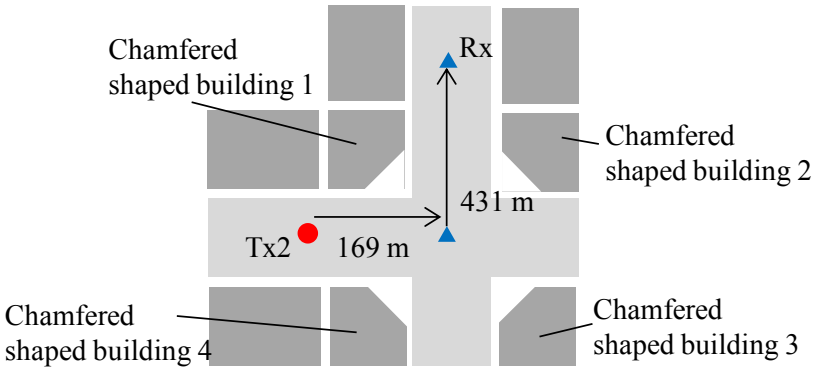

Reference:

Minoru Inomata, Motoharu Sasaki, Wataru Yamada, Yasushi Takatori, Koshiro Kitao, Tetsuro Imai, "Effects of Building Shapes on Path Loss up to 37 GHz Band in Street Microcell Environments," *2017 International Conference on Computational Electromagnetics (ICCEM),* Kumamoto, Japan, pp. 249-251, March.2017.

Figure 2-5 Example of ray tracing simulation model for case (5)

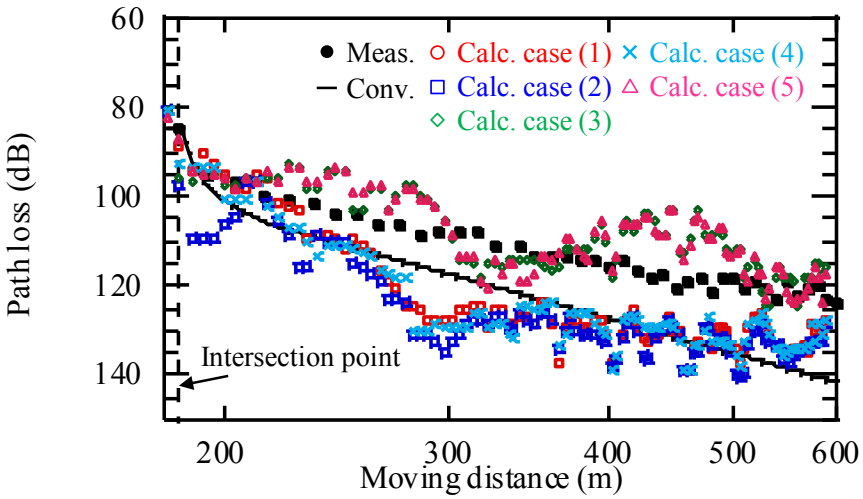

(a) 2.2 GHz

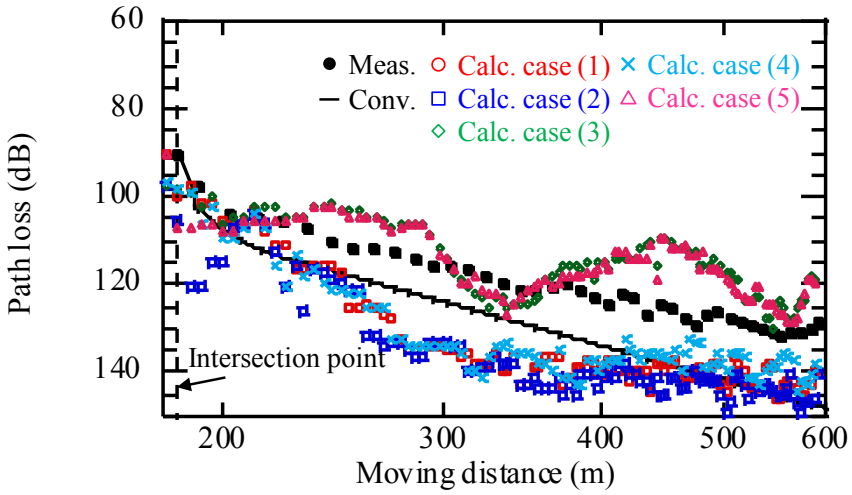

(b) 4.7GHz

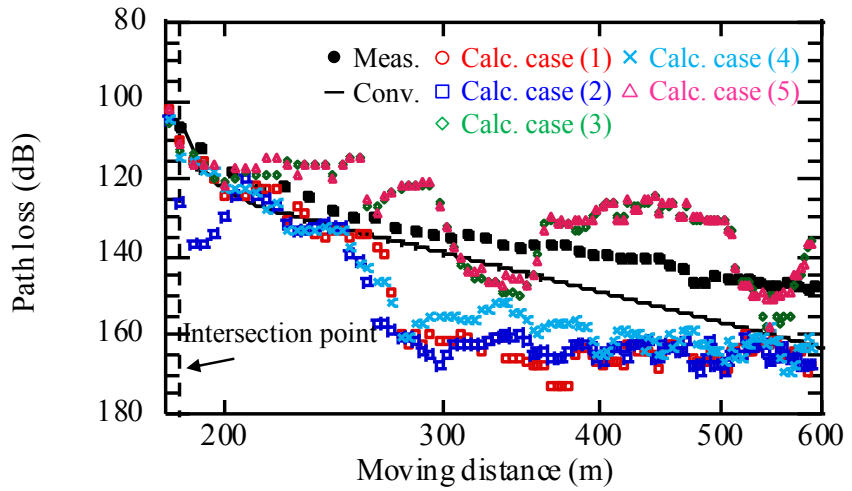

(c) 26.4 GHz.

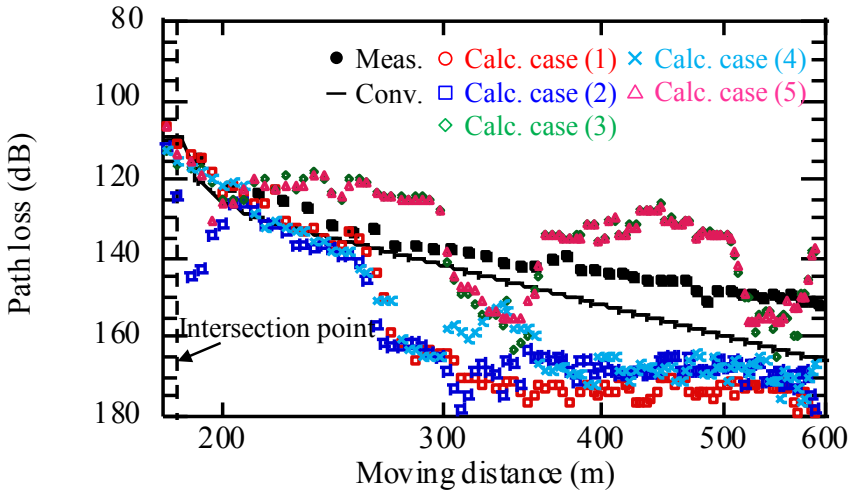

(d) 37.1 GHz.

Reference:

Minoru Inomata, Motoharu Sasaki, Wataru Yamada, Yasushi Takatori, Koshiro Kitao, Tetsuro Imai, "Effects of Building Shapes on Path Loss up to 37 GHz Band in Street Microcell Environments," *2017 International Conference on Computational Electromagnetics (ICCEM),* Kumamoto, Japan, pp. 249-251, March.2017.

Figure 2-6 Comparison results between calculation and measurement

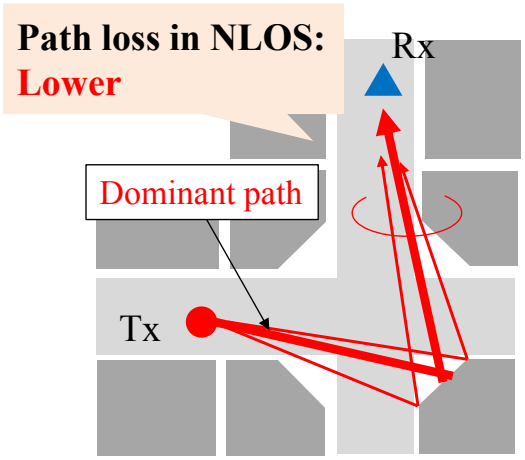

Figure 2-7 Dominant path in NLOS region

2.5 Path Loss Modeling

For less complexity, this section describes how the proposed outdoor path loss model based on the dominant path is developed for chamfered shape buildings from microwave band to millimeter wave band. The attenuation coefficient β is used as a fitting parameter in an NLOS region. The attenuation coefficient β in NLOS region is varied by the frequency and Tx to intersection distance because it is assumed that the relation between size of building and Fresnel zone is affected. Therefore, the attenuation coefficient β is extended in accordance with its dependence on frequency and Tx to intersection distance. Figure 2-8 shows the dependency between β and the Tx to intersection distance; it indicates that β decreases as the distance increases. Figure 2-9 shows the dependency between β and the frequency; it indicates that β increases as the frequency increases. Because the scatter and diffracted waves have frequency dependence, β has frequency dependency. In addition, β is mutually affected by both the Tx to intersection distance and frequency because the slope values vary. These results were used to propose β for chamfered shape buildings, as shown in equation (2.9). The model predicts β by using frequency f and the distance from Tx to the intersection x_1. The fitting parameters are obtained by regressing the measurement results. For applicable range of the model parameters, the maximum Tx-Rx distance was set at 1200 m because the prediction model was verified by using data measured up to that distance and the frequency range is from 2GHz to 37GHz. Figure 2-10 shows the path loss slopes of proposed model. This model provides three slopes and its slopes are continuous. In order to apply to UMi NLOS environment up to millimeter wave band, in NLOS region, the dependency of frequency f and the distance from Tx to the intersection is considered.

$$\beta = 4.2 + (1.4\log_{10} f/1MHz - 7.8)(0.8\log_{10} x_1 - 1.0) \tag{2.9}$$

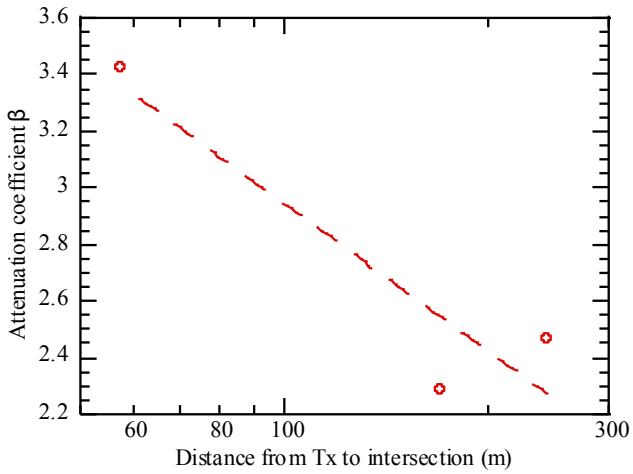

Reference:

Minoru Inomata, Wataru Yamada, Motoharu Sasaki, Masato Mizoguchi, Koshiro Kitao, Tetsuro Imai, “Path loss model for the 2 to 37 GHz band in street microcell environments,” *IEICE Communications Express*, Vol.4, No.5, pp. 149-154, May. 2015.

Figure 2-8 Attenuation coefficient dependency on Tx to intersection distance

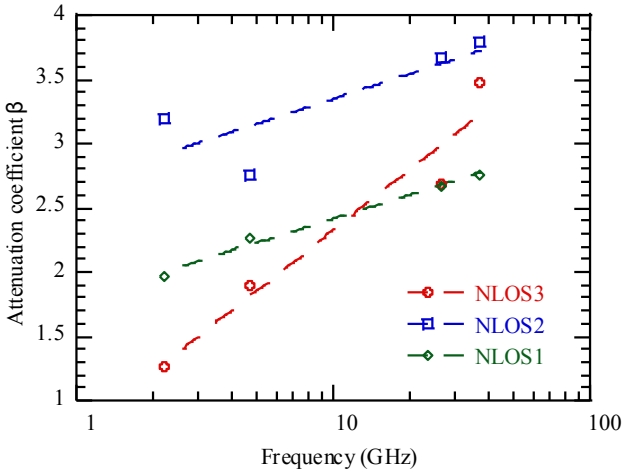

Reference:

Minoru Inomata, Wataru Yamada, Motoharu Sasaki, Masato Mizoguchi, Koshiro Kitao, Tetsuro Imai, “Path loss model for the 2 to 37 GHz band in street microcell environments,” *IEICE Communications Express*, Vol.4, No.5, pp. 149-154, May. 2015.

Figure 2-9 Attenuation coefficient dependency on frequency

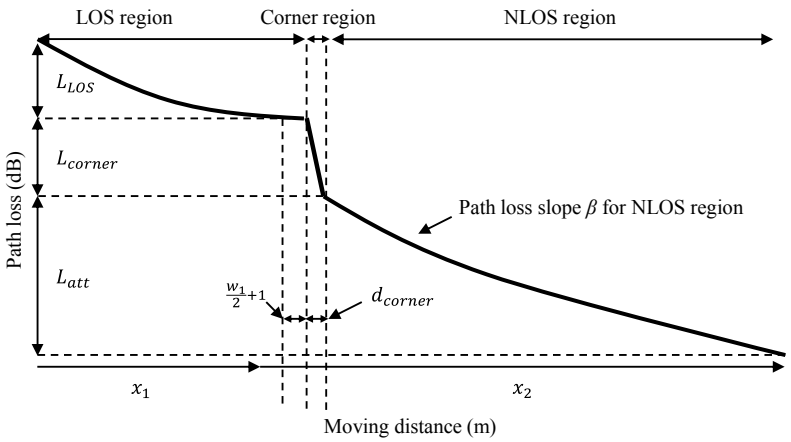

Figure 2-10 Path loss slopes of proposed model

To verify the proposed model's validity, the prediction results obtained are compared with the proposed model for chamfered shape buildings and those given in ITU-R P.1411. Figure 2-11 shows the verification results. The solid lines show the prediction results obtained by using the proposed model. As the figure shows, the prediction error of the proposed model was less than that of the ITU-R P.1411 for chamfered shape buildings in NLOS1, 2 and 3 regions. Table 2-2 summarizes the median, mean and RMSE values of prediction error. Here, the applicable range of the maximum Tx-Rx distance was set at 1200 m because the prediction model was verified by using data measured up to that distance. The applicable range of frequency is up to 37 GHz. This shows that the proposed model can cover the UMi NLOS environment for the frequency range from 2 to 37 GHz.

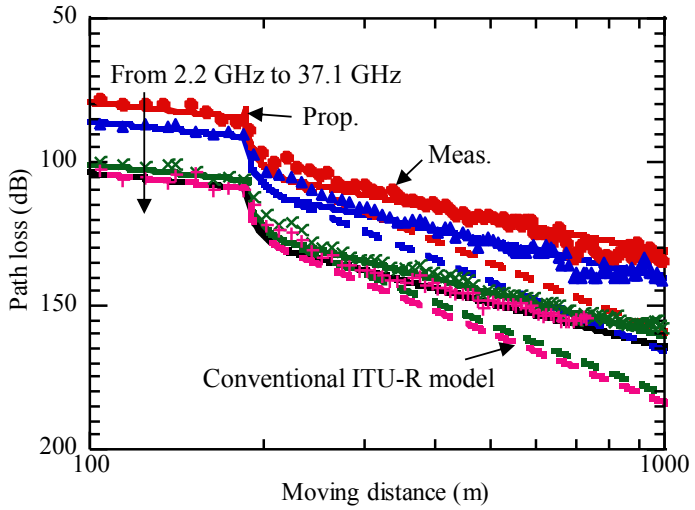

(a) NLOS1

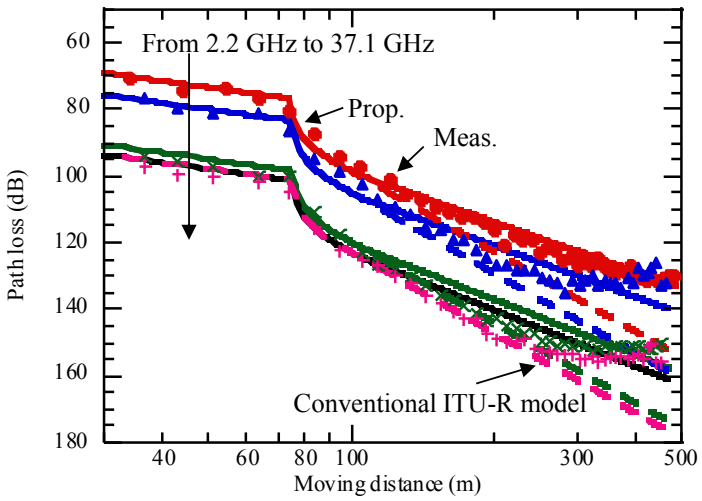

(b) NLOS2

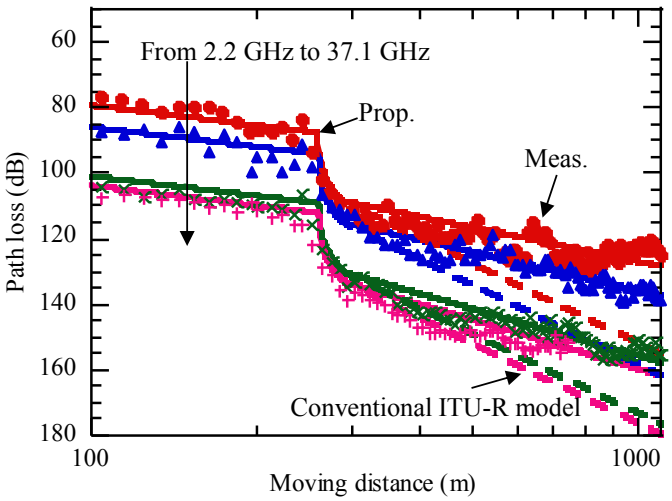

(c) NLOS3

Reference:

Minoru Inomata, Wataru Yamada, Motoharu Sasaki, Masato Mizoguchi, Koshiro Kitao, Tetsuro Imai, “Path loss model for the 2 to 37 GHz band in street microcell environments,” *IEICE Communications Express*, Vol.4, No.5, pp. 149-154, May. 2015.

Figure 2-11 Verification results

Table 2-2 Prediction error

	Proposed model
Median (dB)	-0.7
Mean (dB)	-0.8
R.M.S. (dB)	3.4

2.6 Summary of Chapter 2

In order to clarify dominant path which significantly affect the outdoor path loss and construct the outdoor path loss predictions based on dominant path, the outdoor path loss characteristics are measured in the 2 to 37 GHz band in UMi when the building shape of the intersection is wedge shaped building and chamfered shaped building. A comparison of measurement results and prediction results obtained by an ITU-R model showed that it can cover the frequency band up to 37 GHz for a wedge shaped building. Therefore, when the building shape of the intersection is wedge shaped building, the dominant path is multiple reflection waves which propagate along the street. However, the prediction error in chamfered shaped building cases is large. To clarify the cause of prediction error, ray tracing calculation is used and compared results obtained from it with measurement results. It is clarified that specular reflection from chamfered shaped buildings strongly contributes the power. Therefore, in ray tracing simulation, it is necessary to consider the chamfered shaped building in the intersection.

Based on these dominant paths, it is clarified that path loss depends on distance from Tx antenna to intersection and on frequency. From these results, for more less complexity, an outdoor path loss model based on the dominant paths is proposed and it is confirmed its validity by evaluating the RMSE values of prediction results obtained with it. The evaluations confirmed it can predict path loss with RMSE of less than 4 dB in the 2 to 37 GHz band. Since this path loss model based on chamfered shaped building is not applied to wedge shape building, in the wedge shape building case in the intersection, the conventional model should be applied.

Chapeter 3.

Predictions of Penetration Loss Characteristics through the Building Windows

3.1 Introduction

In this section, the dominant path which penetrates the building window is clarified and building penetration loss prediction is presented in UMi for high frequency band to evaluate 5G cell deployment. In 5G, massive MIMO have been investigated. They are a powerful solution to the problem of how to compensate for high path loss in high frequency bands. Therefore, in order to evaluate the performance of these techniques in practical environments, the path loss model is needed to provide flexibility for the 3D incident angle characteristics. Furthermore, in order to accurately evaluate the indoor coverage and interference at each terminal position in indoor, it is necessary to ascertain distance attenuation characteristics. Although the conventional models in high frequency respond those average characteristics [20], there can be quite some variation. In millimeter-wave bands, since building wall transmission loss increases [49] [50], the specific penetration paths to building windows are dominant.

It is first report how measurements are conducted in the bands ranging from 0.8 to 37.0 GHz. Also 3D incident angle and distance characteristics are measured. Second, ray tracing is used to clarify that the dominant penetration paths affecting path loss characteristics. On the basis of the obtained results, the building penetration loss model is developed by using those results for more simply simulation.

3.2 Measurement Campaign

This Section described the measurement method and parameters. UMi in ITU-R M.2135 [7], which summarizes the wireless interface evaluation method of the IMT-Advanced system, includes grid-layout roads and buildings. The paths between the Tx and building were a LOS environment. Figure 3-1 (a), (b) and (c) respectively show photographs of the measurement area taken at one of the Tx positions, at a corridor inside the building and outdoor buildings. It is regarded as the glass window of the measurement route (marked yellow point) as an LOS environment from a Tx position in the measurement environment. The tall buildings surround the road in the measurement site and Tx antenna is mounted below rooftops.

Figure 3-2 shows the measurement environment and Table 3-1 summarizes the measurement parameters. To analyze the frequency characteristics from microwave bands to millimeter wave

bands, it is set to the measurement frequencies at 0.8, 2.2, 4.7, 8.4, 26.3 and 37.0 GHz, respectively. The continuous waves were simultaneously transmitted from the Tx antennas, which were set up on the roofs of cars positioned on the roadside outside as shown in Figure 3-1 (a). The Rx antenna was located at the indoor corridor in the building where measurements were taken. The Tx antenna positions are shown as A1 and A2 in the Figure 3-2 (a). It is taken repeated measurements on the 1st, 2nd, 4th, 6th and 8th floors (i.e., 1F, 2F, 4F, 6F and 8F). It is also obtained the 3D incident angle characteristics described in Figure 3-2 (c). The 3D incident angle is an angle formed between the incident vector to the building wall and the normal vector of the building wall. Tx antennas were located at A-1 and A-2. Tx antenna height was 2.5 m above the ground. The Rx antenna was set up on a hand truck inside the building, and measurements were carried out with the dolly running as shown in Figure 3-2 (b) and (c). The Rx antenna height was 1.5 m above the floor. The radiation patterns of the Tx and Rx antennas are omni-directional in a horizontal plane. It is noted that vertically polarized waves were transmitted and received in these measurements. The median value of path loss calculated every meter.

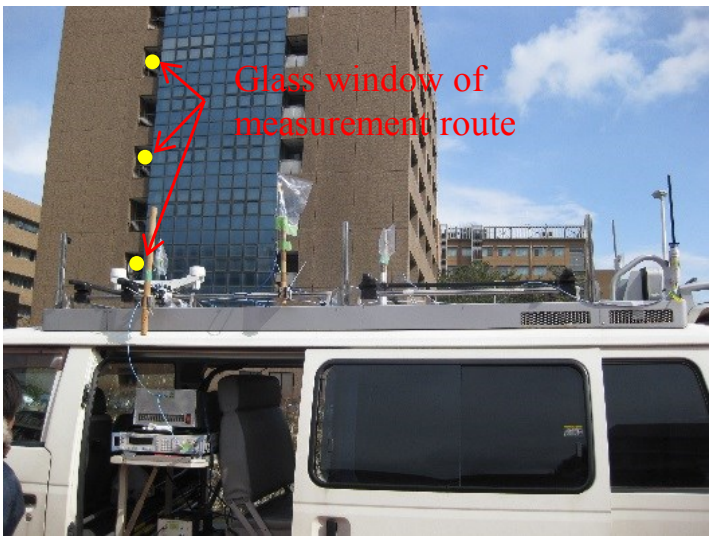

(a) Building from Tx position

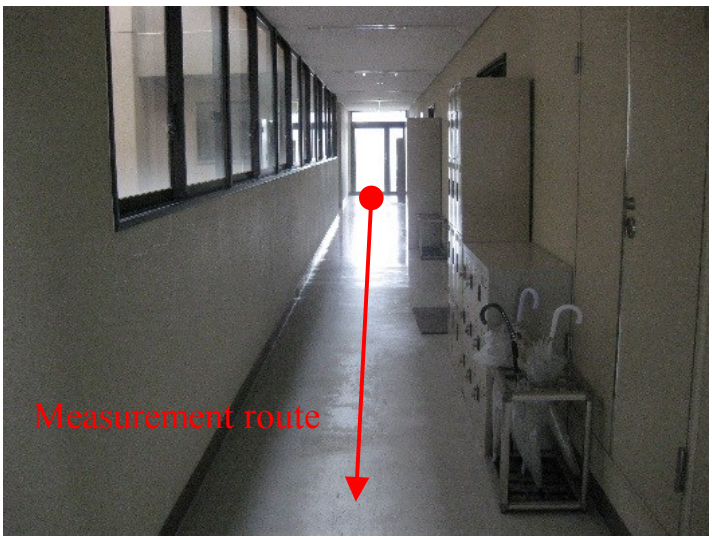

(b) Measurement route at indoor corridor

(c) Outdoor building from 6F

Reference:

Minoru Inomata, Motoharu Sasaki, Wataru Yamada, Takeshi Onizawa, Masashi Nakatsugawa, Nobutaka Omaki, Koshiro Kitao, Tetsuro Imai, Yukihiko Okumura, "Outdoor-to-Indoor Corridor Path Loss Model up to 40 GHz Band in Microcell Environments," *IEICE Trans. on Communication*, Vol.E100-B, No.2, pp.242-251, Feb. 2017.

Figure 3-1 Photographs of measurement area.

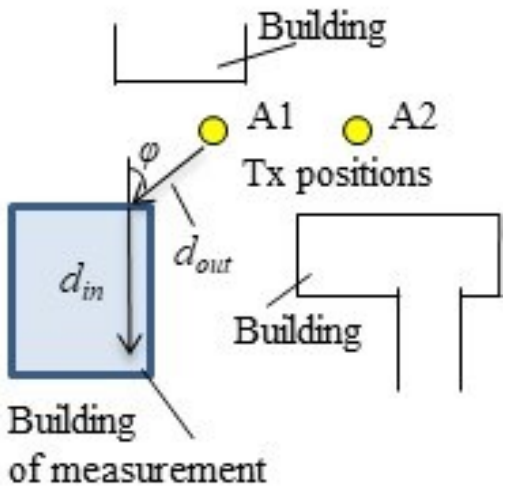

(a) Outdoor building layout and Tx positions.

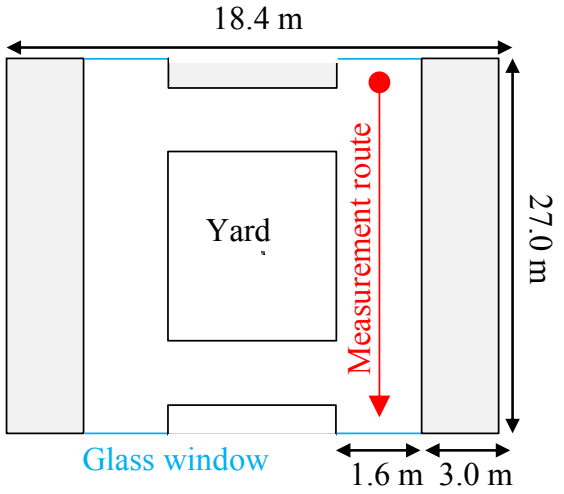

(b) Top view of indoor corridor and measurement route

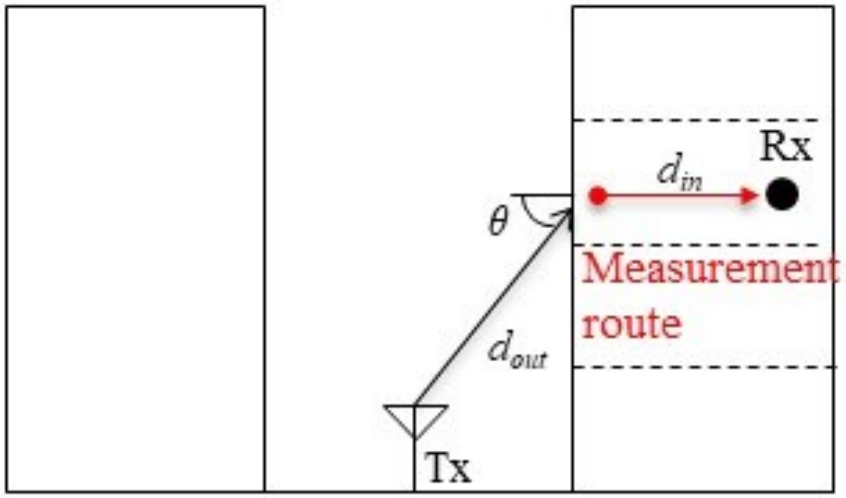

(c) Vertical view of indoor environment and measurement route

Reference:

Minoru Inomata, Motoharu Sasaki, Wataru Yamada, Takeshi Onizawa, Masashi Nakatsugawa, Nobutaka Omaki, Koshiro Kitao, Tetsuro Imai, Yukihiko Okumura, "Outdoor-to-Indoor Corridor Path Loss Model up to 40 GHz Band in Microcell Environments," *IEICE Trans. on Communication*, Vol.E100-B, No.2, pp.242-251, Feb. 2017.

Figure 3-2 Measurement environment

Table 3-1 Measurement parameters

Frequency (GHz)	0.8, 2.2, 4.7, 8.4, 26.3, 37.0
Tx antenna height	2.5 m
Rx antenna height	1.5 m
Floor number of measurement	1F, 2F, 4F, 6F and 8F
Tx/Rx antenna radiation pattern	Omni-directional

3.3 Building Penetration Loss for High Frequency Bands

In this section, a conventional building penetration loss model [7] is described for an UMi that can be applied to microwave bands and the measured path loss characteristics from the 0.8 to the 37.0 GHz band. The conventional model predicts the path loss with basic path loss PL_b which represents loss in an outdoor, penetration loss into building PL_{tw} and loss inside Pl_{in}, which represents path loss characteristics in indoor. The total path loss obtained with a conventional model is shown in equation (3.1), (3.2), (3.3) and (3.4) that follow.

$$PL = PL_b + PL_{tw} + PL_{in} \tag{3.1}$$

$$PL_b = 22\log_{10}(d_{out} + d_{in}) + 28 + 20\log_{10} f/1GHz \tag{3.2}$$

$$PL_{tw} = 14 + 15(1 - \cos\varphi)^2 \tag{3.3}$$

$$PL_{in} = 0.5d_{in} \tag{3.4}$$

where d_{out} is the distance from Tx to the wall next to Rx, d_{in} is the perpendicular distance from the wall to Rx, and φ (azimuth angle) is defined as the angle formed between the unit vector in the azimuth direction of the incident vector and the normal vector.

Figure 3-3 shows the building penetration loss measurement results obtained at A-2 at 37.0 GHz for the route for floors 1F, 2F, 4F, 6F and 8F. The horizontal axis indicates Rx moving distance along the measurement route. The vertical axis indicates the normalized path loss. Figure 3-4 shows that path loss slope of measurement results for each floor. The path loss slope in Figure 3-4 is obtained by linear regression. Figure 3-5 shows the measurement results obtained at A-2 on 8F for the 0.8, 2.2, 4.7, 8.4, 26.3 and 37.0 GHz frequency bands. Figure 3-6 shows the frequency dependence of measurement building penetration loss. The horizontal axis indicates the median value of path loss. The vertical axis indicates the frequency. In order to analyze the path loss dependence on the frequency and 3D incident angle, the path loss PL_{norm} is normalized by free space loss PL_{free} as follows.

$$PL_{norm} = PL_{meas} - PL_{free} \tag{3.5}$$

$$PL_{free} = 20\log_{10}(d_{out} + d_{in}) + 20\log_{10} f/1GHz + 32.4 \tag{3.6}$$

As Figure 3-3 and Figure 3-4 show, the path loss slope tends to increase as the floor number increases. To illustrate, the values are about 0.2 dB/m at 1F and 0.8 dB/m at 8F. Because the values of slope with conventional model is 0.5 dB/m, conventional model predict underestimate the path loss in higher 3D incident angle. As the Figure 3-5 and Figure 3-6 show, the path loss tends to increase as the frequency increases. However, the conventional model underestimates the path loss, which becomes up to as high as 13dB at 37.0 GHz. The frequency dependency of the conventional model is the same as that for free space loss. When the conventional model is normalized by the free space loss as given in equation (3.5), the calculation results PL_{norm} does not depend the frequency. Therefore, it cannot be applied the high frequency bands over 6 GHz.

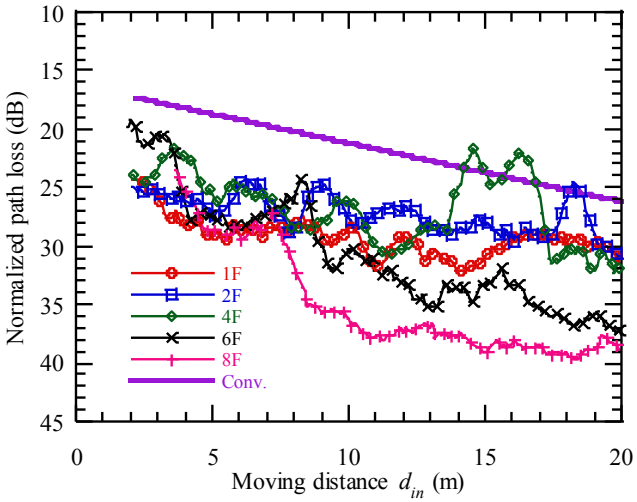

Reference:

Minoru Inomata, Motoharu Sasaki, Wataru Yamada, Takeshi Onizawa, Masashi Nakatsugawa, Nobutaka Omaki, Koshiro Kitao, Tetsuro Imai, Yukihiko Okumura, "Outdoor-to-Indoor Corridor Path Loss Model up to 40 GHz Band in Microcell Environments," *IEICE Trans. on Communication*, Vol.E100-B, No.2, pp.242-251, Feb. 2017.

Figure 3-3 Building penetration loss measurement obtained at A-2 at 37.0 GHz for the route for floors 1F, 2F, 4F, 6F and 8F

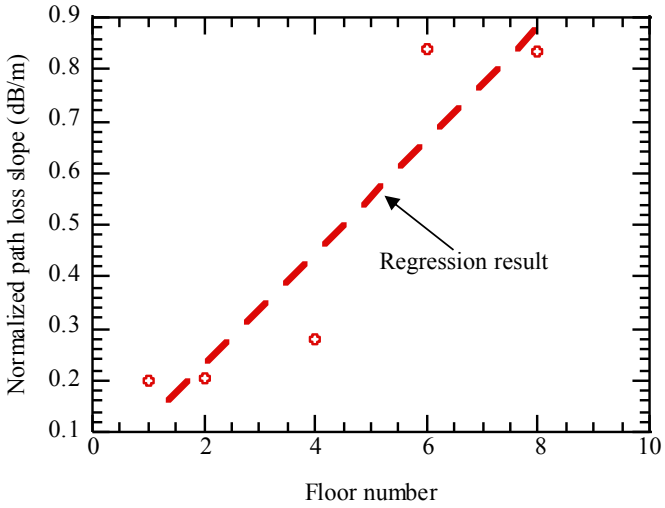

Reference:

Minoru Inomata, Motoharu Sasaki, Wataru Yamada, Takeshi Onizawa, Masashi Nakatsugawa, Nobutaka Omaki, Koshiro Kitao, Tetsuro Imai, Yukihiko Okumura, "Outdoor-to-Indoor Corridor Path Loss Model up to 40 GHz Band in Microcell Environments," *IEICE Trans. on Communication*, Vol.E100-B, No.2, pp.242-251, Feb. 2017.

Figure 3-4 Normalized path loss slope for floors 1F, 2F, 4F, 6F and 8F

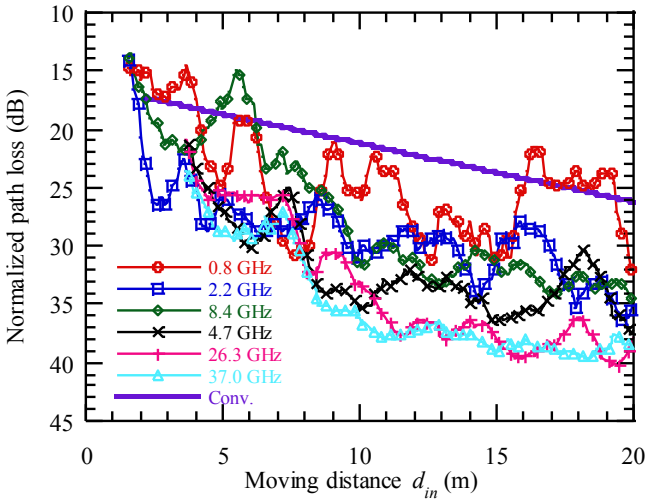

Reference:

Minoru Inomata, Motoharu Sasaki, Wataru Yamada, Takeshi Onizawa, Masashi Nakatsugawa, Nobutaka Omaki, Koshiro Kitao, Tetsuro Imai, Yukihiko Okumura, "Outdoor-to-Indoor Corridor Path Loss Model up to 40 GHz Band in Microcell Environments," *IEICE Trans. on Communication*, Vol.E100-B, No.2, pp.242-251, Feb. 2017.

Figure 3-5 Building penetration loss measurement obtained at A-2 on 8F for the 0.8, 2.2, 4.7, 8.4, 26.3 and 37.0 GHz frequency bands

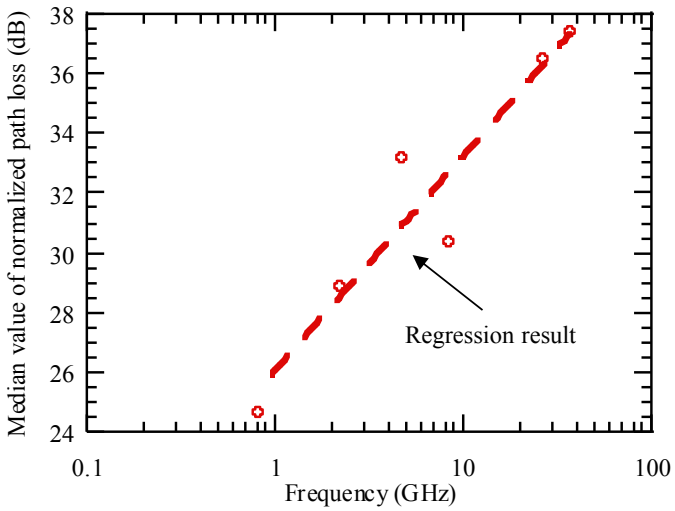

Reference:

Minoru Inomata, Motoharu Sasaki, Wataru Yamada, Takeshi Onizawa, Masashi Nakatsugawa, Nobutaka Omaki, Koshiro Kitao, Tetsuro Imai, Yukihiko Okumura, "Outdoor-to-Indoor Corridor Path Loss Model up to 40 GHz Band in Microcell Environments," *IEICE Trans. on Communication*, Vol.E100-B, No.2, pp.242-251, Feb. 2017.

Figure 3-6 Frequency dependence of median value of normalized path loss for the 0.8, 2.2, 4.7, 8.4, 26.3 and 37.0 GHz frequency bands

3.4 Analysis of Dominant Path at Building Penetration

3.4.1. Analysis of the dominant path at building penetration

This subsection describes the analysis results for the dominant paths at building penetration. In order to analyze and clarify the dominant paths of each propagation path, ray tracing calculation is carried out by considering the simulation model shown in Figure 3-7 (a) and (b) as microcell environments surrounded by buildings. In general UMi environment, reflected rays between external buildings would be observed. Therefore, in order to evaluate those reflected rays, simulation model that the wall of buildings surrounded is constructed. The wall plate material is assumed to be concrete with dielectric constant of 7 and conductivity of 0.0023 S/m. The antenna height, antenna radiation pattern and frequency are same parameter used in measurement. Those calculations were performed every 0.1 m and the results were post-processed in the same manner as measurement. Ray tracing calculations were implemented for different rays as shown in Figure 3-7.

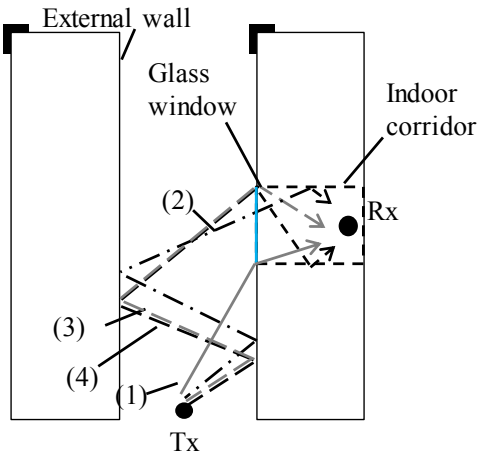

Case (1) A diffracted ray
Case (2) External wall reflected ray
Case (3) External wall reflected, then diffracted ray or diffracted, then indoor wall reflected ray
Case (4) External wall reflected, then diffracted, then indoor wall reflected ray

(a) Top view of ray tracing simulation model and all paths that penetrating building

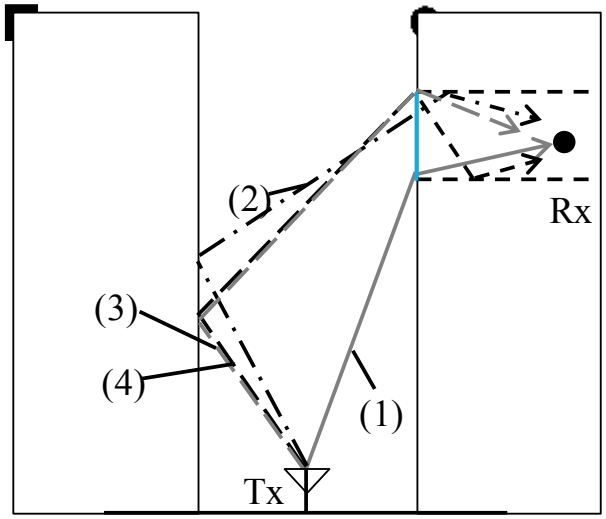

(b) Vertical view of ray tracing simulation model

Reference:

Minoru Inomata, Motoharu Sasaki, Wataru Yamada, Takeshi Onizawa, Masashi Nakatsugawa, Nobutaka Omaki, Koshiro Kitao, Tetsuro Imai, Yukihiko Okumura, “Outdoor-to-Indoor Corridor Path Loss Model up to 40 GHz Band in Microcell Environments,” *IEICE Trans. on Communication*, Vol.E100-B, No.2, pp.242-251, Feb. 2017.

Figure 3-7 Ray tracing simulation model

The rays are as follows:

Case (1): a diffracted ray.

Case (2): rays reflected multiple times between the external walls of buildings.

Case (3): rays reflected multiple times between the external walls of buildings and then diffracted at a window frame, or rays diffracted at a window frame and then reflected multiple times between the internal walls of buildings.

Case (4): rays reflected multiple times between the external walls of buildings, then diffracted at a window frame, then reflected multiple times between the internal walls of buildings.

Case (1) includes a maximum of 4 paths, with 1 diffraction. Case (2) includes a maximum of about 10 paths, with 7 reflections. Case (3) includes a maximum of about 120 paths, with 1 diffraction and 7 reflections. Case (4) includes a maximum of about 280 paths, with 1 diffraction is 1 time and 7 reflections. The paths in case (2), (3) and (4) take rays reflected between the external walls of buildings into consideration but the paths in case (1) do not take those reflection. Therefore, the diffracted angle in case (1) is smaller than (3) and (4) and will cause the diffraction loss in case (1) to be larger than in (3) and (4). Moreover, The paths in case (1), (3) and (4) take rays diffracted at a window frame but the paths in case (2) do not take those diffraction. Therefore, the frequency dependency in case (2) is considerably smaller than in case (1), (3) and (4) because the reflection coefficient in case (2) has little frequency dependency.

Figure 3-8 compares the calculation results obtained by using ray tracing with measurement results. Here, the Tx is at A-2 and the Rx is on 1F and the frequency bands are used at 0.8 and 37.0 GHz. The horizontal axis indicates Rx moving distance along the measurement route. The vertical axis indicates the normalized path loss by subtracting free space loss. First, Figure 3-8 (a) shows in case (1). A diffracted ray tends to be larger than measurement results because of large diffraction loss. The values of RMSE between prediction results and measurement results are 17 dB at 0.8 GHz and 21.4 dB at 37.0 GHz. These results mean that a single diffracted ray has little effect on the path loss characteristics. Second, Figure 3-8 (b) shows in case (2). For these rays the path loss is underestimate compared to the measurement results obtained at 37.0GHz, but these rays cannot contribute to the frequency dependency of the measurement results because the reflection coefficient has little frequency dependency. Furthermore, the steep slope of these rays is different from the gentle slope of the measurement results. The RMSE values are 7.1 dB at 0.8 GHz and 7.3 dB at 37.0 GHz. Last, Figure 3-8 (c) shows in case (3) and (4). Because the path loss in Fig. 8 (c) is calculated by summing up the rays in case 3 and case 4, the figure shows only one calculation result for each frequency. The path loss in these paths can represent the frequency dependency and those gentle slope tend to close to the measurement results because the RMSE values are smaller about 5.3 dB at 0.8 GHz and 4.1 dB at 37.0 GHz than in case (1) and (2). Furthermore, the diffraction loss of these rays are smaller than in case (1) because the diffraction angle of these rays at penetrating buildings in case (3) and (4) are larger than in case (1).

As described in subsection 3.3, the measurement results are dependent on indoor loss, the

frequency and 3D incident angle. Therefore, these dependencies need to be taken into account. The analysis results clarify that paths reflected multiple times between the external walls of buildings and diffracted into a building significantly affect the path loss. As a result, it is found that those paths are dominant. In the ray tracing simulation, it is assumed that since the aperture of window is enough larger than the Fresnel zone in each frequency bands.

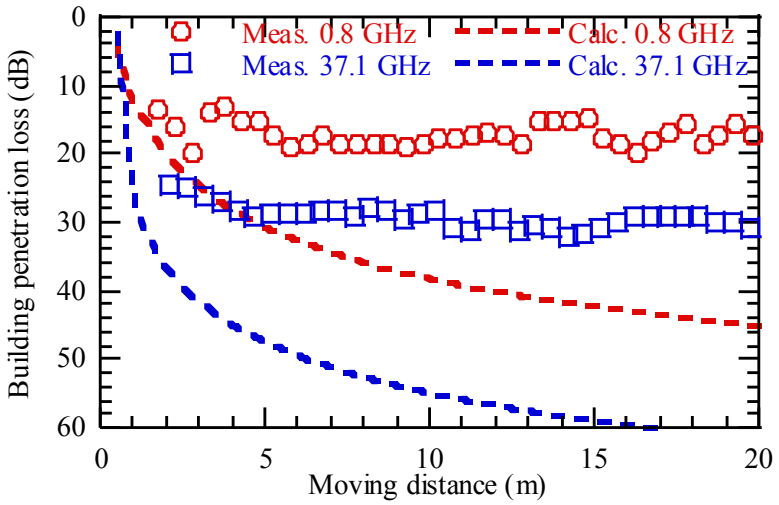

(a) Comparison between calculation results and measurement results in case (1)

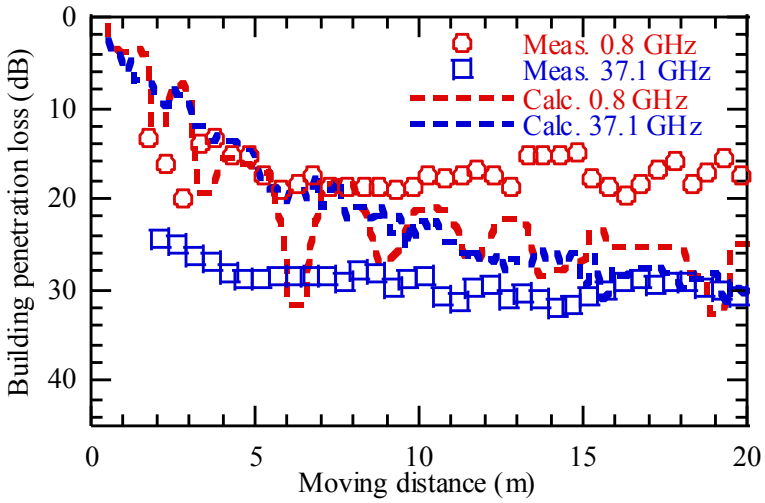

(b) Comparison between calculation results and measurement results in case (2)

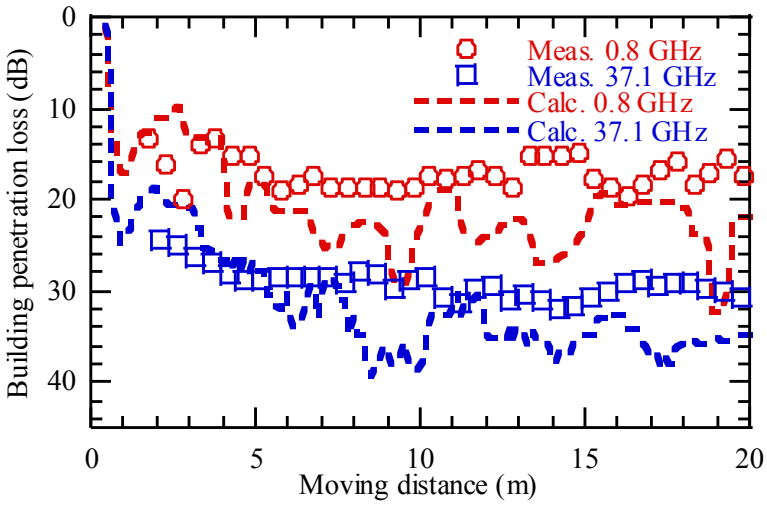

(c) Comparison between calculation results and measurement results in case (3) and (4)

Reference:

Minoru Inomata, Motoharu Sasaki, Wataru Yamada, Takeshi Onizawa, Masashi Nakatsugawa, Nobutaka Omaki, Koshiro Kitao, Tetsuro Imai, Yukihiko Okumura, "Outdoor-to-Indoor Corridor Path Loss Model up to 40 GHz Band in Microcell Environments," *IEICE Trans. on Communication*, Vol.E100-B, No.2, pp.242-251, Feb. 2017.

Figure 3-8 Comparison between calculation results and measurement results

3.4.2 Analysis of Frequency and 3D Incident Angle Dependency

In the previous subsection, it is clarified the dominant paths. Thus, the frequency and 3D incident angle dependency is analyzed by using dominant paths. As mentioned in subsection 3.4.1, the path loss gently sloped after the building penetration because of effect on the diffraction. On the basis of these analysis results, the outdoor-to-indoor path loss is calculated by using the following equation:

$$PL_{prop} = \alpha \log_{10}(d_{in}) + \beta \tag{3.7}$$

where α is the path loss slope and β is the attenuation at the building penetration. The coefficients of the above equation are considered to depend on frequency and 3D incident angle. The relation between the parameter of frequency and 3D incident angle is derived by using the analysis results with dominant paths regressed by (3.7).

Figure 3-9 shows how the path loss slope α (attenuation vs. distance) changed when the floor number from 1F to 8F. Figure 3-10 shows the frequency dependency of the attenuation at building penetraion β. For this analysis, the parameters are same measurement parameters. The path loss slope α and the attenuation at the building penetration β were carried out using the least square method by using the analyzed path loss with dominant paths. The path loss slope α values is

obtained from the fitting results for slope. Also, the attenuation at the building penetration β values is obtained from the fitting results for intercept. From the Figure 3-9, it can be seen that the path loss slope α increases as the floor number increases; this is because the diffraction angle at the building penetration decreases as the floor number increases. Accordingly, it is found that the path loss slope α depends on 3D incident angle. Figure 3-10 shows that the attenuation at building penetration β increases as the frequency increases. The rate of the increment is obtained by logarithmic regression of the results of attenuation at building penetration β. The slope value is about 4.6log$f$, which means that the frequency dependency at the building penetration is larger 4.6 than free space loss.

Accordingly, it can be seen that the attenuation at the building penetration β depends on the frequency. As metioned in this subsection, the frequency and 3D incident angle dependencies tend to close to the measurement results as shown in Figure 3-4 and 3-6. Therefore, it is found that these dependencies need to be taken into account when modeling building penetration loss for less complexity.

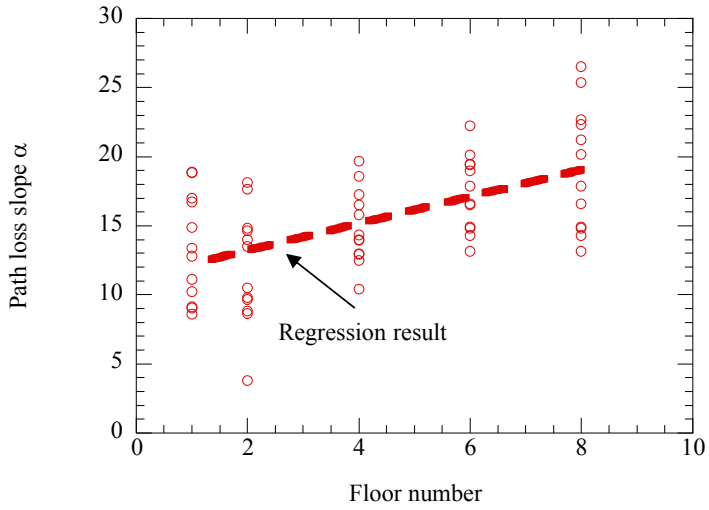

Reference:

Minoru Inomata, Motoharu Sasaki, Wataru Yamada, Takeshi Onizawa, Masashi Nakatsugawa, Nobutaka Omaki, Koshiro Kitao, Tetsuro Imai, Yukihiko Okumura, "Outdoor-to-Indoor Corridor Path Loss Model up to 40 GHz Band in Microcell Environments," *IEICE Trans. on Communication*, Vol.E100-B, No.2, pp.242-251, Feb. 2017.

Figure 3-9 Path loss slope at the floors 1F, 2F, 4F, 6F and 8F

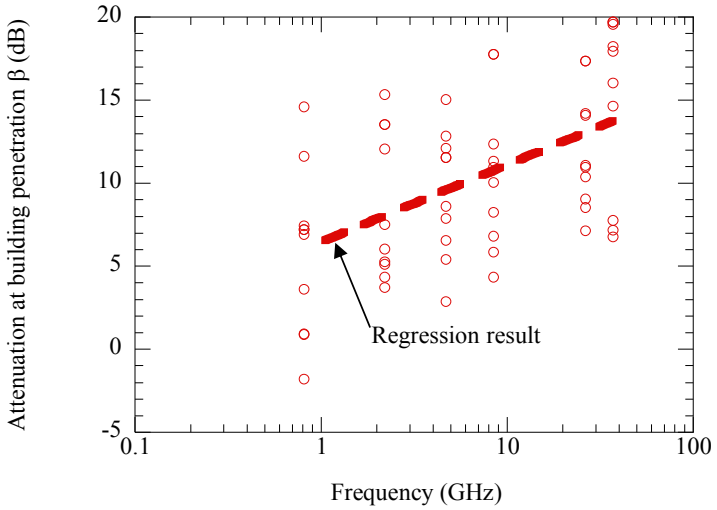

Reference:

Minoru Inomata, Motoharu Sasaki, Wataru Yamada, Takeshi Onizawa, Masashi Nakatsugawa, Nobutaka Omaki, Koshiro Kitao, Tetsuro Imai, Yukihiko Okumura, "Outdoor-to-Indoor Corridor Path Loss Model up to 40 GHz Band in Microcell Environments," *IEICE Trans. on Communication*, Vol.E100-B, No.2, pp.242-251, Feb. 2017.

Figure 3-10 Frequency dependency of the attenuation at building penetration from 0.8 to 37.0 GHz bands

3.5 Building Penetration Loss Modeling

In previous subsection, it is clarified the frequency and 3D incident angle dependecy by using dominant paths. Thus, for less complexity, the path loss model empolying these dependecies is constructed. Equations (3.8) and (3.9) show the proposed building penetration loss model. As the analysis results indicate, the building penetration loss has the gentle slope after the building penetration. Therefore, a logarithmic function is used to represent this characteristic. As the analysis results in subsection 3.4.2 indicate, it is important to take into account the dependency of frequency and 3D incident angle to predict the building penetration loss. It is assumed that the effect of frequency on the attenuation at building penetration β is formulated by logarithmic functions. It is also assumed that the effect of 3D incident angle on the path loss slope α is formulated by trigonometric function. The parameters for proposed model are generated by calculation results with ray tracing. Figure 3-11 and 3-12 shows the definition of the proposed model's parameters. The parameter θ (elevation angle) is defined as the angle formed between the unit vector in the elevation direction of the incident vector and the normal vector of a building wall. The parameter φ (azimuth angle) is defined as the angle formed between the unit vector in the azimuth direction of the incident vector and the normal vector. If the elevation and azimuth angles are equal to 0, it means that the Tx

antenna is in front of the Rx antenna and the Tx antenna height is equal to the Rx antenna height. Here, the fitting parameters of the proposed model carry out multiple regression analysis of the analysis results with dominant paths in all measurement routes and frequencies. Multiple regression is practical method with less complexity to obtaine the prediction model [3] [20]. The multiple regression model is represented by path loss and the distribution of the shadowing which is modelled as log-normal, and its standard deviation is given.

The fitting parameters are calculated for α_φ=3.7, α_θ = 21.2, β = 9.2, α_f = 4.7, γ = 6.5. The unit of frequency is GHz and unit of distance is m.

$$PL = PL_{free} + PL_{prop} \tag{3.8}$$

$$PL_{prop} = \left(\alpha_\varphi \sin\varphi + \alpha_\theta \sin\theta + \beta\right) \log_{10}(d_{in}) + \alpha_f \log_{10} f/1GHz + \gamma \tag{3.9}$$

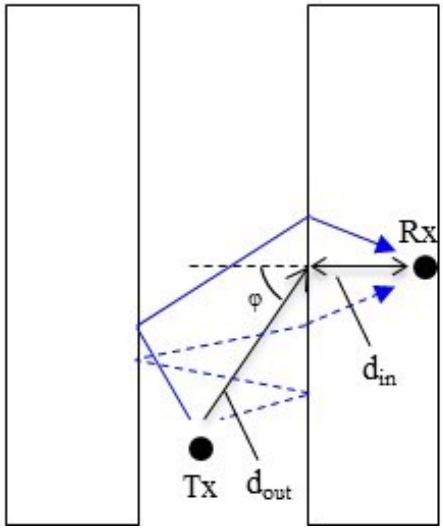

Reference:

Minoru Inomata, Motoharu Sasaki, Wataru Yamada, Takeshi Onizawa, Masashi Nakatsugawa, Nobutaka Omaki, Koshiro Kitao, Tetsuro Imai, Yukihiko Okumura, “Outdoor-to-Indoor Corridor Path Loss Model up to 40 GHz Band in Microcell Environments,” *IEICE Trans. on Communication*, Vol.E100-B, No.2, pp.242-251, Feb. 2017.

Figure 3-11 Top view of proposed model definition and example of dominant paths at building penetration

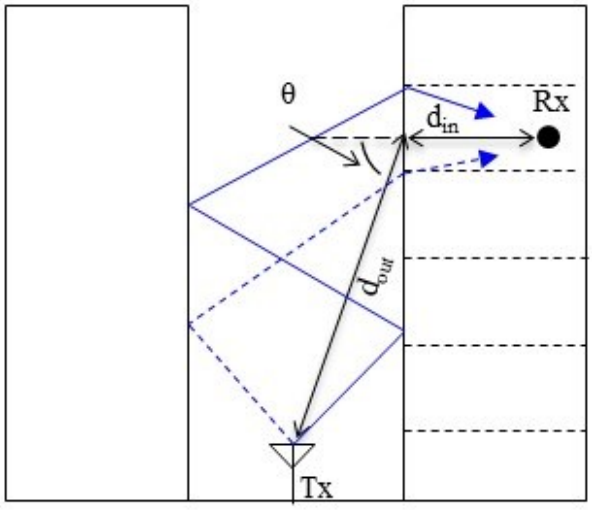

Reference:

Minoru Inomata, Motoharu Sasaki, Wataru Yamada, Takeshi Onizawa, Masashi Nakatsugawa, Nobutaka Omaki, Koshiro Kitao, Tetsuro Imai, Yukihiko Okumura, "Outdoor-to-Indoor Corridor Path Loss Model up to 40 GHz Band in Microcell Environments," *IEICE Trans. on Communication*, Vol.E100-B, No.2, pp.242-251, Feb. 2017.

Figure 3-12 Vertical view of proposed model definition and example of dominant paths at building penetration

3.6 Performance of Proposed Building Penetration Loss Model

In this section, to verify the performance of the proposed model, the prediction results obtained with proposed model and the conventional model are compared. Furthermore, the applicable range of proposed model is described. Figure 3-13 show the proposed model's prediction results from 0.8 to 37.0 GHz band as well as the measurement results at A-2 on 8F. Table 3-2 shows the RMSE values between predicted results with proposed model and conventional model in each frequency band. Because the parameters for proposed model were regressed only by using calculation results obtained with ray tracing, separate measurement results are compared with proposed model and conventional model. From Figure 3-13, it can be seen that for both routes the prediction error of the proposed model was less than that of the conventional model. It reduces the RMSE value by about 6.2 dB. From these results, the distance attenuation obtained with the proposed model is better fitting compared with the conventional model.

Figure 3-14 shows prediction error as a function of frequency for the proposed model and the conventional model. In order to analyze the effect of frequency on prediction error, the RMSE value is calculated for each frequency. As the Figure 3-14 shows, the prediction errors are considerably lower for the former than for the latter. For the former the RMSE values were from 3.3 dB to 5.5 dB,

while for the latter they were from 4.3 to 8.7 dB. For the conventional model these values tend to steadily increase with increasing frequency, but they do not for the proposed model. In particular, at 37.0 GHz, the RMSE value is improved about 5.4 dB with proposed model. This is because the conventional model takes no account of the frequency dependency, which becomes larger with increasing diffraction loss. Figure 3-15 shows prediction error as a function of the 3D incident angle for the proposed model and the conventional model. The 3D incident angle is an angle formed between the incident vector to the building wall and the normal vector of the building wall. As the figure shows, the prediction errors with proposed model are improved than that with conventional model. The RMSE values with conventional model are from 3.3 dB to 11 dB, while with proposed model the RMSE values are from 2.5 dB to 6.4 dB. This result means that the proposed model achieved the better performance of the 3D incident angle. Therefore, these results indicate that the proposed model can accurately predict the actual path loss.

Table 3-3 shows the applicable range of the proposed model parameters. Because the model was verified by using data measured up to the 20 m distance given in the table, the maximum indoor distance din was set at that distance. The frequency and 3D incident angle characteristics are few changes on the basis of theoretical analysis results for lower angle below 25 degrees and frequency bands below 0.8 GHz. Therefore, the range of the frequency is applicable up to 37 GHz and the range of the 3D incident angle is applicable up to 60 degrees.

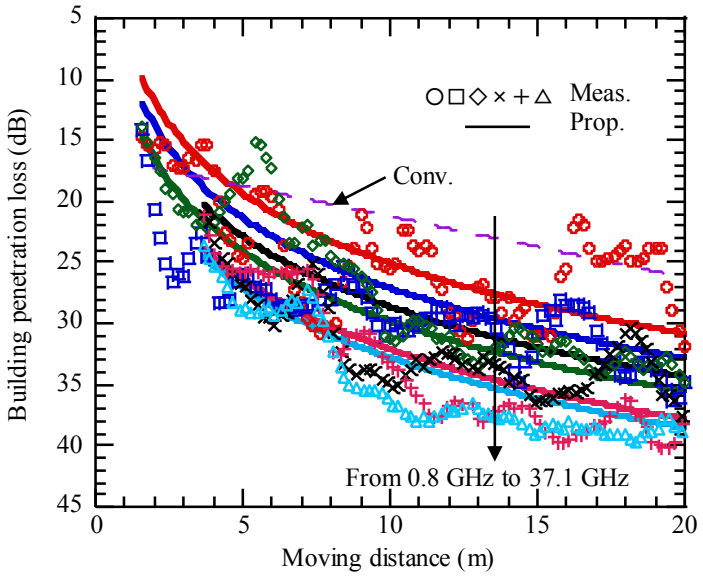

Reference:

Minoru Inomata, Motoharu Sasaki, Wataru Yamada, Takeshi Onizawa, Masashi Nakatsugawa, Nobutaka Omaki, Koshiro Kitao, Tetsuro Imai, Yukihiko Okumura, “Outdoor-to-Indoor Corridor Path Loss Model up to 40 GHz Band in Microcell Environments,” *IEICE Trans. on*

Communication, Vol.E100-B, No.2, pp.242-251, Feb. 2017.

Figure 3-13 Measurement and prediction results with proposed model and with conventional model

Table 3-2 The RMSE values between predicted results with proposed model and conventional model

	RMSE (dB)	
	Prop.	Conv.
0.8 GHz	4.7	4.2
2.2 GHz	3.7	5.2
4.7 GHz	4.3	6.7
8.4 GHz	5.7	5.7
26.3 GHz	4.0	7.9
37.0 GHz	3.3	8.7

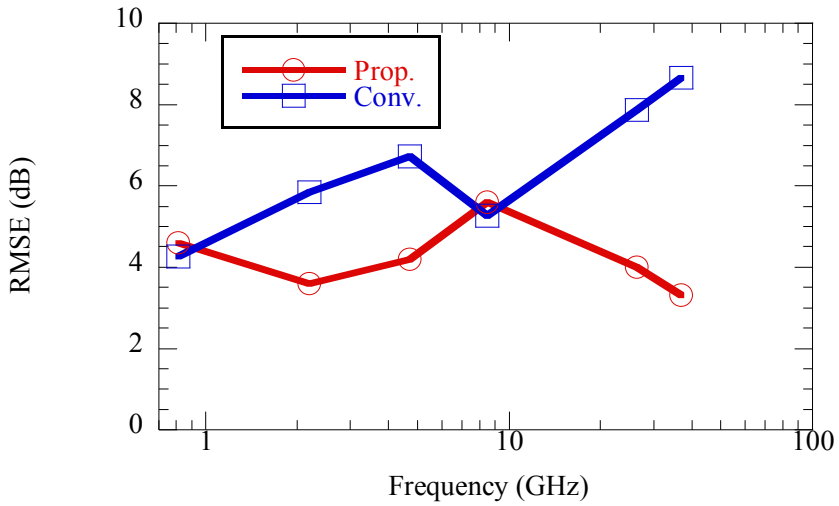

Reference:

Minoru Inomata, Motoharu Sasaki, Wataru Yamada, Takeshi Onizawa, Masashi Nakatsugawa, Nobutaka Omaki, Koshiro Kitao, Tetsuro Imai, Yukihiko Okumura, "Outdoor-to-Indoor Corridor Path Loss Model up to 40 GHz Band in Microcell Environments," *IEICE Trans. on Communication*, Vol.E100-B, No.2, pp.242-251, Feb. 2017.

Figure 3-14 Comparison of prediction error as function of frequency

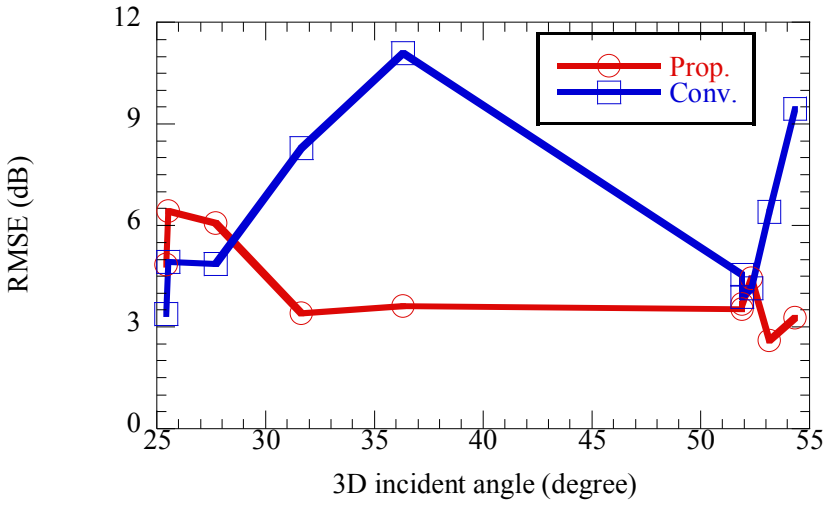

Reference:

Minoru Inomata, Motoharu Sasaki, Wataru Yamada, Takeshi Onizawa, Masashi Nakatsugawa, Nobutaka Omaki, Koshiro Kitao, Tetsuro Imai, Yukihiko Okumura, "Outdoor-to-Indoor Corridor Path Loss Model up to 40 GHz Band in Microcell Environments," *IEICE Trans. on Communication*, Vol.E100-B, No.2, pp.242-251, Feb. 2017.

Figure 3-15 Comparison of prediction error as function of 3D incident angle

Table 3-3 Applicable range of proposed model.

d_{in}: Distance in indoor	1 – 20 (m)
f: Frequency	0.8-37 (GHz)
3D incident angle	Up to 60 (degree)

3.7 Summary of Chapter 3

In this section, in order to clarify the dominant path which penetrates to building window and construct the building penetration loss predictions, it is measured the building penetration loss in the 0.8 to 37 GHz bands in UMi environment. To clarify the dominant path, ray tracing is used to carry out calculation and compare measurement with calculation results. It is clarified that paths reflected multiple times between the external walls of buildings and then diffracted into one of the building were dominant. It is also clarified their effects on the accurate modeling of path loss characteristics. For implementation with less computation, dominant paths are used to develop a building penetration loss model based on analysis results that is obtained for frequency and 3D incident angle dependency. The proposed model's validity was confirmed by comparing the RMSE values obtained with proposed model and conventional model. It is found that it can improve the predicted error maximum 5.4 dB in bands up to 37 GHz. In order to construct a model with general versatility, further experiments and verification in various environments including the indoor office case are required and these will be subjects for our future work.

Chapeter 4.

Predictions of Channel Characteristics considering Buildings Surface Irregularity

4.1 Introduction

In this section, propagation channel prediction based on scattering from the structure irregularities is proposed in UMi LOS environment for high frequency band for cell deployment. Diffuse scattering waves due to scattering objects that have structure irregularities such as the shape of buildings, windows, and balconies, significantly affect the propagation characteristics in high frequency band. Therefore, the RT method must be extended so that it can properly handle diffuse scattering characteristics.

An ER model based on Gaussian surface roughness was described in [72]. The ER model is one solution that accurately predicts diffuse scattering from various scattering objects. There have been several studies on the hybrid of RT method and ER model [12]. However, since the building model in an urban environment is generated by means of conventional commercially available map databases based on the smooth surface, the structure irregularities are not considered and the scattering coefficient is set to empirical value based on measurement data. Thus, prediction results are not suitable for channel characteristics in high frequency bands in an actual urban environment.

Therefore, in this chapter, a radio propagation prediction method is proposed using point cloud data based on a hybrid of the RT method and ER model in an urban environment for high frequency bands. A point cloud is acquired by using laser scanning, which is a widely accepted method to obtain detailed structure data from environments in recent architecture and civil engineering research. Since the parameters related to structure irregularities in the proposed prediction method can be obtained by point cloud data, the prediction method takes into consideration the diffuse scattering from the structure irregularities. First the prediction method process is reported. Then, it is verified that the prediction accuracy based on comparison between measurements and prediction results using the proposed method. On the basis of the obtained results, it is clarified that the validity of the proposed method and statistical parameters that properly represent the propagation characteristics considering diffuse scattering in an urban environment for high frequency bands.

4.2 Conventional Prediction Method

4.2.1 Procedure

The procedure for the hybrid method is described as follows. The electric field E_{RT}, of the direct wave, and the specular reflections and diffractions from smooth surfaces are calculated using the RT method. In the ER model, the electric field is basically calculated by assuming a Gaussian random rough surface as shown in Figure 4-1. In order to consider specular reflections based on this Gaussian rough surface, the electric field of the specular reflections is calculated using effective reflection coefficient R_s. It is defined as

$$R_s = \rho R \tag{4.1}$$

where

$$\rho = \exp\left\{-\frac{1}{2}\left(\frac{4\pi\sigma_h \cos\theta_i}{\lambda}\right)\right\} \tag{4.2}$$

ρ is the roughness attenuation factor, and R is the Fresnel reflection coefficient. Factor ρ is calculated based on wavelength λ, incident angle θ_i, and the standard deviation of roughness, σ_h.

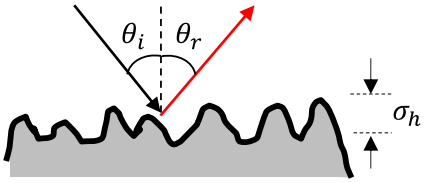

Reference:

Minoru Inomata, Tetsuro Imai, Koshiro Kitao, Yukihiko Okumura, Motoharu Sasaki, Yasushi Takatori, “Radio Propagation Prediction Method Using Point Cloud Data Based on Hybrid of Ray-Tracing and Effective Roughness Model in Urban Environments,” *IEICE Trans. on Communication*, Vol.E102-B, No.1, pp.51-62, July. 2019.

Figure 4-1 Gaussian random rough surface

Then, diffuse scattered electric field E_s is calculated using the ER model. In this model, each surface of the scattering object is divided into multiple surface elements as shown in Figure 4-2. Then, scattered electric field E_s is calculated from each surface element. There are a few scattering radiation patterns for the ER model [72] as shown in Figure 4-3: the Lambertian model and the directive model. The Lambertian model assumes that the scattering is non-coherent. The scattering radiation lobe has its maximum in the direction perpendicular to the wall. The electric field of the Lambertian model, $E_{S\_Lambertian,}$ is obtained by

$$\left|E_{s\_Lambertian}\right|^2 = \left(\frac{KS}{|\boldsymbol{r}_i||\boldsymbol{r}_s|}\right)^2 \frac{cos\theta_i cos\theta_s}{\pi} dS \tag{4.3}$$

where K is a constant depending on the amplitude of the impinging wave, θ_i is the incident angle, θ_s is the scattering angle, $\boldsymbol{r}_i$ is the incident direction, $\boldsymbol{r}_s$ is the scattering direction, and dS is the size of the surface elements. Term S is a scattering coefficient calculated by roughness attenuation factor ρ and Fresnel reflection coefficient R as indicated below.

$$S = \sqrt{1-\rho^2}|R| \tag{4.4}$$

Equation (4.4) is obtained from the power balance between reflections and scattering, i.e., the scattering power becomes lower as the reflection power increases. The directive model is based on the assumption that the scattering lobe is steered towards the direction of the specular reflection. The electric field of the directive model $E_{S\_directive}$, is defined as

$$\left|E_{s\_directive}\right|^2 = \left(\frac{KS}{|\boldsymbol{r}_i||\boldsymbol{r}_s|}\right)^2 \frac{dS\cos\theta_i}{F_\alpha}\left(\frac{1+\cos\Psi_r}{2}\right)^\alpha \tag{4.5}$$

$$F_\alpha = \int_0^{\pi/2}\int_0^{2\pi}\left(\frac{1+\cos\Psi_r}{2}\right)^\alpha \sin\theta_s \, d\theta_s d\varphi_s \tag{4.6}$$

where F_α and α are constants defining the scattering pattern, and Ψ_r is the angle between the reflection direction and the scattering direction. Term α is related to the width of the scattering lobe width, and the greater that α becomes, the wider the scattering lobe width. Reference [22] evaluates the ER model using α =1, 2, 3, 4 as an empirical value and the evaluation results are varied in accordance with this parameter. Also, in this dissertation, α is given as an empirical value and optimized using measurement results. Figure 4-4 shows a comparison of the scattering patterns between Lambertian and directive models assuming α =1, 5, 10, 50. In calculations, R = 0.6, $\theta_r = \pi/6$, σ_h = 1 mm is set.

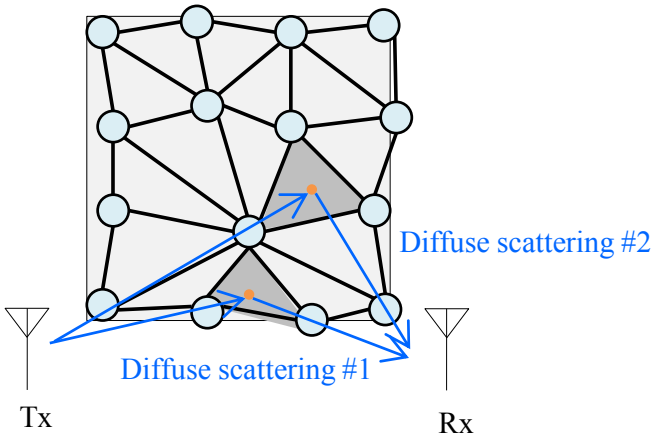

Reference:

Minoru Inomata, Tetsuro Imai, Koshiro Kitao, Yukihiko Okumura, Motoharu Sasaki, Yasushi Takatori, “Radio Propagation Prediction Method Using Point Cloud Data Based on Hybrid of Ray-Tracing and Effective Roughness Model in Urban Environments,” *IEICE Trans. on*

Communication, Vol.E102-B, No.1, pp.51-62, July. 2019.

Figure 4-2 Surface elements of scattering object

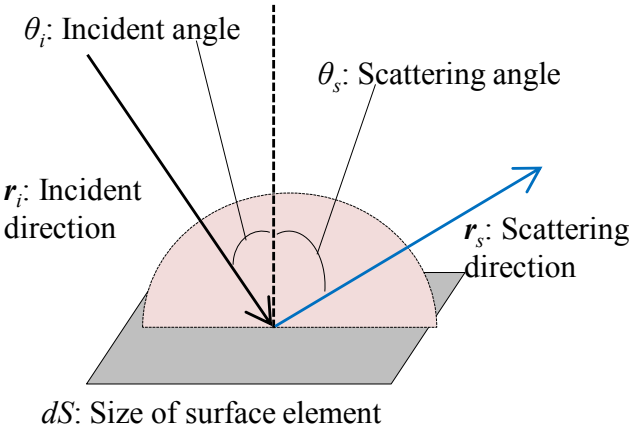

(a) Lambertian model

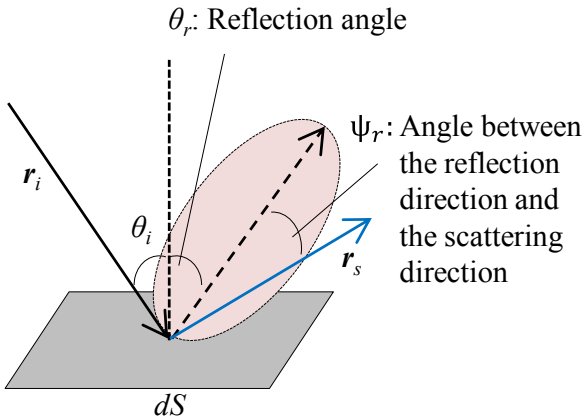

(b) Directive model

Reference:

Minoru Inomata, Tetsuro Imai, Koshiro Kitao, Yukihiko Okumura, Motoharu Sasaki, Yasushi Takatori, “Radio Propagation Prediction Method Using Point Cloud Data Based on Hybrid of Ray-Tracing and Effective Roughness Model in Urban Environments,” *IEICE Trans. on Communication*, Vol.E102-B, No.1, pp.51-62, July. 2019.

Figure 4-3 Scattering radiation lobe.

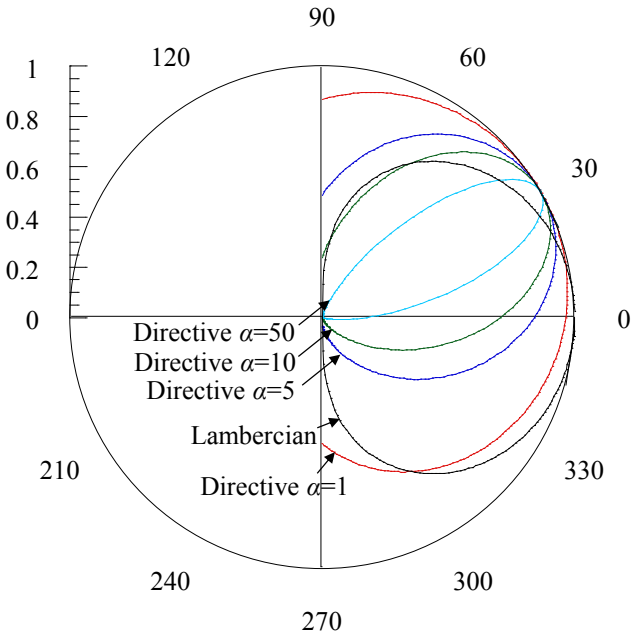

Reference:

Minoru Inomata, Tetsuro Imai, Koshiro Kitao, Yukihiko Okumura, Motoharu Sasaki, Yasushi Takatori, "Radio Propagation Prediction Method Using Point Cloud Data Based on Hybrid of Ray-Tracing and Effective Roughness Model in Urban Environments," *IEICE Trans. on Communication*, Vol.E102-B, No.1, pp.51-62, July. 2019.

Figure 4-4 Comparison of Lambercian and directive scattering patterns.

The total electric field E_{total} is the sum of electric field E_{RT} of the direct, specular reflections, and diffractions obtained through the RT method and scattered electric field E_s obtained through the Lambertian model $E_{s\_Lambertian}$ and the directive model $E_{s\_directive}$. Therefore, total electric field E_{total} is expressed as equation (4.7). Fig. 4 shows the hybrid method.

$$|E_{total}|^2 = \sum|E_{RT}|^2 + \sum|E_s|^2 \tag{4.7}$$

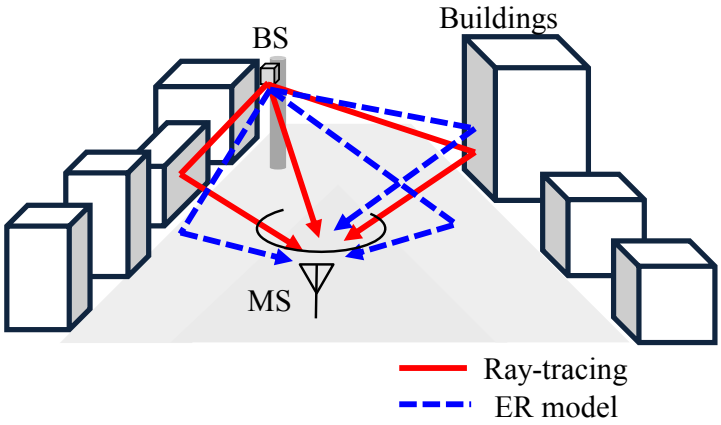

Reference:

Minoru Inomata, Tetsuro Imai, Koshiro Kitao, Yukihiko Okumura, Motoharu Sasaki, Yasushi Takatori, "Radio Propagation Prediction Method Using Point Cloud Data Based on Hybrid of Ray-Tracing and Effective Roughness Model in Urban Environments," *IEICE Trans. on Communication*, Vol.E102-B, No.1, pp.51-62, July. 2019.

Figure 4-5 Hybrid method of RT and ER model

4.2.2 Conventional Map Database

A detailed description of the urban environment is essential for evaluating the appropriate propagation channel. In urban environments, the RT method using a building model that is constructed based on a commercial map database is often employed as shown in Figure 4-6 [84]. Buildings are generated by means of a vector database that describes their exact position and size. In recent map databases, height profiles of buildings are available by extracting aerially obtained laser scanning data. However, in commercially available map databases, the structure irregularities including the shape of buildings, windows, and balconies are not considered. Therefore, even if commercial map databases are simply utilized in the hybrid method, since the influence of diffuse scattering from those irregularities is increased in higher frequency bands, propagation channel considering diffuse scattering in urban environments cannot be evaluated.

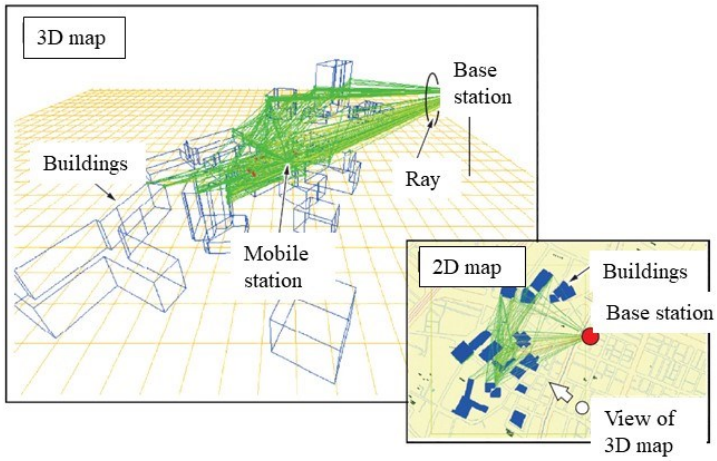

Reference:

Minoru Inomata, Tetsuro Imai, Koshiro Kitao, Yukihiko Okumura, Motoharu Sasaki, Yasushi Takatori, "Radio Propagation Prediction Method Using Point Cloud Data Based on Hybrid of Ray-Tracing and Effective Roughness Model in Urban Environments," *IEICE Trans. on Communication*, Vol.E102-B, No.1, pp.51-62, July. 2019.

Figure 4-6 RT method using conventional commercial map database

4.3 Proposed Prediction Method

In this section, to evaluate propagation channel considering the diffuse scattering, it is show that the proposed hybrid method with point cloud data.

4.3.1 Hybrid Method with Point Cloud Data

In order to predict accurately propagation channel in high frequency bands, a detailed structure model must be constructed that considers scattering objects. Therefore, a hybrid method that employs a structure model constructed based on point cloud data is proposed in urban environments for high frequency bands. Point cloud data are acquired through laser scanning, which is a widely accepted method used in recent architecture and civil engineering research to obtain detailed structure data in environments. A detailed structure model can be obtained with an accuracy of several millimeters using laser scanning.

Figure 4-7 shows the proposed method and the procedure is described as follows. First, the specular reflection and diffraction electric fields from structures constructed based on computer aided design (CAD) software or a commercial map database are calculated using the RT method as shown in Figure 4-7 (a). Reflection coefficient is represented by effective reflection coefficient R_s. Second, a detailed description of the urban environment in the form of point cloud data is acquired using laser scanning. In order to apply point cloud data to the ER model, the raw point cloud data must be converted into a structure model constructed using multiple surface elements. The point cloud data

are divided into multiple triangular surface elements with a mesh reconstruction algorithm, e.g., Delaunay triangulation. The ER model parameters are extracted from each of these surface elements. Finally, the diffuse scattered electric field is calculated using the ER model with those parameters as shown in Figure 4-7 (b). The total electric field is calculated by combining the electric field with the ER model and RT method.

Since the structure irregularities can be obtained to an accuracy of several millimeters, the proposed prediction method takes into consideration the diffuse scattering from those irregularities, specular reflection, and diffraction.

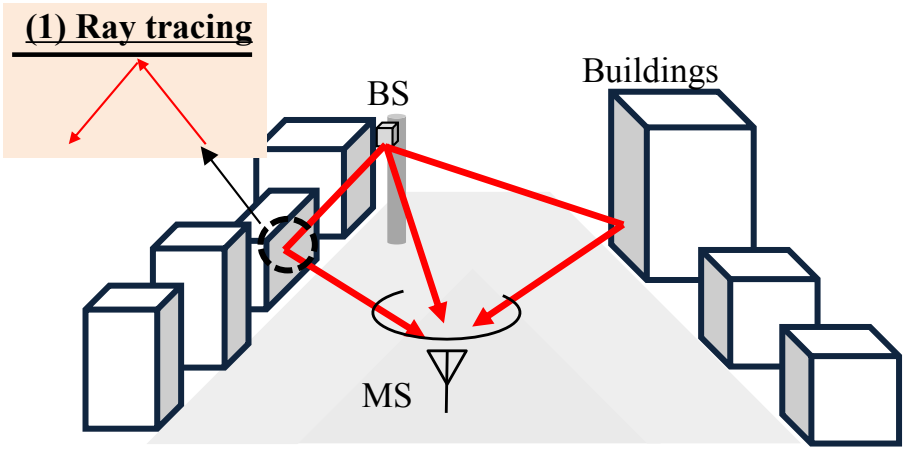

(a) RT method using commercial map database

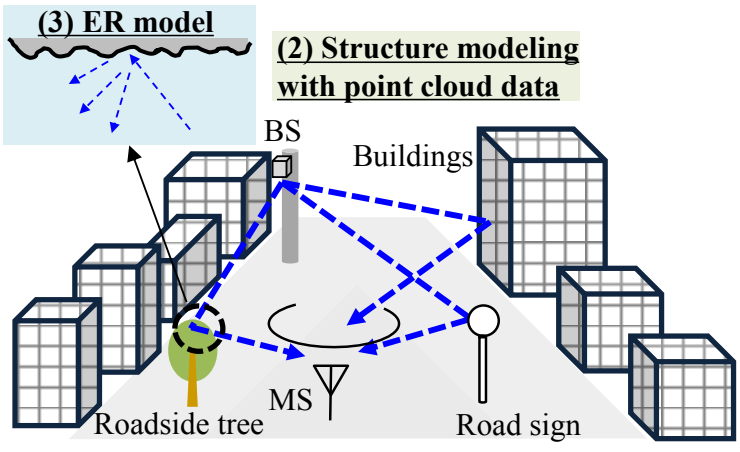

(b) ER model using point cloud data

Reference:

Minoru Inomata, Tetsuro Imai, Koshiro Kitao, Yukihiko Okumura, Motoharu Sasaki, Yasushi Takatori, “Radio Propagation Prediction Method Using Point Cloud Data Based on Hybrid of Ray-Tracing and Effective Roughness Model in Urban Environments,” *IEICE Trans. on*

Communication, Vol.E102-B, No.1, pp.51-62, July. 2019.

Figure 4-7 Proposed method

4.3.2 Structure Model Based on Point Cloud Data

Figure 4-8 shows the point cloud data of an urban environment using laser scanning. It is found that detailed structures such as building irregularities, road signs, roadside trees, and subway entrances can be acquired. If these are appropriately converted into multiple surface elements, the proposed method can calculate the diffuse scattering from these structures. However, in this paper, since the diffuse scattering from building irregularities is greater due to their larger scattering size, prediction is focused on diffuse scattering from the building irregularities.

Figure 4-9 shows a structure model constructed based on the point cloud data. It is confirmed that multiple triangular surface elements can be obtained. It is necessary to specify the size when dividing raw point cloud data into multiple surface elements. So in this paper, the size of surface elements dS to 100 cm^2 is set in equation (4.3) and (4.5). ER model parameters θ_i, θ_s, $\boldsymbol{r}_i$, $\boldsymbol{r}_s$, and Ψ_r, are extracted from each surface element. The parameter values for θ_i, θ_s, $\boldsymbol{r}_i$, $\boldsymbol{r}_s$, Ψ_r, σ_h, dS, and α are required to calculate the ER model. Angles θ_i and θ_s indicate the incident angle and scattering angle, respectively. The incident angle of the surface elements, θ_i, is the angle between the normal vector of the surface elements and the vector from the Tx position to the gravity of the surface elements. The gravity of the surface elements is calculated using the position of each vertex of the surface elements. Terms $\boldsymbol{r}_i$ and $\boldsymbol{r}_s$ indicate the vector from the Tx position to the gravity of the surface elements and from the gravity of the surface elements to the Rx position, respectively. In addition, Ψ_r indicates the difference in reflected angle θ_r and scattered angle θ_s. Reflected angle θ_r equals incident angle θ_i and is the angle between the direction of reflection and the direction of the normal vector of the surface elements. Scattered angle θ_s is the angle between the direction of scattering and the direction of the normal vector of the surface elements.

On the other hand, in the calculation of the prediction method using point cloud data, the building irregularities and the standard deviation of roughness σ_h are necessary. The accuracy of the laser scanner is approximately 2 mm, that for the standard deviation of roughness σ_h is lower at approximately 2 mm, and that for the building irregularities is greater at approximately 2 mm. The building irregularities can be obtained using point cloud data; however, the standard deviation of roughness σ_h cannot be obtained, and so σ_h is given as a parameter in this paper. In addition, [22] evaluated the ER model using α =1, 2, 3, 4 as an empirical value and the evaluation results are varied in accordance with this parameter. Therefore, α is also given as a parameter in this paper.

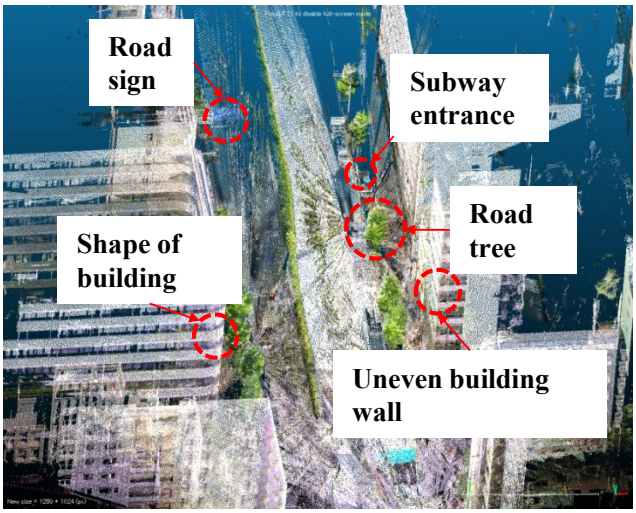

Reference:

Minoru Inomata, Tetsuro Imai, Koshiro Kitao, Yukihiko Okumura, Motoharu Sasaki, Yasushi Takatori, “Radio Propagation Prediction Method Using Point Cloud Data Based on Hybrid of Ray-Tracing and Effective Roughness Model in Urban Environments,” *IEICE Trans. on Communication*, Vol.E102-B, No.1, pp.51-62, July. 2019.

Figure 4-8 Acquisition of point cloud data.

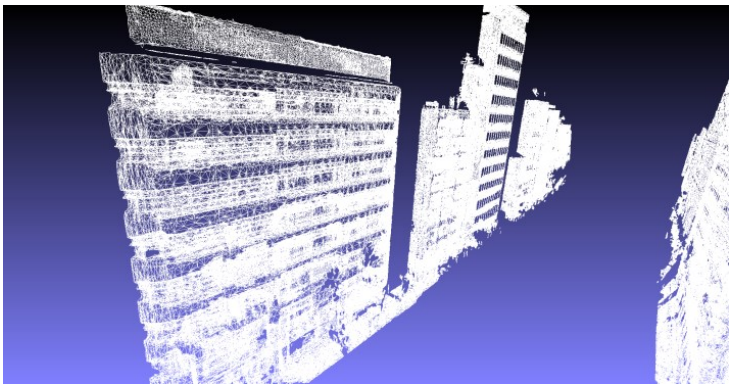

Reference:

Minoru Inomata, Tetsuro Imai, Koshiro Kitao, Yukihiko Okumura, Motoharu Sasaki, Yasushi Takatori, “Radio Propagation Prediction Method Using Point Cloud Data Based on Hybrid of Ray-Tracing and Effective Roughness Model in Urban Environments,” *IEICE Trans. on Communication*, Vol.E102-B, No.1, pp.51-62, July. 2019.

Figure 4-9 Structure model constructed based on point cloud data.

4.4 Measurement Campaign

In this section, the measurement campaign is described for the radio propagation measurement method and point cloud measurement method using laser scanning.

4.4.1 Measurement Method

This section describes the radio propagation measurement method and parameters. Figure 4-10 shows a photograph of the measurement area in Japan, around Tokyo station. Tall buildings line the road in the measurement site. Figure 4-11 shows the measurement point and Table 4-1 gives a summary of the measurement parameters. To analyze the diffuse scattering in high frequency bands, the measurement frequencies are set to the 20-GHz band. The Tx antenna is omni-directional and the Rx has channel sounders for the 20-GHz band. An OFDM signal is transmitted from the Tx antenna, which is established on the roof of a car positioned along the roadside as shown in Figure 4-10 (b) and the signal is received at the Rx using a planar array antenna. The Rx planar array antenna is affixed to a pole mounted on the car. The Tx antenna height is 2.5 m and the Rx antenna height is 5 m. The Tx and the Rx antennas are placed in the same lane of the road and the Tx antennas are fixed along the roadside. The Tx is a MS and the Rx is a BS.

For the measurements, in order to obtain data from 360 degrees in the horizontal plane, the planar array antenna records measurements in 4 directions: 0, 90, 180 and -90 degrees. The recording duration per direction is 30 s in 1 s intervals.

For data processing, the angular delay profile is obtained using the IFFT and beamforming processing in four different Rx directions. The 4 angular delay profiles are concatenated in the azimuth angle and the angular delay profile with 360 degree azimuth angle is obtained. The profile of the maximum power value of the 180 degree elevation angle for each propagation delay is extracted. Then, the power delay profile is obtained by extracting the maximum power value of the 360 degree azimuth angle for each propagation delay. The angular profile is obtained by extracting the maximum power value of the propagation delay for each azimuth angle. In order to obtain the angular profile, beamforming processing on the received signal is used. The angular profile is obtained by calculating the correlation between the measurement mode vector of the planar array antenna and the measurement data as described in [85]. In order to eliminate the effect of fading, power delay profiles recorded over the 30 s duration is averaged.

(a) View from Rx antenna

(b) Rx antenna established on the roof of a car

Reference:

Minoru Inomata, Tetsuro Imai, Koshiro Kitao, Yukihiko Okumura, Motoharu Sasaki, Yasushi Takatori, “Radio Propagation Prediction Method Using Point Cloud Data Based on Hybrid of Ray-Tracing and Effective Roughness Model in Urban Environments,” *IEICE Trans. on Communication*, Vol.E102-B, No.1, pp.51-62, July. 2019.

Figure 4-10 Measurement environment

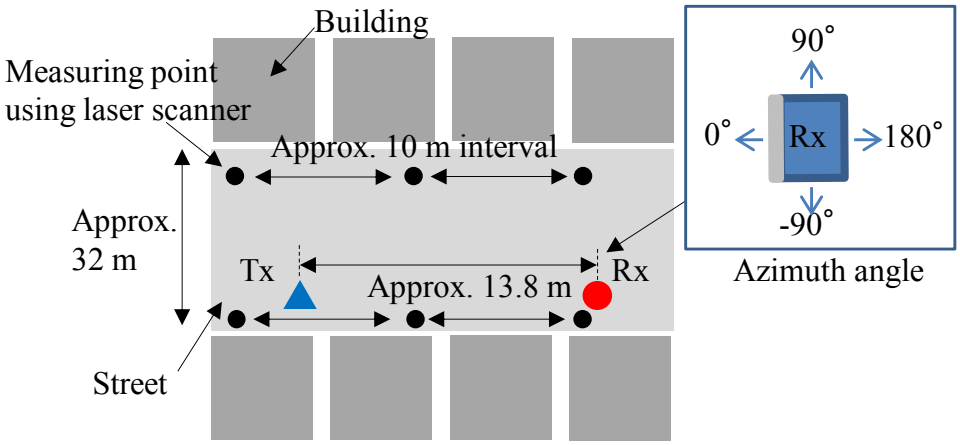

Reference:

Minoru Inomata, Tetsuro Imai, Koshiro Kitao, Yukihiko Okumura, Motoharu Sasaki, Yasushi Takatori, "Radio Propagation Prediction Method Using Point Cloud Data Based on Hybrid of Ray-Tracing and Effective Roughness Model in Urban Environments," *IEICE Trans. on Communication*, Vol.E102-B, No.1, pp.51-62, July. 2019.

Figure 4-11 Measurement point

Table 4-1 Measurement parameters

Tx	Frequency	19.85 GHz
	Signal transmission power	30 dBm
	Polarization	Vertical
	Bandwidth	50 MHz
	Modulation	OFDM
	Antenna	Sleeve antenna
	Antenna height	2.5 m
Rx	Antenna	Planar array antenna (256 elements)
	Polarization	Vertical
	Antenna height	5 m

4.4.2 Acquisition of Point Cloud Data

Figure 4-12 shows a photograph from the laser scanner and Table 4-2 gives the laser scanner specifications. The structure model is obtained using a FARO Laser scanner Focus 3D X330 [86], which emits a laser beam at the wavelength of 1550 nm in different directions, and the model identifies bouncing points with the precision of approximately 2 mm to build a point cloud. The maximum scanning area is 330 m. The laser scanner is established on the roof of a car positioned along the roadside as shown in Figure 4-12. For the measurements, point cloud data in 360 degrees in the horizontal plane were obtained. The density of the point cloud was non-uniform because of

spherical scanning. Therefore, laser scanning at multiple positions is performed in the measurement environment as shown in Figure 4-11. We acquired the point cloud data at 10 m intervals in the same and opposite lanes in the road from the Rx antenna. Point cloud data is combined to obtain accurate building irregularities.

Reference:

Minoru Inomata, Tetsuro Imai, Koshiro Kitao, Yukihiko Okumura, Motoharu Sasaki, Yasushi Takatori, “Radio Propagation Prediction Method Using Point Cloud Data Based on Hybrid of Ray-Tracing and Effective Roughness Model in Urban Environments,” *IEICE Trans. on Communication*, Vol.E102-B, No.1, pp.51-62, July. 2019.

Figure 4-12 View from laser scanner

Table 4-2 Laser scanner specifications

Laser scanner	FARO Laser scanner Focus 3D X330
Scanning area	Maximum 330 m
Accuracy	2 mm

4.5 Performance of Proposed Prediction Method

In this section, it is verified the performance of the proposed prediction method. Since the proposed prediction method is implemented based on the RT method, ER model, and point cloud data, improvement is evaluated from the prediction method using the RT method as a reference. Furthermore, the derived appropriate parameters for the proposed method are described.

4.5.1 Measurement Results

Figure 4-13 shows the power angular-delay profile of the measurement results. In Figure 4-13, the azimuth angle in the direction of the MS at 0 degrees is represented on the horizontal axis and the

delay distance is represented on the vertical axis. In addition, the power of each azimuth angle is obtained by extracting the maximum value of the elevation angle direction. From Figure 4-13, it is confirmed the arrival direction of the direct ray, 1 bounce reflection, and 2 bounce reflection. The 2 bounce reflection represents the propagation path that is first reflected from the building opposite the Rx antenna, reflected from the building on the same side as the Rx antenna, and then arrives at the Rx antenna. It is also found that the diffuse scattering spreads radially from both the 1 and 2 bounce reflection points. These waves are scattered due to the building irregularities and small scattering objects such as roadside trees and road signs. Therefore, in order to clarify the influence of diffuse scattering, measurement results are compared with the prediction results using the RT method.

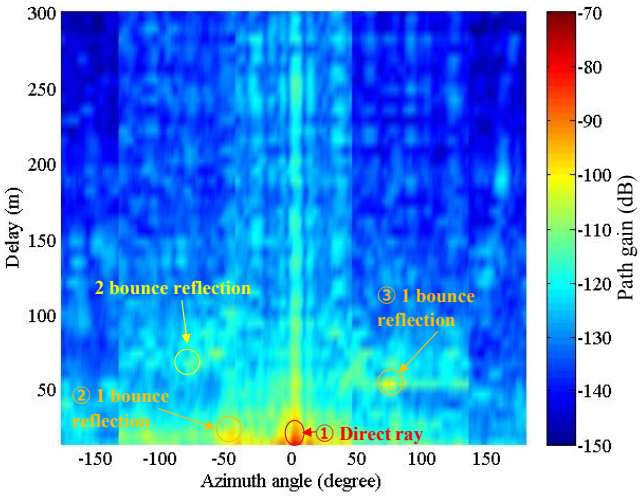

Reference:

Minoru Inomata, Tetsuro Imai, Koshiro Kitao, Yukihiko Okumura, Motoharu Sasaki, Yasushi Takatori, “Radio Propagation Prediction Method Using Point Cloud Data Based on Hybrid of Ray-Tracing and Effective Roughness Model in Urban Environments,” *IEICE Trans. on Communication*, Vol.E102-B, No.1, pp.51-62, July. 2019.

Figure 4-13 Measurement power angular-delay profile

4.5.2 Prediction of Specular Reflection and Diffraction with RT Method

In order to verify the influence of diffuse scattering, the prediction results using the RT method and measurement results are compared based on the angular-delay profiles. Table 4-3 gives the simulation parameters for the RT method. Figure 4-14 shows the power angular-delay profile predicted using the RT method. In the RT method, direct ray, 1 bounce reflection, 2 bounce reflection, and 1 diffraction waves are calculated using buildings constructed based on CAD software. Those

building surfaces are constructed using multiple smooth surfaces. From Figure 4-14, it is confirmed the direction that the direct wave, 1 bounce, and 2 bounce reflections arrive. Since the path gain of the diffraction is relatively low, i.e., below -150 dB, diffraction is not depicted. However, Figure 4-14 shows that since the RT method does not consider the diffuse scattering that can be observed in the measurement results, the number of incoming waves is underestimated. As described in Subsections 4.5.1 and 4.5.2, the analysis results clarify that the power of the diffuse scattering from scattering objects is relatively strong and affect the propagation characteristics. Therefore, diffuse scattering need to be taken into account.

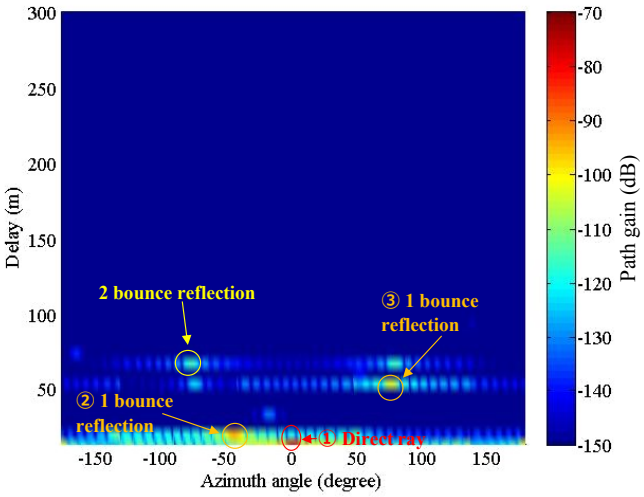

Reference:

Minoru Inomata, Tetsuro Imai, Koshiro Kitao, Yukihiko Okumura, Motoharu Sasaki, Yasushi Takatori, "Radio Propagation Prediction Method Using Point Cloud Data Based on Hybrid of Ray-Tracing and Effective Roughness Model in Urban Environments," *IEICE Trans. on Communication*, Vol.E102-B, No.1, pp.51-62, July. 2019.

Figure 4-14 Power angular-delay profile predicted using RT method

Table 4-3 Simulation parameters in RT method

Building material	Concrete
Relative permittivity	6.76
Conductivity	0.0023 S/m
Maximum number of reflection/diffraction	2/1

4.5.3 Diffuse Scattering Prediction with ER Model

Figure 4-15 shows the prediction results when using only the ER model. Table 4-4 gives the simulation parameters for the ER model. The roughness value, σ_h, is set to 0.5 mm and the diffuse

scattering calculations using the ER model consider one-time scattering. In the figure, diffuse scattering power from each surface element using the ER model is mapped on to the point cloud. The figure shows that relatively strong diffuse scattering from the buildings arrives near the Rx antenna. It is also found that the scattering spreads radially from the 1 bounce reflection point. The diffuse scattering that is obtained with the ER model is summed with predictions using the RT method.

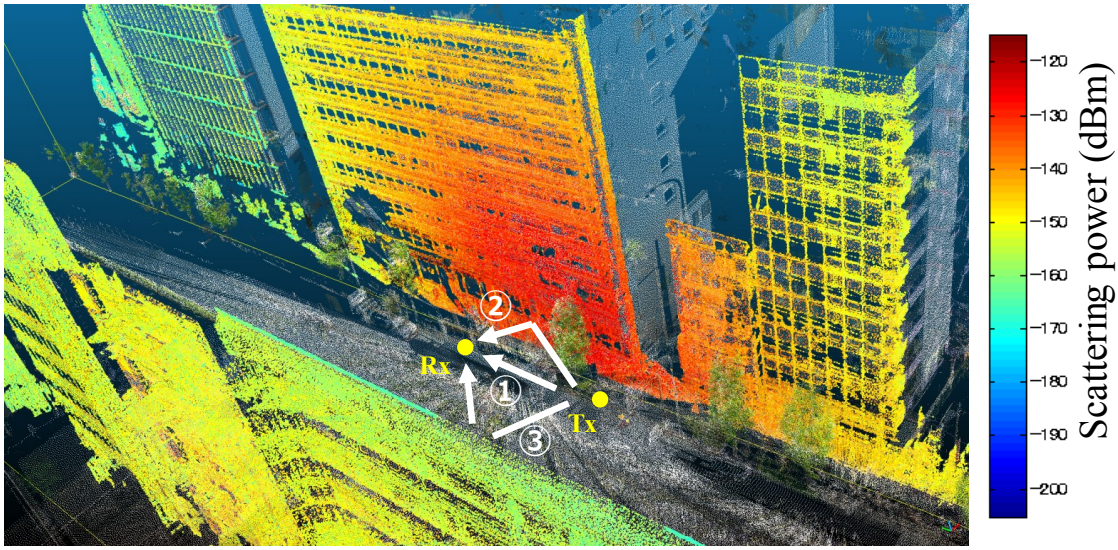

①：Direct ray
②③：1 bounce reflection from the wall using RT method

Reference:
Minoru Inomata, Tetsuro Imai, Koshiro Kitao, Yukihiko Okumura, Motoharu Sasaki, Yasushi Takatori, “Radio Propagation Prediction Method Using Point Cloud Data Based on Hybrid of Ray-Tracing and Effective Roughness Model in Urban Environments,” *IEICE Trans. on Communication*, Vol.E102-B, No.1, pp.51-62, July. 2019.

Figure 4-15 The received power from the wall is mapped to the scattered points of the wall

Table 4-4 Simulation parameters in ER model

The size of surface elements dS	100 cm^2
Scattering lobe width α	1, 5, 10, 50
Surface roughness σ_h	0.5, 1, 5 mm

4.5.4 Comparison between Proposed Method and Measurements

Verification results based on the power angular-delay profile by comparing measurements and prediction results using the proposed method are described. To clarify the validity of the proposed

method, measurements are compared with prediction results using the proposed method and RT method. In the calculations for the proposed method, total electric field E_{total} is obtained by adding electric field Es of the diffuse scattering to electric field E_{RT} with the RT method. In the proposed prediction method, roughness σ_h and α are given as parameters and these values are varied as σ_h = 0.5 mm, 1 mm, 5 mm and α = 1, 5, 10, 50. Moreover, prediction results are calculated using both scattering radiation patterns of the Lambertian and directive models.

Figure 4-16 (a) and (b) show the power angular-delay profile predicted using the proposed method. In Figure 4-16 (a), the scattering radiation pattern is obtained using the directive model, while in Figure 4-16 (b) the pattern is obtained using the Lambertian model. Figure 4-16 shows the effect of the power of diffuse scattering around the 1 bounce reflection. From Figure 4-16, it is confirmed that scattering is radially dispersed in a U shape from the 1 bounce reflection point and it is found the scattering in Figure 4-13.Therefore, regarding the scattering from building irregularities, the tendencies found in Figure 4-13 and Figure 4-16 are similar. However, from Figure 4-13, it is found other scattering around the 1 bounce reflection point and it is assume that scattering from trees, road signs, and vehicles. However, further experiments and verification are required to identify the scattering from the trees, road signs, and vehicles and these will be subjects for future work to improve the accuracy of the prediction method.

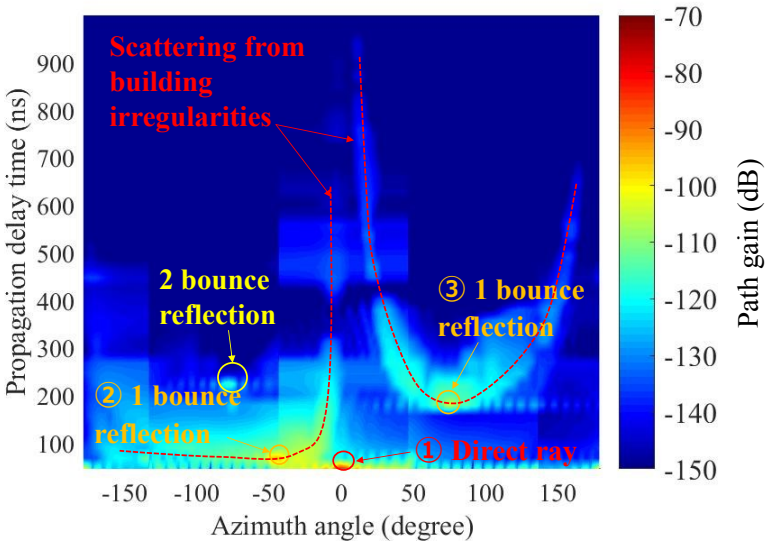

(a) Prediction using power angular-delay profile
(scattering radiation pattern is obtained by directive model, α is set to 5 and σ_h is set to 1 mm)

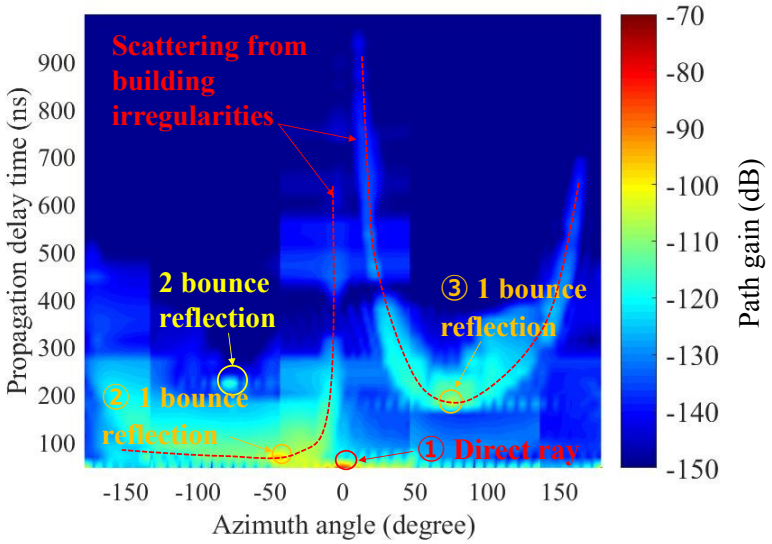

(b) Prediction using power angular-delay profile
(scattering radiation pattern is obtained by Lambertian model)

Reference:

Minoru Inomata, Tetsuro Imai, Koshiro Kitao, Yukihiko Okumura, Motoharu Sasaki, Yasushi Takatori, "Radio Propagation Prediction Method Using Point Cloud Data Based on Hybrid of Ray-Tracing and Effective Roughness Model in Urban Environments," *IEICE Trans. on Communication*, Vol.E102-B, No.1, pp.51-62, July. 2019.

Figure 4-16 Prediction results based on power angular-delay profile

Figure 4-17 shows a comparison of the power delay profiles. Under the same conditions as the measurements, the predictions were made using a bandwidth limited to 50 MHz. In addition, in order to eliminate the spuriousness of the OFDM signal, the azimuth angle data within -10 to 10 degrees are not used. The power delay profile is obtained by extracting the maximum power value of the 360 degree azimuth angle for each delay distance. In Figure 4-17, markers 1, 2, and 3 indicate the direct ray, reflected rays from the building wall near the Rx antenna, and reflected rays from the building wall far from the Rx antenna, respectively. As Figure 4-17 (a) and (b) shows, as roughness σ_h increases, the power of the reflected waves from the building wall decreases, while the power except for the reflections indicated by markers 2 and 3 are increased. This is because effective reflection coefficient R_s and scattering coefficient S are in a trade-off relationship. The prediction results for the proposed method exhibit a similar tendency as the measurement results than those for the RT method. The prediction results using σ_h = 1 mm for the proposed prediction method are the most similar to the measurement results when the roughness value is varied as σ_h = 0.5, 1, 5 mm. Figure 4-17 (c) shows the results set to σ_h = 1 mm and α = 1, 5, 10, 50. The scattering power from 80 ns to 180 ns becomes larger as α is larger. Based on the difference between the prediction and measurements, it is

confirmed that when $\alpha = 5$, the results are in the best agreement with measurement results. Therefore, in evaluating the power delay profile, it is found that the directive model assuming $\sigma_h = 1$ mm and $\alpha = 5$ is relatively similar to that for the measurements.

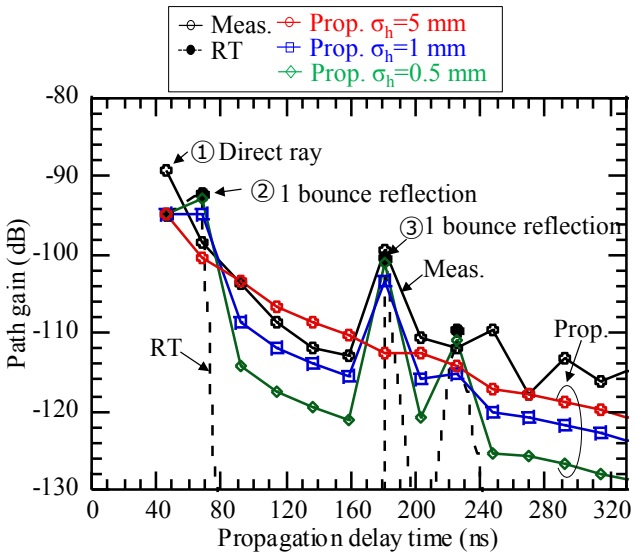

(a) Prediction using power delay profile
(scattering radiation pattern is obtained by directive model, α is set to 1)

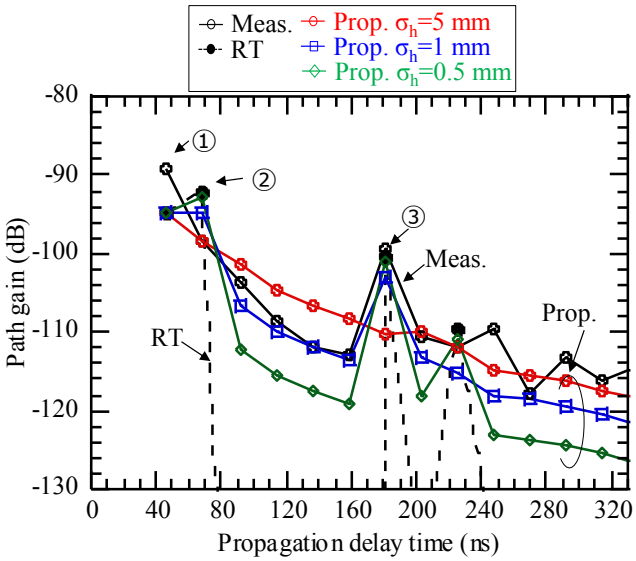

(b) Prediction using power delay profile
(scattering radiation pattern is obtained by Lambertian model)

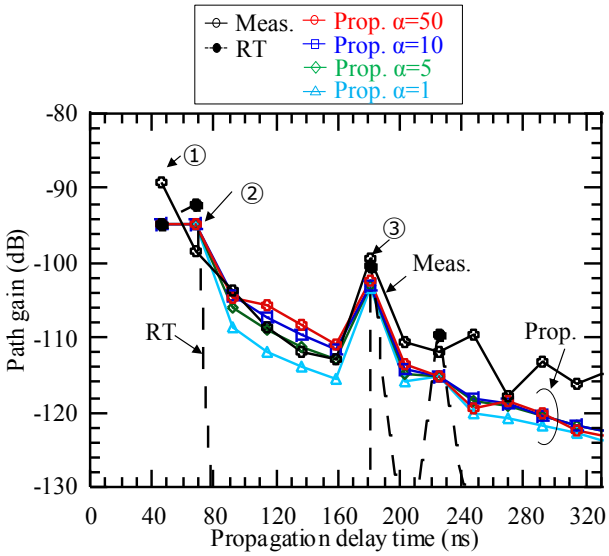

(c) Prediction using power delay profile

(scattering radiation pattern is obtained by directive model, σ_h is set to 1 mm)

Reference:

Minoru Inomata, Tetsuro Imai, Koshiro Kitao, Yukihiko Okumura, Motoharu Sasaki, Yasushi Takatori, "Radio Propagation Prediction Method Using Point Cloud Data Based on Hybrid of Ray-Tracing and Effective Roughness Model in Urban Environments," *IEICE Trans. on Communication*, Vol.E102-B, No.1, pp.51-62, July. 2019.

Figure 4-17 Comparison results based on power delay profile

For verification of the delay spread given in Table 4-5, it is showed that the prediction error of the delay spread using the proposed method is smaller than that using the RT method. The delay profile of 20 dB lower than the peak of the path gain is extracted and the delay spread is obtained by calculating the standard deviation of the propagation delay time weighted by the path gain. The difference between the prediction results using the proposed method and the measurements is from 2.1 ns to 9.7 ns. On the other hand, the difference for the RT method is 9.8 ns. The difference using the proposed method is the smallest when roughness value σ_h is set to 5 mm and α is set to 1; however, the prediction results with the roughness value set to 5 mm and α = 1 underestimated the reflection power at marker 3 by approximately 13 dB and underestimated total path gain by approximately 5 dB compared to measurements. On the other hand, the prediction results with the roughness value set to 1 mm and α = 1 underestimated the reflection power at marker 3 by approximately 3 dB and underestimated total path gain by approximately 3.6 dB. Therefore, it is confirmed that prediction results assuming the roughness value of σ_h = 1 mm is similar to measurements. In addition, when σ_h = 1 mm and α = 1, 5, 10, 50, the difference between prediction of α = 50 and measurement is lower. However, based on the difference of the path gain of each

propagation delay time between prediction and measurement, it is confirmed that prediction result with $\alpha = 5$ is relatively similar to measurement than that with $\alpha = 50$. Moreover, it is found that the variable range of the delay spread when varying roughness σ_h is greater than when varying α. This indicates that roughness σ_h is a dominant parameter compared to α. Although it is confirmed the tendency when changing the parameters σ_h and α by these evaluations, verification of setting optimum value in various environments is a future work.

Table 4-5 Comparison based on delay spread

	Roughness	α	Delay spread
Meas.			48.0 ns
RT method			38.2 ns
Prop. (directive model)	0.5 mm	1	38.3 ns
	1.0 mm	1	39.2 ns
	5.0 mm	1	43.8 ns
Prop. (directive model)	1.0 mm	5	40.0 ns
	1.0 mm	10	40.5 ns
	1.0 mm	50	42.1 ns
Prop. (Lambertian model)	0.5 mm	1	38.6 ns
	1.0 mm	1	40.5 ns
	5.0 mm	1	45.9 ns

Figure 4-18 shows comparison delay profiles between proposed method and hybrid method with smooth surface based on the prediction method as shown in [75]. In calculation of hybrid method with smooth surface, the building model constructed by smooth surface is divided to the surface elements. Then, the ER model is applied to the scattering calculation from surface elements. The result is set to Lambertian model, $\sigma_h = 1$ mm, and $dS = 400$ cm^2, because variation of the size does not affect the scattering characteristics in smooth surface. From this result, it is found that the received power of the scattering using proposed method is higher than hybrid method with smooth surface. This is because the proposed method considers the building irregularities acquired by point cloud. Also, it is clarified that the prediction results with proposed method is similar tendency to the measurement results. The RMSE values of each delay tap is 3.8 dB with proposed method, 6.3 dB with smooth surface. Therefore, in 5G cell deployment, it is better to use the point cloud than smooth surface.

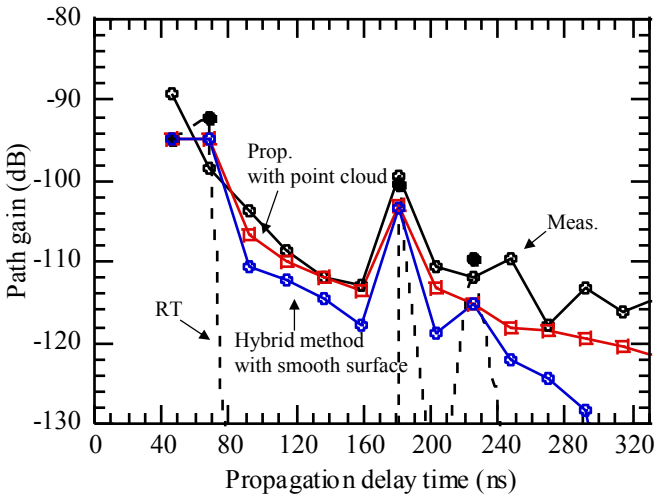

Figure 4-18 Comparison results between predictions using hybrid method with point cloud and with smooth surface

Figure 4-19 shows comparison results based on the angular profile. In order to obtain the angular profile under the same conditions as the measurements, prediction results are calculated by beamforming processing. The angular profile is obtained by extracting the maximum power value of the delay distance for each azimuth angle. From Figure 4-19 (b) and (c), when the roughness value is varied from 0.5 mm, 1 mm, 5 mm and α = 1, the prediction results with the roughness value set to 1 mm exhibit the best agreement with the measurement results. In particular, at markers 2 and 3, both of which are 1 bounce reflections, the error of the reflection power is 5.4 dB at marker 2, 1.2 dB at marker 3 for a roughness value of 0.5 mm, 3.3 dB at marker 2, 3.1 dB at marker 3 for the roughness of 1 mm, and 5.4 dB at marker 2, 10 dB at marker 3 for the roughness of 5 mm. In addition, we confirm that the characteristics are similar between the Lambertian and directive models in terms of the angular profiles. It is assumed that similar characteristics are obtained due to the randomness of the direction of the multiple surface elements. Figure 5-4 shows the scattering pattern when using the directive model assuming α = 1, 5, 10, 50 and when the Lambertian model is used. When there is no randomness in the direction of the multiple surface elements, it is assumed that the difference in the scattering patterns between the Lambertian and directive models affects the characteristics. However, in this paper, it is confirmed that the characteristics are similar between the Lambertian and directive models. Therefore, because the direction of the multiple surface elements is relatively random, the characteristics of the directive model become similar to those of the Lambertian model. As shown in Figure 4-19 (a) and (b), the prediction error when using the proposed prediction method is lower than when using the RT method. This approximately 6 dB improvement in the directions from -90 to -60 degrees is due to considering the scattering from building irregularities in the proposed prediction method. In addition, based on Figure 4-19 (b) and (d), when α = 1, 5, 10, 50 and σ_h = 1 mm, the prediction results exhibit similar characteristics to the measurement results. It is confirmed

that roughness σ_h = 1 mm is an appropriate value to predict the power angular profile.

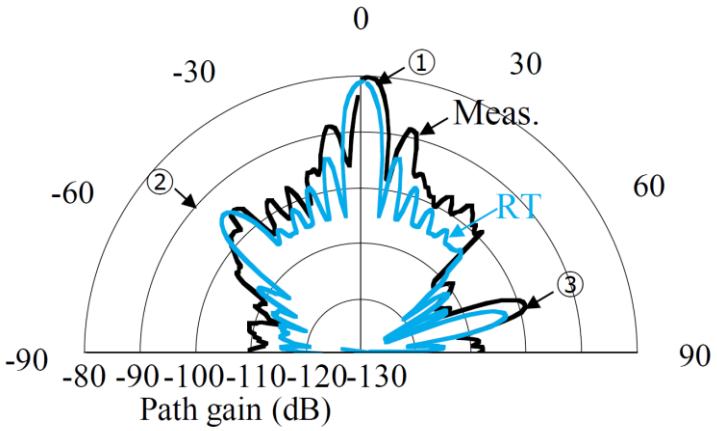

(a) Prediction angular profile using RT

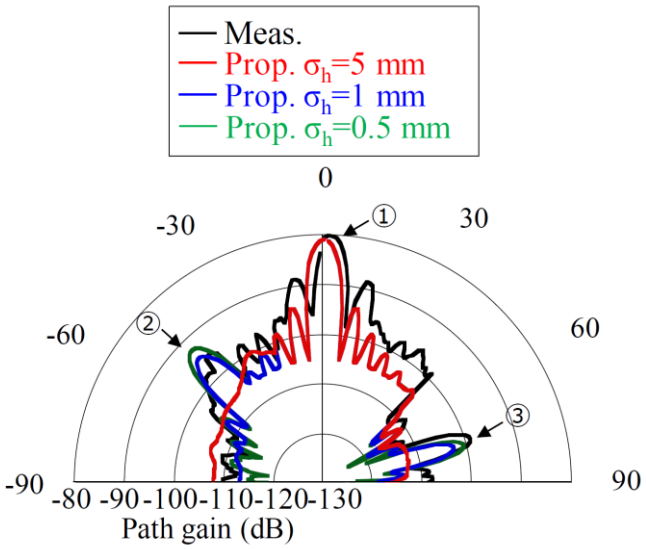

(b) Prediction angular profile using directive model.(α is set to 1)

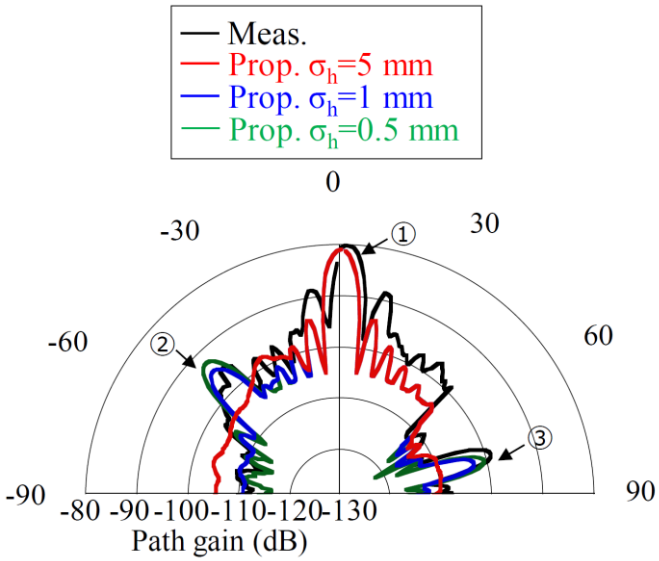

(c) Prediction angular profile using Lambertian model

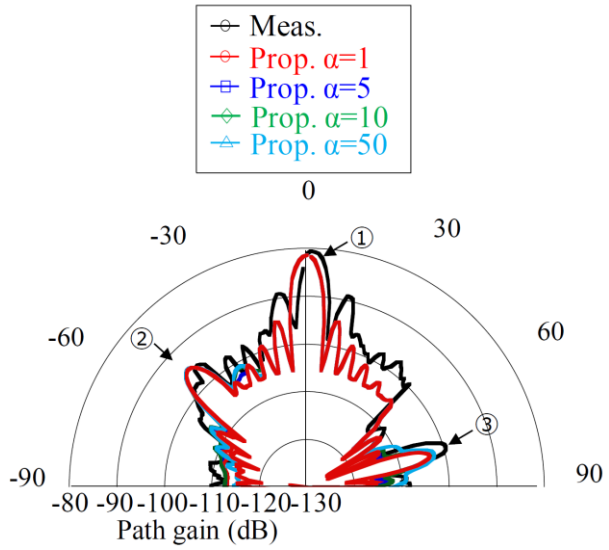

(d) Prediction angular profile using Lambertian model

Reference:

Minoru Inomata, Tetsuro Imai, Koshiro Kitao, Yukihiko Okumura, Motoharu Sasaki, Yasushi Takatori, “Radio Propagation Prediction Method Using Point Cloud Data Based on Hybrid of Ray-Tracing and Effective Roughness Model in Urban Environments,” *IEICE Trans. on Communication*, Vol.E102-B, No.1, pp.51-62, July. 2019.

Figure 4-19 Comparison results based on angular profile

As mentioned in this section, by comparing measurement results with the prediction results using

the RT and proposed method, it is found the following. First, it is found that the prediction of the power delay and angular profiles show good agreement for roughness σ_h = 1 mm and α = 5. These results show that the proposed method accurately predicts propagation channel considering the diffuse scattering from the building irregularities for high frequency bands in UMi environments. Second, these results considering the diffuse scattering from building irregularities yield accurate predictions. This means that the diffuse scattering from building irregularities is dominant in UMi LOS environments. This is because the scattering size of buildings is larger than that of small scattering objects on roads such as roadside trees and road signs.

4.6 Summary of Chapter 4

In this section, in order to the construct channel predictions based on the scattering form building irregularities in UMi LOS environment for high frequency bands. Propagation channel prediction method that uses point cloud data based on a hybrid of the RT method and the ER model is proposed. The validity of the proposed method was confirmed based on comparison of measurement results and prediction results using the proposed method based on the power delay profile and angular profile. From predictions with the power delay and angular profile, it is found that the predictions using proposed prediction method assuming the roughness of σ_h = 1 mm and α = 5 in directive model and the roughness of σ_h = 1 mm Lambercian model yield a similar tendency to the measurement propagation channel in the 20 GHz band for UMi environments. The prediction error of the delay spread is approximately 2.1 ns to 9.7 ns in an UMi environment.

In this chapter, although channel prediction which consider the scattering from building irregularities based on point cloud is constructed, several millions scattering paths is calculated and the computation complexity is considerably high which it takes about several days using graphics processing unit. Therefore, in terms of implement, construction of a high-speed algorithm is a future work.

Chapeter 5.

Predictions of Dynamic Channel Characteristics due to Vehicles

5.1 Introduction

Chapter 5 shows the effect of the scattering from the vehicle on the site-specific propagation channel in UMi NLOS environment for high frequency band. In 5G, a massive MIMO technique using a large number of antenna elements is being investigated to compensate for the large propagation loss in high frequency bands, and the application of beamforming is being considered to obtain a higher antenna gain. Therefore, in order to evaluate these techniques, it is necessary to clarify dynamic channel properties based on the effect of vehicle around the MS in a NLOS urban environment. METIS [12] and mmMAGIC [20] [83] construct scattering model which represents the scattering from randomly placed small objects. However, it is not clear how scattering from vehicles affect the dynamic channel characteristic in actual environment and the validity have not been enough investigated. Therefore, the dynamic channel characteristics are investigated based on scattering from vehicles in high frequency band in UMi NLOS environment and clarify the dominant paths based on the measured power delay angular profile using a 20-GHz band channel sounder. Also, proposed propagation channel prediction method is described based on the scattering from the specific vehicle model in actual UMi NLOS environment.

5.2 Measurement Campaign

Figure 5-1 is a photograph of the measurement area in Japan, around Tokyo station. Figure 5-2 shows the measurement point. To analyze diffuse scattering in high frequency bands, the measurement frequencies are set to the 19.85 GHz band. Tx antenna is an omni-directional antenna and the Rx antenna is a planar array antenna that has 256 elements. An OFDM signal is transmitted from the Tx antenna, which is established on the roof of a vehicle positioned along the roadside. The Rx antenna is affixed to a pole mounted on the car. The Tx antenna height is 2.5 m and the Rx antenna height is 5 m. The Tx antenna and the Rx antenna is placed as shown in Figure 5-2. The Tx signal power is 30 dBm and the bandwidth is 50 MHz. For the measurements, in order to obtain data from 360 degrees in the horizontal plane, the planar array antenna records measurements in 3 directions: 0, 90 and -90 degrees. For data processing, the angular delay profile is obtained using the IFFT and beamforming processing in three different Rx directions. The three angular delay profiles are concatenated based on the azimuth angle. The profile of the maximum power value of the 180-degree elevation angle for each propagation delay is extracted. Then, the power delay profile is obtained by extracting the maximum power value of the azimuth angle for each propagation delay. The angular profile is obtained by extracting the maximum power value of the propagation delay for each azimuth angle. In order to obtain the angular profile, beamforming processing on the received signal is used. The recording duration per direction is 30 s and 15 snapshots of the power angular delay profiles are obtained.

Figure 5-1 Photo from Rx antenna

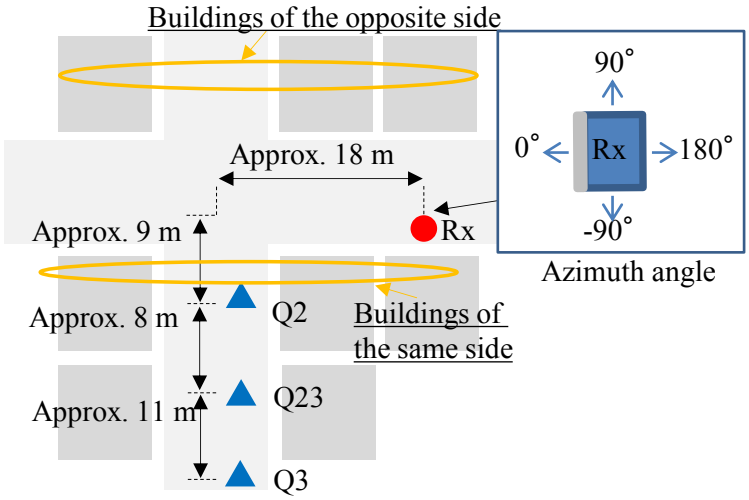

Reference:

Minoru Inomata, Tetsuro Imai, Koshiro Kitao, Yukihiko Okumura, "Dynamic Channel Properties Based on Diffuse Scattering from Vehicles for High Frequency Bands in NLOS Urban Environments," *IEICE Communications Express*, Vol. 7, No. 12, pp.438-443, Dec. 2018.

Figure 5-2 Measurement point

5.3 Investigation of Dynamic Channel Characteristics for NLOS Environment

In order to evaluate the dynamic channel properties based on diffuse scattering from the moving objects, the 15 snapshots of the power angular delay profiles are compared with analyzed the time fading characteristics. Figure 5-3 shows the measurement power delay profile. In the figure, all 15 snapshots of the power delay profiles are represented. From Figure 5-3, it is confirmed that (1) 1-bounce reflection and then the diffraction at the building in the same lane as the Rx antenna, (2) the diffraction and then 1-bounce reflection at the building in the opposite lane, and (3) the 2-bounce reflections. The 2-bounce reflections represent a propagation path that is first reflected from the building opposite the Rx antenna, reflected from the building on the same side as the Rx antenna, and then arrives at the Rx antenna. It is found that the time fading of paths (1), (2), and (3) is relatively stable; however, the fading of the paths at the propagation distance of 34 m for Q2, 47 m for Q23 and 60 m for Q3 is relatively greater. The fading of paths (1), (2) and (3) is approximately 3 dB. On the other hand, the fading of the scattering paths between (1) and (2) is approximately 7 dB for each measurement points. Since these scattering paths are between the path (1) and (2), and the scattering paths fade in accordance with the time variation, it is assumed that these scattering paths occur from vehicles on the road.

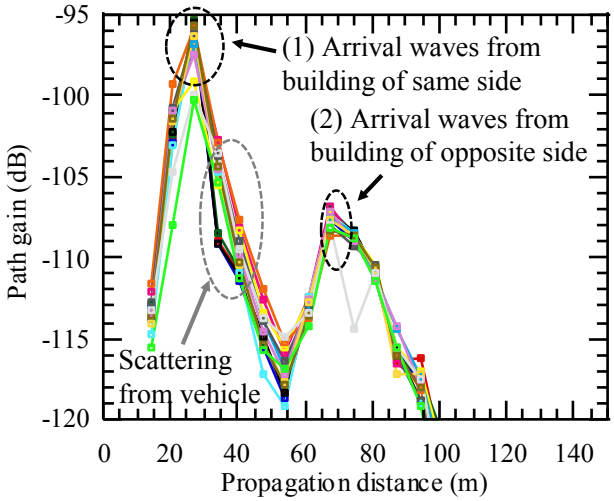
-95
-100
-105
-110
-115
-120
Path gain (dB)
0
20
40
60
80
100
120
140
Propagation distance (m)
(1) Arrival waves from building of same side
(2) Arrival waves from building of opposite side
Scattering from vehicle

(a) Q2

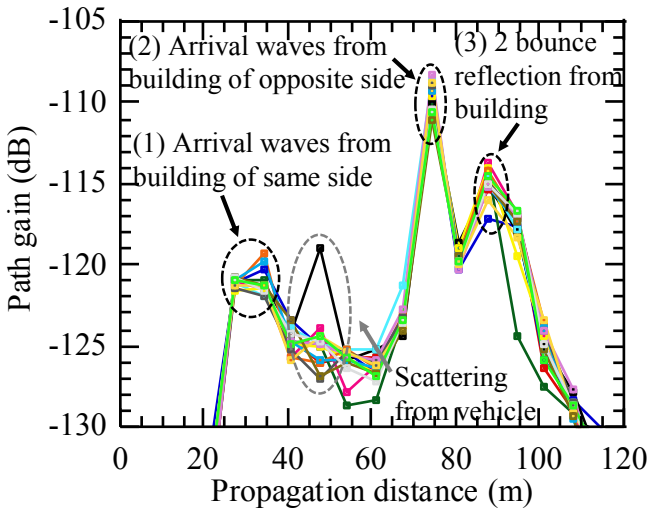
-105
-110
-115
-120
-125
-130
Path gain (dB)
0
20
40
60
80
100
120
Propagation distance (m)
(2) Arrival waves from building of opposite side
(3) 2 bounce reflection from building
(1) Arrival waves from building of same side
Scattering from vehicle

(b) Q23

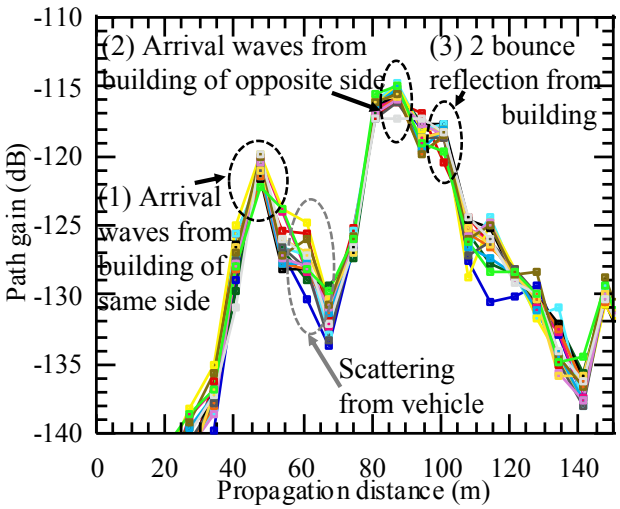

(d) Q3

Reference:

Minoru Inomata, Tetsuro Imai, Koshiro Kitao, Yukihiko Okumura, “Dynamic Channel Properties Based on Diffuse Scattering from Vehicles for High Frequency Bands in NLOS Urban Environments,” *IEICE Communications Express*, Vol. 7, No. 12, pp.438-443, Dec. 2018.

Figure 5-3 Measurement power delay profiles

In order to analyze the arrival angle of the scattering paths from vehicles, the angular profiles are analyzed. Figure 5-4 shows the angular profiles. The angular profiles at the propagation distance of 34 m for Q2, 47 m for Q23 and 60 m for Q3 are extracted and 15 snapshots of the angular profiles are shown. From Figure 6-4, it is confirmed that the scattering paths from vehicles arrive from the direction of -50 degrees. This indicates that based on the propagation distance of the scattering paths from the vehicles and the arrival angle, the scattering paths from the vehicles are first reflected from the buildings around the Tx antenna, scattered from the vehicle, reflected from the building on the same side as the Rx antenna, and arrive at the Rx antenna.

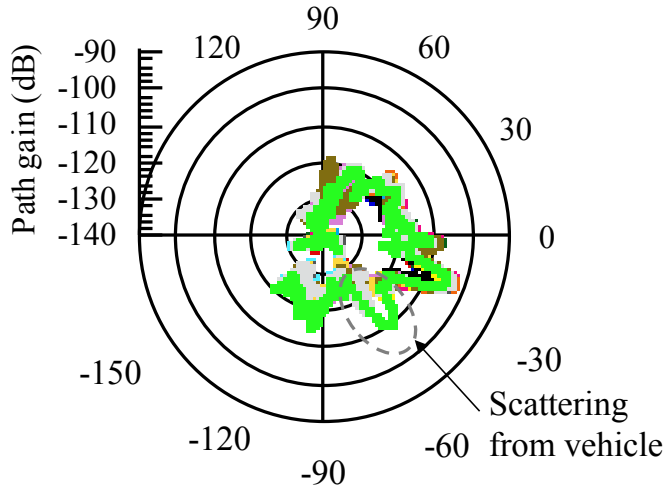
90
120
60
30
0
-30
-60
-90
-120
-150
-90
-100
-110
-120
-130
-140
Path gain (dB)
Scattering
from vehicle

(a) Q2

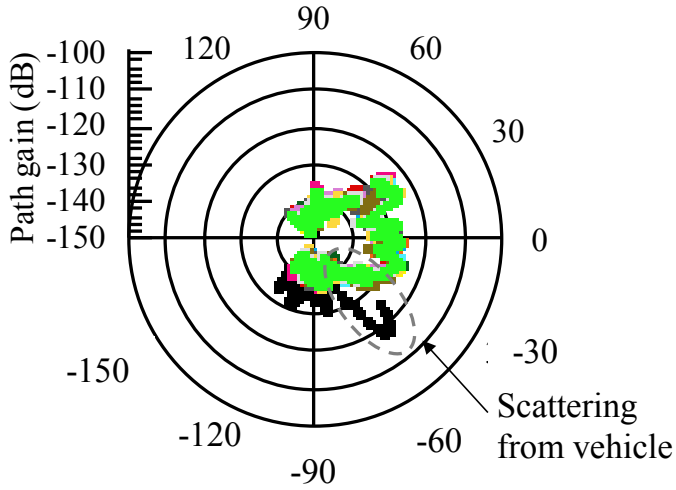
90
120
60
30
0
-30
-60
-90
-120
-150
-100
-110
-120
-130
-140
-150
Path gain (dB)
Scattering
from vehicle

(b) Q23

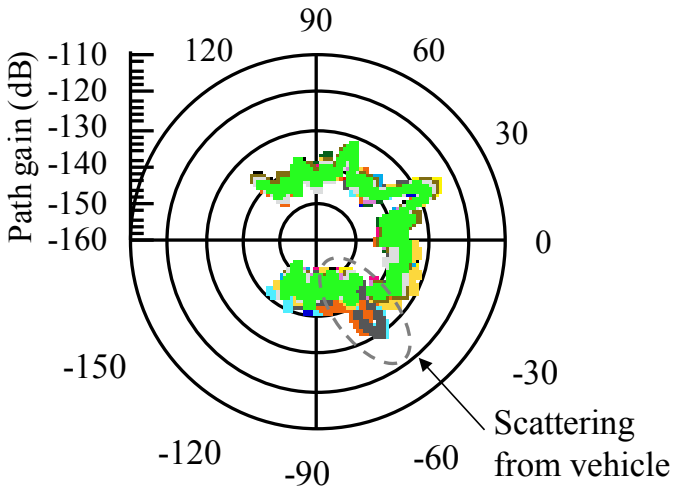

(c) Q3

Reference:

Minoru Inomata, Tetsuro Imai, Koshiro Kitao, Yukihiko Okumura, "Dynamic Channel Properties Based on Diffuse Scattering from Vehicles for High Frequency Bands in NLOS Urban Environments," *IEICE Communications Express*, Vol. 7, No. 12, pp.438-443, Dec. 2018.

Figure 5-4 Measurement angular profiles

In order to obtain the time fading characteristics, Figure 5-5 and Figure 5-6 show the power angular delay profiles at 2 different snapshots, 3 and 4, that are obtained over a 2 s measurement duration, at Q23. At the propagation distance of 47 m and the arrival angle of -50 degrees, it is found that the scattering paths from the vehicles are born and die between each snapshot.

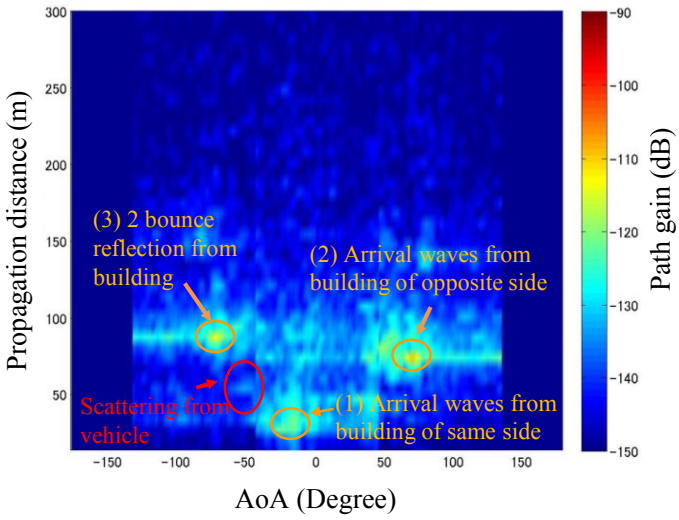

Reference:

Minoru Inomata, Tetsuro Imai, Koshiro Kitao, Yukihiko Okumura, "Dynamic Channel

Properties Based on Diffuse Scattering from Vehicles for High Frequency Bands in NLOS Urban Environments," *IEICE Communications Express*, Vol. 7, No. 12, pp.438-443, Dec. 2018.

Figure 5-5 Power angular delay profile at snapshot 3

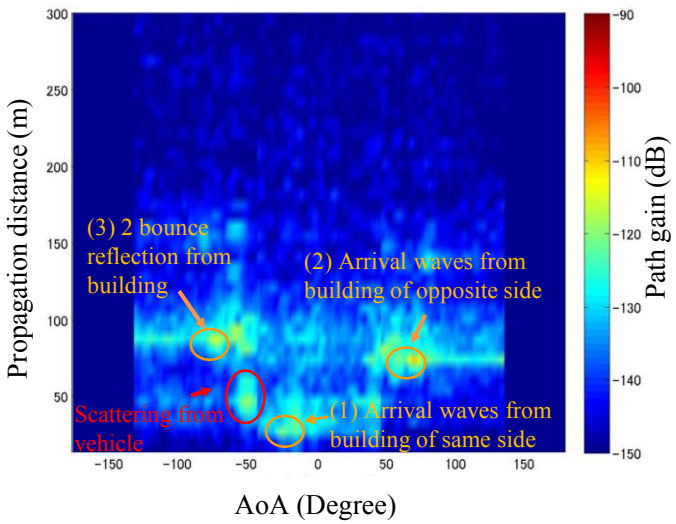

Reference:

Minoru Inomata, Tetsuro Imai, Koshiro Kitao, Yukihiko Okumura, "Dynamic Channel Properties Based on Diffuse Scattering from Vehicles for High Frequency Bands in NLOS Urban Environments," *IEICE Communications Express*, Vol. 7, No. 12, pp.438-443, Dec. 2018.

Figure 5-6 Power angular delay profile at snapshot 4

Figure 5-7 shows the time fading of the path gain at the propagation distance of 34 m and the arrival angle of -50 degrees for Q2, 47 m and the arrival angle of -50 degrees for Q23 and 60 m and the arrival angle of -50 degrees. As a result, it is found that the fading of the path gain is approximately 26 dB when those paths are born and die. Figure 5-8 shows the dominant paths in a NLOS urban environment. Based on these results, it is confirmed that (1) 1-bounce reflection and then the diffraction at the building in the same lane as the Rx antenna, (2) the diffraction and then 1-bounce reflection at the building in the opposite lane, (3) the 2-bounce reflections, and (4) the scattering path from the vehicles on the road are dominant for high frequency bands in a NLOS urban environment. Conventional method construct scattering model which represent the scattering from randomly placed small objects. However, from these results, since the scattering from vehicle in NLOS environment is relatively high and received from the vehicle in road of LOS environment, it is necessary to consider the specular reflection from vehicles in LOS environment.

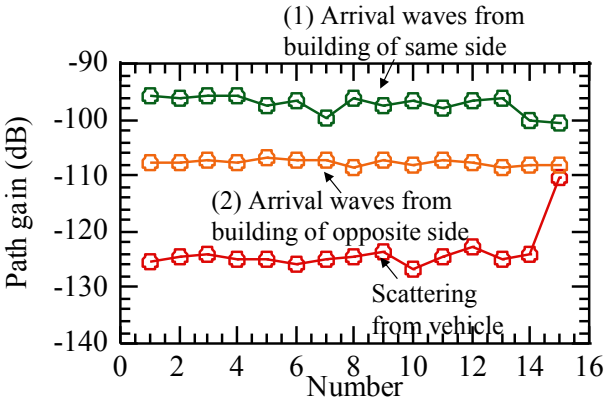

(a) Q2

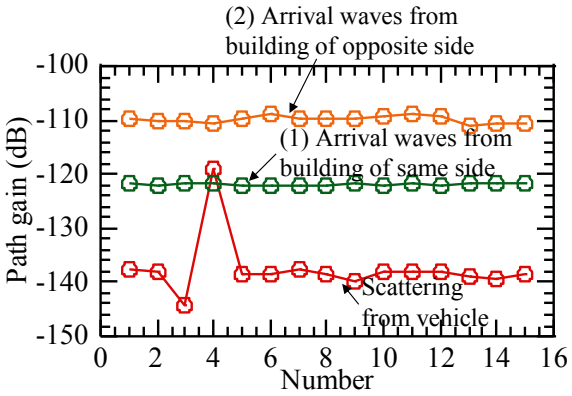

(b) Q23

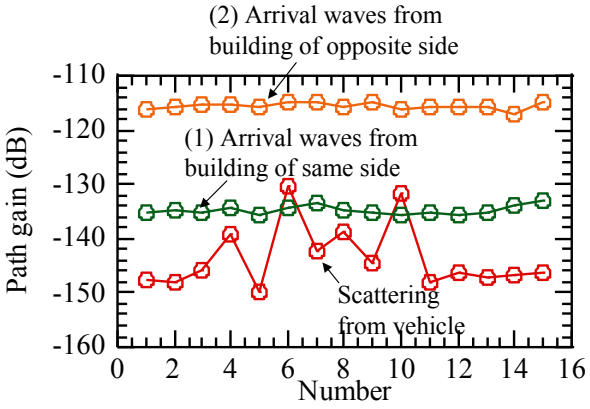

(c) Q3

Reference:

Minoru Inomata, Tetsuro Imai, Koshiro Kitao, Yukihiko Okumura, “Dynamic Channel Properties Based on Diffuse Scattering from Vehicles for High Frequency Bands in NLOS Urban Environments,” *IEICE Communications Express*, Vol. 7, No. 12, pp.438-443, Dec. 2018.

Figure 5-7 Measurement time fading characteristics

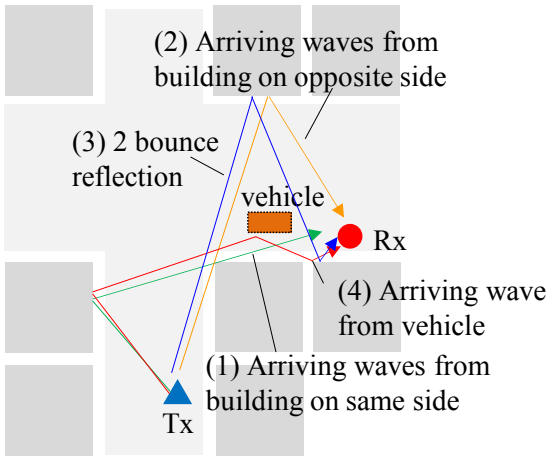

Reference:

Minoru Inomata, Tetsuro Imai, Koshiro Kitao, Yukihiko Okumura, "Dynamic Channel Properties Based on Diffuse Scattering from Vehicles for High Frequency Bands in NLOS Urban Environments," *IEICE Communications Express*, Vol. 7, No. 12, pp.438-443, Dec. 2018.

Figure 5-8 Dominant paths in NLOS urban environment

5.4 Prediction of specular reflection from vehicles in NLOS environment

5.4.1 Procedure

In order to predict accurately channel properties in the urban NLOS environment, specular reflecting from vehicles must be considered. In this subsection, propagation prediction method using a vehicle model with a rectangular smooth screen is proposed.

Figure 5-9 shows the procedure of the prediction method. This procedure takes into account the building irregularities based on the point cloud data in Chapter 4. First, the specular reflection and diffraction electric fields from the building model constructed based on computer aided design software or a commercial map database are calculated using the RT method as shown in Figure 5-9 (a). The reflection coefficient is represented by the effective reflection coefficient. Also, the specular reflection electric fields from the vehicle models with a rectangular screen are calculated using the RT method. Then, the electric field using RT, E_{RT}, is calculated by combining the specular reflection from the building model and the specular reflection from the vehicle model. Second, a detailed description of the building in the form of point cloud data is acquired using laser scanning. In order to apply point cloud data to the ER model, the building point cloud data are converted into multiple triangle surface elements. Diffuse scattered electric field E_s is calculated using the ER model and RT method. For example, in the paths that are reflected and then scattered, the incident electric field of scattering surfaces is calculated using the RT method and then scattered electric field E_s is calculated using the ER model based on the strength of incident electric field using RT method. In the paths that are twice scattered, the scattered electric field E_s is calculated by applying twice ER

model in scattering building surfaces. Finally, the total electric field, E_{total}, is calculated by combining the electric field with the ER model and RT method.

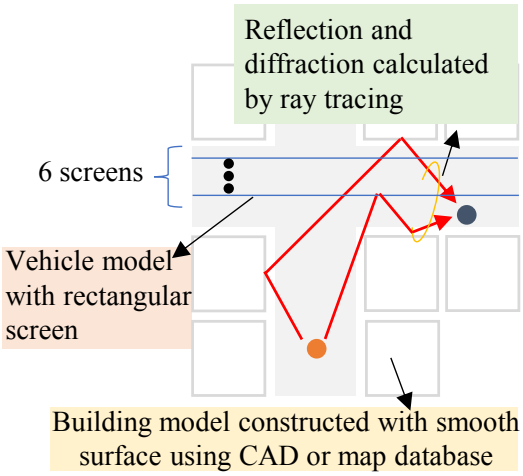

(a) Calculation of specular reflection

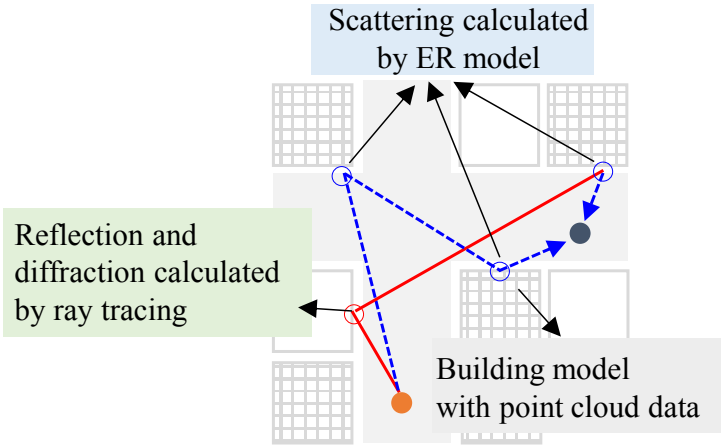

(b) Calculation of diffuse scattering electric field

Figure 5-9 Procedure of prediction method

5.4.2 Vehicle Model with Rectangular Smooth Screen

A vehicle model is implemented with a rectangular screen that is physically placed in the simulation as shown in Figure 5-10. The number of screens, their height, locations, and the vehicle shielding probability are all parameters assumed in the simulation. Using this vehicle model, only specular reflection using the RT method is considered.

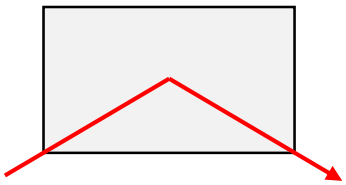

Reference:

Minoru Inomata, Tetsuro Imai, Koshiro Kitao, Takahiro Asai, “Proposal on Propagation Prediction Method Based on Dynamic Channel Properties for High Frequency Bands in Urban NLOS Environment,” *PhotonIcs & Electromagnetics Research Symposium (PIERS) 2019*, Roma, Italy, June.2019.

Figure 5-10 Vehicle model with rectangular screen

5.5 Performance of Proposed Method

In this subsection, the verification results for the proposed prediction method are described. To clarify the validity of the proposed prediction method, measurement delay profiles are compared to the prediction results using the proposed method. Table 5-1 gives the simulation parameters. In the reflection and scattering calculation with building model, size of surface elements is set to 100m^2, scattering lobe width is set to $\alpha = 5$ and surface roughness is set to 1mm. Scattering pattern using directive model is calculated. In the calculation with vehicle model, since there are six lanes on the roads in this measurement environment, six rectangular screens is set in the center of each lane. Each screen height is set to 1.8 m as a typical vehicle height. Also, the shielding probability is given as a parameter that is set to 10%, 25%, 50%, 75%, and 90% in this paper. In the simulation, each screen is physically placed in the simulation with a shielding probability. When the ray reaches the screen, the diffraction and reflection is occurred.

Figure 5-14 shows a comparison between the measured power delay profiles and calculation with reflection and scattering with building model only. The predictions were made using a bandwidth limited to 50 MHz. As Figure 5-14 shows, the received power from the simulation results using only

the building model is lower than the measured values. Markers (1), (2), and (3) indicate the arriving waves that are 1-bounce reflected and then diffracted at the building in the same lane as the Rx antenna, arriving waves that are diffracted and then 1-bounce reflected at the building in the opposite lane, and the 2-bounce reflected waves. As Figure 5-14 shows, the received power from the simulation results using only the building model has a similar tendency to the measurement power at markers (1), (2), and (3). However, the received power between 40 m and 60 m is lower than the measured values because the scattering from vehicle is not considered.

Table 5-1 Simulation parameters

Building material	Concrete
Size of surface elements	100 cm^2
Scattering pattern from surface elements	Directive model
Scattering lobe width from surface elements	$\alpha = 5$
Surface roughness	1 mm
Vehicle material	Metal
Vehicle model height	1.8 m
Vehicle model position	Center of the road
Number of vehicle model	6
Shielding probability of vehicle model	10%, 25%, 50%, 75%, and 90%
Maximum number of reflection / diffraction / scattering	3/1/1

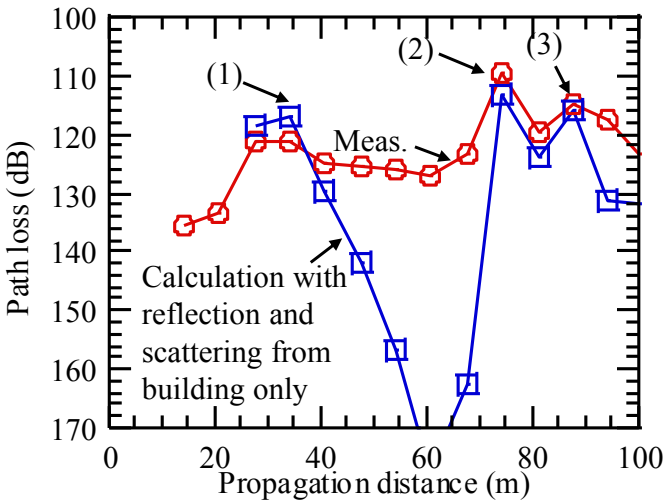

Reference:

Minoru Inomata, Tetsuro Imai, Koshiro Kitao, Takahiro Asai, “Proposal on Propagation Prediction Method Based on Dynamic Channel Properties for High Frequency Bands in Urban NLOS Environment,” *PhotonIcs & Electromagnetics Research Symposium (PIERS) 2019*, Roma, Italy, June.2019.

Figure 5-14 Comparison between measurements and simulations with building only or with building and vehicle

Figure 5-15 shows a comparison between the measurement and simulation results using vehicle and building model with the vehicle shielding probabilities of 10%, 25%, 50%, 75%, and 90%. From Figure 5-15, the received power in the simulation results using the vehicle and building models is similar to the measured values, especially, the received power between 40 m and 60 m. Also, it is confirmed that when the vehicle shielding probability is set to 50%, the results are in the best agreement with the measurement results. For verification of the root mean square error for each delay tap, the difference is 7.4 dB at 10%, 6.3 dB at 25%, 6.2 dB at 50%, 6.5 dB at 75%, and 6.6 dB at 90%. Therefore, in evaluating the power delay profile, it is found that the results using proposed method are good agreement based on arriving waves from the vehicles and buildings assuming the vehicle shielding probability of 50% in the urban NLOS environment

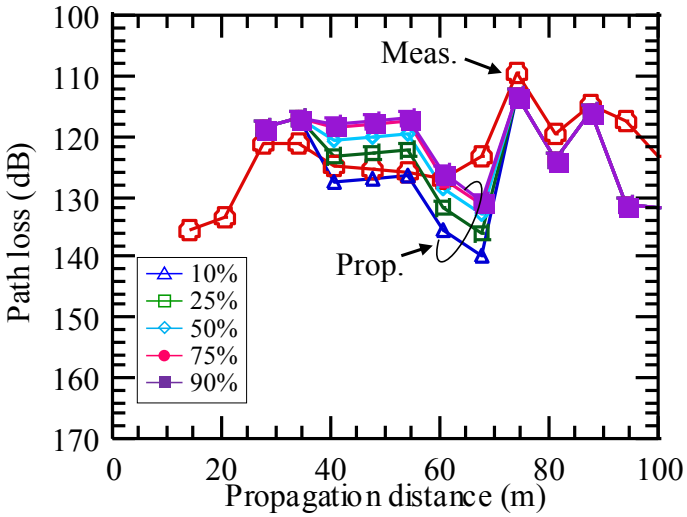

Reference:

Minoru Inomata, Tetsuro Imai, Koshiro Kitao, Takahiro Asai, “Proposal on Propagation Prediction Method Based on Dynamic Channel Properties for High Frequency Bands in Urban NLOS Environment,” *PhotonIcs & Electromagnetics Research Symposium (PIERS) 2019*, Roma, Italy, June.2019.

Figure 5-15 Comparison between measurement and simulation results with different vehicle shielding probabilities

5.6 Summary of Chapter 5

In this section, in order to clarify the effect on the specular reflection from the vehicles for high frequency bands in an UMi NLOS environment, it is investigated the dominant paths based on the measured power delay angular profile using a 20-GHz band channel sounder. It is confirmed based on these results that the arrival waves from the building on the same or opposite side of the Rx antenna and the scattering path from the vehicles on the road are dominant in an UMi NLOS environment. Also, from those results, reflection from vehicle in NLOS environment is relatively high and received from the vehicle in road of LOS environment.

Therefore, a prediction method using a vehicle model with a rectangular screen is proposed in actual UMi NLOS environment. In vehicle model with a rectangular screen, the number of screens, their height, locations, and the vehicle shielding probability are all parameters assumed in the simulation. It is confirmed the validity of the proposed prediction method based on comparison results between measurements and simulations using proposed method. From the results, it is found that the result based on specular reflection from vehicle assuming vehicle shielding probability 50% are similar tendency to the measurement channel characteristics.

Chapeter 6. Conclusions

This dissertation has explored the radio propagation predictions for 5G cell deployment in high frequency band in UMi environment. The path loss and channel characteristics have been clarified based on dominant path of detailed structure. The major results and proposals are shown in the followings.

Chapter 2 deals with outdoor path loss predictions in the 2 to 37 GHz band for the coverage evaluation with the aim of clarify a dominant path from the various building shapes in actual environment. In addition, outdoor path loss model is constructed based on the dominant paths that can cover the frequency range from microwave to millimeter-wave bands for more less complexity.

In chapter 2, a comparison of measurement results and prediction results obtained by an ITU-R model showed that it can cover the frequency band up to 37 GHz for wedge shaped building. Therefore, when the building shape of the intersection is wedge shaped building, the dominant path is multiple reflection waves which propagate along the street. However, the prediction error in chamfered shaped building cases is large. From the ray tracing calculation, it is clarified that specular reflection from chamfered shaped buildings strongly contributes the power. For less complexity, outdoor path loss model is proposed based on the dominant path. It is confirmed its validity for 5G cell deployment by evaluating the RMSE values of prediction results obtained with it and the evaluations confirmed it can predict path loss with RMSE of less than 4 dB in the 2 to 37 GHz band.

From these results, if the building structure can be changed, the building shape of the intersection is changed to chamfered or rounded shape, the coverage in the NLOS may be improved because of the specular reflection from those building shape. However discussions are still needed about the balance between the improvement of the communication quality and construction cost.

Chapter 3 deals with building penetration loss predictions for the coverage evaluation in bands raging up to 37 GHz. It is clarified the dominant penetration path to the building window based on measurement results and proposed a prediction based on the dominant paths with more less complexity.

In chapter 3, to clarify the dominant penetration path to building windows, ray tracing is used to carry out calculation and compare measurement with calculation results. Based on the ray tracing calculation, it is clarified that paths reflected multiple times between the external walls of buildings and then diffracted into the building window were dominant. For less complexity, dominant paths are used to develop a building penetration loss model based on analysis results. It is found that it can improve the predicted error maximum 5.4 dB in bands up to 37 GHz. Therefore, it is concluded that

the proposed model can accurately predict the actual building penetration loss in UMi environments and confirm the validity.

From these results, it is clarified that the penetration path to building window is dominant in high frequency bands. However, because of the high path loss, indoor coverage cannot be enough. Therefore, a transparent glass antenna for building window is developed described in [87] [88] [89] [90]. The relay systems using glass antenna in building window may be improve the millimeter wave indoor coverage but this new installation method is also future work.

Chapter 4 describes the propagation channel prediction method for system performance evaluation that uses point cloud data based on a hybrid of the RT method and the ER model in an UMi LOS environment in high frequency bands in order to consider the scattering from the building irregularities.

In the chapter 4, the validity of the proposed method was confirmed based on comparison of measurement results and prediction results using the proposed method based on the power delay profile and angular profile. From predictions with the power delay and angular profile, it is found that the predictions using proposed prediction method assuming the roughness of σ_h = 1 mm and α = 5 in directive model and the roughness of σ_h = 1 mm Lambercian model yield a similar tendency to the measurement propagation channel in the 20 GHz band for UMi environments. Therefore, it is concluded that the proposed method with point cloud data to consider the building irregularities is valid for propagation channel prediction in order to deploy 5G small cell in high frequency bands. In this calculation, several millions scattering paths is calculated and the computation complexity is considerably high which it takes about several days using graphics processing unit. Therefore, in terms of implement, construction of a high-speed algorithm is a future work.

Chapter 5 describes the propagation channel prediction method for system performance evaluation that considers the scattering from vehicles for high frequency bands in an UMi NLOS environment.

In the chapter 5, it is investigated the dominant paths based on the measured power delay angular profile using a 20 GHz band channel sounder. It is confirmed based on these results that the arrival waves from the building on the same or opposite side of the Rx antenna and the scattering path from the vehicles on the road are dominant in an UMi NLOS environment. Therefore, prediction method using a vehicle model with a rectangular screen is proposed based on actual measurement channel. In vehicle model with a rectangular screen, the number of screens, their height, locations, and the vehicle shielding probability are all parameters assumed in the simulation. It is confirmed the validity of the proposed prediction method based on comparison results between measurements and simulations using proposed method. From the results, it is found that the result based on arrival waves from vehicle assuming vehicle shielding probability 50% and buildings are similar tendency to the measurement channel characteristics.

In this dissertation, it is clarified the path loss and channel characteristic based on detailed building structure or objects for 5G cell deployment of high frequency bands in UMi environment. Also, the predictions are constructed based on the dominant path. In the implementation, the prediction with practical computational complexity and reasonable accuracy should be considered for implementation in 5G multi-cell deployment tool. In conventional method, the stochastic characteristics are used for cell deployment. Those characteristics in low frequency band are obtained by stochastic model constructed by measurements or RT method with uniform building structure. The conventional RT method is seen as a sufficiently accuracy for above purposes, with an acceptable level of complexity. However, in high frequency band, since the accuracy is insufficient because the detailed structure affects the propagation characteristics. The prediction in chapter 2, 3 and 5 is constructed based on RT method which building shape, window, vehicles are considered, therefore, the complexity are acceptable level for evaluation of coverage and system performance in high frequency bands. On the other hand, since predictions in chapter 4 are constructed based on the scattering using point cloud data, the complexity is considerably larger than conventional RT method. Therefore the construction of high speed algorism is future subject.

Reference

[1] Ministry of Internal Affairs and Communications, "http://www.soumu.go.jp/johotsusintokei/field/tsuushin06.html," March 2019. (*Japanese edition*)

[2] NTT DOCOMO, INC., “DOCOMO 5G white paper, 5G radio access: Requirements, concept and technologies,” July 2014.

[3] NTT DOCOMO, INC. Aalto University, Nokia, AT&T, BUPT, New York University, CMCC, Qualcomm, Ericsson, Samsung, Huawei, University of Bristol, INTEL, University of Southern California, KT Corporation, “White paper on 5G channel model for bands up to 100 GHz,” *Global Communications Conference, 3rd Workshop on Mobile Communications in Higher Frequency Bands,* May 2016.

[4] ITU-R, “IMT Vision Framework and overall objectives of the future development of IMT for 2020 and beyond,” *M.2083-0*, Sep 2015.

[5] Y. Hosoya, “Radiowave Propagation Handbook,” Realize Science & Engineering, 1999. (*Japanese edition*)

[6] T. Imai, “Ray-tracing Method for Radio Propagation Analysis -Fundamentals and Practical Applications-,” *CORONA PUBLISHING CO., LTD.* Aug 2016. (*Japanese edition*)

[7] ITU-R, “Guidelines for evaluation of radio interface technologies for IMT-Advanced,” *M.2135-1* vol.1, 2009.

[8] T. Imai, K. Kitao, N. Tran, N. Omaki, Y. Okumura, M. Sasaki, and W. Yamada, “Development of high frequency band over 6 GHz for 5G mobile communication systems,” *The 9th European Conference on Antennas and Propagation,* pp.1-4, May 2015.

[9] WINNER, “WINNER II Channel Models,” *IST-4-027756 WINNER II D1.1.2 V1.2*, Sep 2007.

[10] 3GPP, “Study on 3D channel model for LTE,” *TR 36.873 (V12.2.0)*, July 2015.

[11] METIS, “Simulation Guidelines,” *METIS document number ICT-317669-METIS/D6.1*, Oct 2013.

[12] METIS, “METIS Channel Models,” *Deliverable D1.4*, Feb 2015.

[13] MiWEBA, “Channel modeling and characterization,” *Deliverable D5.1*, June 2014.

[14] T. S. Rappaport et al., "Millimeter Wave Mobile Communications for 5G Cellular: It Will Work!," *IEEE Access*, vol.1, pp. 335-349, 2013.

[15] M. K. Samimi, T. S. Rappaport, and G. R. MacCartney, Jr., “Probabilistic omnidirectional path loss models for millimeter-wave outdoor communications,” *IEEE Wireless Communications*

Letters, vol. 4, no. 4, pp. 357-360, Aug 2015.

[16] M. K. Samimi and T. S. Rappaport, "3-D Millimeter-Wave Statistical Channel Model for 5G Wireless System Design," *IEEE Transactions on Microwave Theory and Techniques*, vol. 64, no. 7, pp. 2207-2225, July 2016.

[17] ITU-R, "Guidelines for evaluation of radio interface technologies for IMT-2020," *M.2412-0*, Oct 2017.

[18] 3GPP, "Study on channel model for frequencies from 0.5 to 100 GHz (Release 14)," *TR 38.901 V14.0.0*, March 2017.

[19] mmMAGIC, "6–100 GHz Channel Modelling for 5G: Measurement and Modelling Plans in mmMAGIC," *White Paper W2.1*, Feb 2016.

[20] mmMAGIC, "Measurement Results and Final mmMAGIC Channel Models," *Deliverable D2.2*, May 2017.

[21] T. S. Rappaport, F. Gutierrez, E. Ben-Dor, J. Murdock, Y. Qiao, and J. Tamir, "Broadband millimeter-wave propagation measurements and models using adaptive-beam antennas for outdoor urban cellular communications," *IEEE Trans. Antennas Propagation*, vol. 61, no. 4, pp. 1850–1859, Apr 2013.

[22] T. S. Rappaport, Y. Qiao, J. I. Tamir, J. N. Murdock, and E. Ben-Dor, "Cellular broadband millimeter wave propagation and angle of arrival for adaptive beam steering systems," *2012 IEEE Radio and Wireless Symposium (RWS)*, pp. 151-154, Jan 2012.

[23] J. Andersen, T. Rappaport, and S. Yoshida, "Propagation measurements and models for wireless communications channels," *IEEE Communications Magazine*, vol. 33, no. 1, pp. 42–49, Jan 1995.

[24] T. S. Rappaport, G. R. MacCartney, M. K. Samimi and S. Sun, "Wideband Millimeter-Wave Propagation Measurements and Channel Models for Future Wireless Communication System Design," *IEEE Transactions on Communications*, vol. 63, no. 9, pp. 3029-3056, Sep 2015.

[25] S. Sun, T. A. Thomas, T. S. Rappaport, H. Nguyen, I. Z. Kovacs and I. Rodriguez, "Path Loss, Shadow Fading, and Line-of-Sight Probability Models for 5G Urban Macro-Cellular Scenarios," *2015 IEEE Globecom Workshops (GC Wkshps)*, San Diego, CA, 2015, pp. 1-7.

[26] S. Sun *et al.*, "Investigation of Prediction Accuracy, Sensitivity, and Parameter Stability of Large-Scale Propagation Path Loss Models for 5G Wireless Communications," *IEEE Transactions on Vehicular Technology*, vol. 65, no. 5, pp. 2843-2860, May 2016.

[27] H.-K. Kwon, M.-D. Kim and Y.-J. Chong, "Implementation and performance evaluation of mmWave channel sounding system," *Proc. IEEE APS/URSI*, 2015.

[28] G. R. MacCartney, Jr., *et al*, "Indoor Office Wideband Millimeter-Wave Propagation

Measurements and Channel Models at 28 GHz and 73 GHz for Ultra-Dense 5G Wireless Networks (Invited)," *IEEE Access*, vol. 3, pp. 2388-2424, Oct. 2015

[29] S. Piersanti, L. Annoni, and D. Cassioli, "Millimeter waves channel measurements and path loss models," *in 2012 IEEE International Conference on Communications (ICC),* June 2012, pp. 4552–4556.

[30] G. R. MacCartney, Jr., J. Zhang, S. Nie, and T. S. Rappaport, "Path loss models for 5G millimeter wave propagation channels in urban microcells," *2013 IEEE Global Communications Conference (GLOBECOM)*, Dec 2013, pp. 3948–3953.

[31] K. Haneda, N. Omaki, T. Imai, L. Raschkowski, M. Peter and A. Roivainen, "Frequency-Agile Pathloss Models for Urban Street Canyons," *IEEE Transactions on Antennas and Propagation*, vol. 64, no. 5, pp. 1941-1951, May 2016.

[32] S. Sun, T. S. Rappaport, S. Rangan, T. A. Thomas, A. Ghosh, I. Z. Kovacs, I. Rodriguez, O. Koymen, A. Partyka and J. Jarvelainen, "Propagation path loss models for 5G urban micro- and macro-cellular scenarios," *IEEE VTC2016-Spring*, 2016.

[33] M. Hata, "Empirical formulas for propagation loss in land mobile radio service," *IEEE Trans. Veh. Technol.*, vol. 29, no. 3, pp. 317–325, Aug 1980

[34] Maltsev, V. Erceg and E. Perahia, "Channel models for 60 GHz WLAN systems", *Document IEEE 802.11-09/0334r8*, 2010.

[35] IEEE, "Channel Models for 60 GHz WLAN Systems," *IEEE 802.11-09/0334r8*, May 2010.

[36] ITU-R, "Propagation data and prediction methods for the planning of short-range outdoor radiocommunication systems and radio local area networks in the frequency range 300 MHz to 100 GHz," *P.1411-10*, vol.7, Aug 2019.

[37] H. Masui, M. Ishii, K. Sakawa, H. Shimizu, T. Kobayashi and M. Akaike, "Microwave path-loss characteristics in urban LOS and NLOS environments," *IEEE VTS 53rd Vehicular Technology Conference*, Spring 2001. Rhodes, Greece, pp. 395-398.

[38] V. Erceg, S. Ghassemzadeh, M. Taylor, D. Li and D. L. Schilling, "Urban/suburban out-of-sight propagation modeling," *IEEE Communications Magazine*, vol. 30, no. 6, pp. 56-61, June 1992.

[39] N. Omaki, K. Kitao, T. Imai and Y. Okumura, "Investigation of Ray Tracing accuracy in street cell environment in high-SHF band," *2014 International Symposium on Antennas and Propagation Conference (ISAP)*, Kaohsiung, 2014, pp. 441-442.

[40] N. Omaki, T. Imai, K. Kitao and Y. Okumura, "Improvement of ray tracing in urban street cell environment of non line-of-site (NLOS) with consideration of building corner and its surface roughness," *2016 10th European Conference on Antennas and Propagation (EuCAP)*, Davos,

2016, pp. 1-5.

[41] Dieter J. Cichon, Thomas Kurner, “DIGITAL MOBILE RADIO TOWARDS FUTURE GENERATION SYSTEM COST 231 Final Report,”chapter4 Propagation Prediction Models.

[42] H. Omote, M. Miyashita, R. Yamaguchi, “Time-Spatial Characteristics Between Indoors of Different LOS Buildings in Mobile Communications,” *IEICE Tech. Report,* AP2015-114, Nov 2015. (*Japanese edition*)

[43] H. Zhao, R. Mayzus, S. Sun, M. Samimi, J. K. Schulz, Y. Azar, G. N. Wong, F. Gutierrez, and T. S. Rappaport, “28GHz millimeter wave cellular communication measurements for reflection and penetration loss in and around buildings in New York City” International Conference on Communications,” pp.5163-5167, June 2013.

[44] C. R. Anderson, T. S. Rappaport, K. Bae, A. Verstak, N. Ramakrishnan, W. H. Tranter, C. A. Shaffer, and L. T. Walson, “In-Building wideband multipath characteristics at 2.5 and 60 GHz,” *Vehicular Technology Conference fall,* vol. 1, pp.97-101, Sep 2002.

[45] C. Larsson, F. Harrysson, B. Olsson, and J. Berg, “An outdoor-to-indoor propagation scenario at 28 GHz,” *The 8th European Conference on Antennas and Propagation,* pp.3301-3304, April 2014.

[46] Rodriguez, H. C. Nguyen, N. T. K. Jorgensen, T. B. Sorensen and P. Mogensen, "Radio Propagation into Modern Buildings: Attenuation Measurements in the Range from 800 MHz to 18 GHz," *2014 IEEE 80th Vehicular Technology Conference (VTC2014-Fall)*, Vancouver, BC, 2014, pp. 1-5.

[47] S. Nie, G. R. MacCartney, Jr., S. Sun, T. S. Rappaport, “72 GHz Millimeter Wave Indoor Measurements for Wireless and Backhaul Communications,” *2013 IEEE 24th Annual International Symposium on Personal, Indoor and Mobile Radio Communications, (PIMRC)*, Sept. 2013, pp. 2429.

[48] E. Semaan, F. Harrysson, A. Furuskär and H. Asplund, "Outdoor-to-indoor coverage in high frequency bands," *2014 IEEE Globecom Workshops (GC Wkshps)*, Austin, TX, 2014, pp. 393-398.

[49] C. Larsson, F. Harrysson, B. E. Olsson and J. E. Berg, "An outdoor-to-indoor propagation scenario at 28 GHz," *The 8th European Conference on Antennas and Propagation (EuCAP 2014)*, The Hague, 2014, pp. 3301-3304.

[50] K. Haneda *et al.*, "5G 3GPP-Like Channel Models for Outdoor Urban Microcellular and Macrocellular Environments," *2016 IEEE 83rd Vehicular Technology Conference (VTC2016-Spring)*, Nanjing, 2016, pp. 1-7.

[51] N. Tran, T. Imai, K. Kitao and Y. Okumura, “A study on wall scattering characteristics based

on ER model with point cloud data," *2017 IEEE International Conference on Computational Electromagnetics (ICCEM),* pp. 252-253, March 2017.

[52] L. Minghini, R. D'Errico, V. D. Esposti and E. M. Vitucci, "Electromagnetic simulation and measurement of diffuse scattering from building walls", *Proc. 8th European Conference on Antennas and Propagation (EuCAP)*, 2014.

[53] P. Pongsilamanee and H. L. Bertoni, "Specular and nonspecular scattering from building facades", *IEEE Transactions on Antennas and Propagation*, vol 52, no 7, pp. 1879-1889, 2004.

[54] Q.H. Spencer, B. D. Jeffs, M. A. Jensen, and A. L. Swindlehurst, "Modeling the Sta-tistical Time and Angle of Arrival Characteristics of an Indoor Multipath Channel", IEEE J. Sel. Areas Commun., vol. 18, no. 3, pp. 347-360, March 2000.

[55] S. Hur *et al.*, "Wideband spatial channel model in an urban cellular environments at 28 GHz," *2015 9th European Conference on Antennas and Propagation (EuCAP)*, Lisbon, 2015, pp. 1-5.

[56] S. Hur, et al., "Proposal on Millimeter-Wave Channel Modeling for 5G Cellular System", *IEEE Journal of Selected Topics in Signal Processing*, April 2016.

[57] mmMAGIC, "Measurement campaigns and initial channel models for preferred suitable frequency ranges," *ICT-671650 mmMAGIC Deliverable D2.1*, 2016.

[58] J. Medbo, H. Asplund, J.-E. Berg and N. Jalden, "Directional channel characteristics in elevation and azimuth at an urban macrocell base station", *Proc. 6th EuCAP*, Prague, Czech Republic, March 2012.

[59] J. Poutanen, J. Salmi, K. Haneda, V. Kolmonen and P. Vainikainen, "Angular and shadowing characteristics of dense multipath components in indoor radio channels", *IEEE Transactions on Antennas and Propagation*, Vol 59, no 1, 245-253, 2011.

[60] O. Landron, M. J. Feuerstein and T. S. Rappaport, "A comparison of theoretical and empirical reflection coefficients for typical exterior wall surfaces in a mobile radio environment", *IEEE Transactions on Antennas and Propagation*, vol. 44, no. 3, pp. 341-351, 1996.

[61] O. Landron, M. J. Feuerstein and T. S. Rappaport, "In situ microwave reflection coefficient measurements for smooth and rough exterior wall surfaces", *Proc. 43rd IEEE Vehicular Technology Conference*, 1993.

[62] E. J. Violette, R. H. Espeland, R. O. DeBolt and F. K. Schwering, "Millimeter- wave propagation at street level in an urban environment,"," *IEEE Transactions on Geoscience and Remote Sensing, , vol. 26,* pp. 368-380, 1988.

[63] H. J. Thomas, R. S. Cole and G. L. Siqueira, "An experimental study of the propagation of 55 GHz millimeter waves in an urban mobile radio environment," I*EEE Transactions on Vehicular Technology, vol. 43,* pp. 140- 146, 1994.

[64] A. M. Hammoudeh, M. G. Sanchez and E. Grindrod, "Experimental analysis of propagation at 62 GHz in suburban mobile radio microcells," *IEEE Transactions on Vehicular Technology, vol. 48,* pp. 576-588, 1999.

[65] L. M. Correia, J. J. Reis and P. O. Frances, "Analysis of the average power to distance decay rate at the 60 GHz band," *IEEE in Vehicular Technology Conference*, 1997.

[66] A. V. Raisanen, J. Ala-Laurinaho, K. Haneda, J. Jarvelainen, A. Karttunen, M. Kyro, V. Semkin, A. Lamminen and J. Saily, "Studies on E-band antennas and propagation," *Antennas and Propagation Conference (LAPC)*, Loughborough, 2013 .

[67] M. Kyro, V. Semkin and V. Kolmonen, "Empirical characterization of scattering pattern of built surfaces at mm-wave frequencies," in *European Conference on Antennas and Propagation (EuCAP)*, 2013.

[68] M. Kyro, S. Ranvier, V. Kolmonen, K. Haneda and P. Vainikainen, "Long range wideband channel measurements at 81-86 GHz frequency range," *European Conference Antennas and Propagation (EuCAP)*, 2010.

[69] A. Hammoudeh, M. Sanchez and E. Grindrod, "Modelling of Propagation in Outdoor Microcells at 62.4GHz," *Microwave Conference ,* vol.1, pp.119-123, 1997.

[70] K. Sarabandi, E. Li and A. Nashashibi, "Modeling and measurements of scattering from road surfaces at millimeter-wave frequencies," *IEEE Transactions on Antennas and Propagation,* vol. 45, no. 11, pp. 1679-1688, 1997.

[71] H. Sawada, "Intra-cluster response model and parameter for channel modeling at 60 GHz (Part 3)," *IEEE doc. 802.11-10/0112r1*, January 2010.

[72] V. Degli-Esposti, "A diffuse scattering model for urban propagation prediction," *IEEE Trans. AP,* vol. 49, no. 7, pp.1111-1113, July 2001.

[73] E. M. Vitucci, F. Mani, V. Degli-Esposti and C. Oestges, "Polarimetric Properties of Diffuse Scattering From Building Walls: Experimental Parameterization of a Ray-Tracing Model," *IEEE Transactions on Antennas and Propagation,* vol. 60, no. 6, pp.2961-2969, June 2012.

[74] V. Degli-Esposti, D. Guiducci, A. de' Marsi, P. Azzi, and F. Fuschini, "An advanced field prediction model including diffuse scattering," *IEEE Trans. AP,* vol. 52, no. 7, pp.1717-1728, July 2004.

[75] T. Fugen, J. Maurer, T. Kayser, and W. Wiesbeck, "Capability of 3-D ray tracing for defining parameter sets for the specification of future mobile communications systems," *IEEE Trans. AP,* vol. 54, no. 11, pp.3125-3137, Nov 2006.

[76] V. Degli-Esposti, F. Fuschini, E. Vitucci, and G. Falciasecca, "Measurement and modelling of scattering from buildings," *IEEE Trans. AP,* vol. 55, no. 1, pp.143-153, Jan 2007.

[77] J. Pascual-Garcia, J. M. Molina-Garcia-Pardo, M. T. Martinez-Ingles, J. V. Rodriguez and N. Saurin-Serrano, “On the Importance of Diffuse Scattering Model Parameterization in Indoor Wireless Channels at mm-Wave Frequencies,” *IEEE Access,* vol. 4, pp.688-701, 2016.

[78] J. Hyyppä, , D. Fritsch, Ed., “State of the art in laser scanning,” *Photogrammetric Week 2011. Stuttgart*, Germany: Wichmann, 2011, pp. 203–216.

[79] G. Vosselman and H.-G. Maas, "Airborne and Terrestrial Laser Scanning Caithes," *Whittles Publishing*, 2010.

[80] P. Ökvist, N. Seifi, B. Halvarsson, A. Simonsson, M. Thurfjell, H. Asplund and J. Medbo, “15 GHz Street-Level Blocking Characteristics Assessed with 5G Radio Access Prototype,” *2016 IEEE 83rd Vehicular Technology Conference (VTC2016-Spring)*, Nanjing, 2016, pp. 1-5.

[81] G. R. MacCartney, Jr., S. Deng, S. Sun, and T. S. Rappaport, “Millimeter-Wave Human Blockage at 73 GHz with a Simple Double Knife-Edge Diffraction Model and Extension for Directional Antennas,” *2016 IEEE 84th Vehicular Technology Conference (VTC2016-Fall)*, Sep 2016.

[82] X. Chen, L. Tian, P. Tang and J. H. Zhang, "Modelling of Human Body Shadowing Based on 28 GHz Measurement Results," *Proc. 84th Veh. Tech. Conf (VTC2016-Fall)*, Montreal, Canada, Sep 2016.

[83] A. Maltsev et al., "Quasi-deterministic approach to mmWave channel modeling in a non-stationary environment," *2014 IEEE Globecom Workshops*, Austin, TX, 2014, pp. 966-971.

[84] K. Kitao, “Mobile radio propagation research: Evolutions for future,” The journal of the IEICE, vol. 99, no. 8, pp.820-825, Aug 2016. (*Japanese edition*)

[85] N. Kikuma, “Adaptive signal processing with array anntena,” Kagaku Gijutsu shuppan, Inc., Chapter 9, 1998. (*Japanese edition*)

[86] FARO, "http://www.faro.com/ja-jp/products/construction-bim-cim/faro-focus/,"

[87] Toshiki Sayama, Osamu Kagaya, Shoji Hideaki, Shoichi Takeuchi, Kiyoshi Nobuoka, Minoru Inomata, Tetsuro Imai "Study on Using Vehicle Glass Windows as Mounting Locations for 28GHz Band Antennas," *IEICE Tech. Report,* AP2018-142, Nov 2018. (*Japanese edition*)

[88] Tetsuro Imai, Minoru Inomata, Toshiki Sayama, Osamu Kagaya, Shoji Hideaki, Shoichi Takeuchi, Kiyoshi Nobuoka, " Performance evaluation of Vehicle Glass Mounted Antenna for 28 GHz Band in Microcellular Environment," *IEICE Tech. Report,* AP2018-143, Nov 2018. (*Japanese edition*)

[89] Minoru Inomata, Tetsuro Imai, Toshiki Sayama, Osamu Kagaya, Shoji Hideaki, Shoichi Takeuchi, Kiyoshi Nobuoka, " Downlink Performance using Vehicle Glass Mounted Antenna

for 28 GHz Band in High Mobility Environment," *IEICE Tech. Report,* AP2018-144, Nov 2018. (*Japanese edition*)

[90] NTT DOCOMO, INC., " https://www.nttdocomo.co.jp/english/info/media_center/pr/2019/0529_00.html," May 2019

Appendix

List of Publications

Journal Papers

1. Minoru Inomata, Motoharu Sasaki, Wataru Yamada, Takeshi Onizawa, Masashi Nakatsugawa, Nobutaka Omaki, Koshiro Kitao, Tetsuro Imai, Yukihiko Okumura, "Outdoor-to-Indoor Corridor Path Loss Model up to 40 GHz Band in Microcell Environments," *IEICE Trans. on Communication*, Vol.E100-B, No.2, pp.242-251, Feb. 2017.
2. Minoru Inomata, Wataru Yamada, Motoharu Sasaki, Masato Mizoguchi, Koshiro Kitao, Tetsuro Imai, "Path loss model for the 2 to 37 GHz band in street microcell environments," *IEICE Communications Express*, Vol.4, No.5, pp. 149-154, May. 2015.
3. Minoru Inomata, Tetsuro Imai, Koshiro Kitao, Yukihiko Okumura, Motoharu Sasaki, Yasushi Takatori, "Radio Propagation Prediction Method Using Point Cloud Data Based on Hybrid of Ray-Tracing and Effective Roughness Model in Urban Environments," *IEICE Trans. on Communication*, Vol.E102-B, No.1, pp.51-62, July. 2019.
4. Minoru Inomata, Tetsuro Imai, Koshiro Kitao, Yukihiko Okumura, "Dynamic Channel Properties Based on Diffuse Scattering from Vehicles for High Frequency Bands in NLOS Urban Environments," *IEICE Communications Express*, Vol. 7, No. 12, pp.438-443, Dec. 2018.

International Conference

1. Minoru Inomata, Wataru Yamada, Motoharu Sasaki, Takeshi Onizawa, "Outdoor to Indoor Path loss model for 8 to 37 GHz Band," *2015 International Symposium on Antennas and Propagation (ISAP),* Hobart, Australia, pp. 1-4, Nov.2015.
2. Minoru Inomata, Motoharu Sasaki, Takeshi Onizawa, Koshiro Kitao, Tetsuro Imai, "Effect of Reflected Waves from Outdoor Buildings on Outdoor-to-Indoor Path Loss in 0.8 to 37 GHz Band," *2016 International Symposium on Antennas and Propagation (ISAP),* Okinawa, Japan, pp. 62-63, Oct.2016.
3. Minoru Inomata, Motoharu Sasaki, Mitsuki Nakamura, Yasushi Takatori, "Simulating Diffuse Scattering for 26GHz Band in Indoor Office Environments," *2017 International Symposium on Antennas and Propagation (ISAP),* Phuket, Thailand, Oct.2017.
4. Minoru Inomata, Motoharu Sasaki, Wataru Yamada, Yasushi Takatori, Koshiro Kitao, Tetsuro

Imai, “Effects of Building Shapes on Path Loss up to 37 GHz Band in Street Microcell Environments,” *2017 International Conference on Computational Electromagnetics (ICCEM),* Kumamoto, Japan, pp. 249-251, March.2017.

5. Minoru Inomata, Tetsuro Imai, Koshiro Kitao, Motoharu Sasaki, Yasushi Takatori, “Prediction Accuracy of Hybrid Method Based on Ray-traing and Effective Roughness Model in Indoor Environment for Millimeter Waves,” *2017 International Conference on Antenna Measurements and Applications (CAMA),* Japan, Dec. 2017.
6. Minoru Inomata, Tetsuro Imai, Koshiro Kitao, Yukihiko Okumura, Motoharu Sasaki, Yasushi Takatori, “Radio Propagation Prediction for High Frequency Bands Using Hybrid Method of Ray-Tracing and ER Model with Point Cloud of Urban Environments,” *12th European Conference on Antennas and Propagation (EuCAP)*, London, UK, March.2018.
7. Minoru Inomata, Tetsuro Imai, Koshiro Kitao, Yukihiko Okumura, “Investigation of Channel Properties for 28 GHz Band in Urban Street Microcell Environments,” *2018 International Symposium on Antennas and Propagation (ISAP),* Busan, Korea, pp.1-2, Oct. 2018.
8. Minoru Inomata, Tetsuro Imai, Koshiro Kitao, Takahiro Asai, “Proposal on Propagation Prediction Method Based on Dynamic Channel Properties for High Frequency Bands in Urban NLOS Environment,” *PhotonIcs & Electromagnetics Research Symposium (PIERS) 2019*, Roma, Italy, June.2019.

Domestic Conference

1. Minoru Inomata, Wataru Yamada, Motoharu Sasaki, Takatoshi Sugiyama, Masato Mizoguchi, Koshiro Kitao, Tetsuro Imai, “Propagation Loss Characteristics for Millimeter-wave Band in NLOS Street Microcell Environment,” *IEICE Tech. Rep.*, vol. 114, no. 396, AP2014-178, pp. 97-102, Jan. 2015.
2. Minoru Inomata, Wataru Yamada, Motoharu Sasaki, Takatoshi Sugiyama, Masato Mizoguchi, Nobutaka Omaki, Koshiro Kitao, Tetsuro Imai, “Prediction Method for Propagation Loss Characteristics in NLOS Street Microcell Environment,” *IEICE General Conference*, March.2015
3. Minoru Inomata, Wataru Yamada, Motoharu Sasaki, Takatoshi Sugiyama, Masato Mizoguchi, Nobutaka Omaki, Koshiro Kitao, Tetsuro Imai, ” Propagation Loss Characteristics for Millimeter-wave Band in NLOS Street Microcell Environment”, *URSI-F*, March.2015.
4. Minoru Inomata, Wataru Yamada, Motoharu Sasaki, Takeshi Onizawa, Koshiro Kitao, Tetsuro Imai, “Fast Fading Characteristics for Microwave to Millimeter-wave Band in Street Microcell Environments,” *IEICE Tech. Rep.*, vol. 115, no. 79, AP2015-38, pp. 35-40, June 2015.
5. Minoru Inomata, Wataru Yamada, Motoharu Sasaki, Takeshi Onizawa,“Building entry loss model from microwave band to millimeter-wave band,” *IEICE Society Conference*, Sep.2016.

6. Minoru Inomata, Wataru Yamada, Motoharu Sasaki, Takeshi Onizawa,“Outdoor-to-Indoor Path Loss Characteristics for 8GHzto 37GHzBand,” *IEICE Tech. Rep.*, vol. 115, no. 286, AP2015-115, pp. 29-34, Nov. 2015.
7. Minoru Inomata Motoharu Sasaki Naoki Kita Takeshi Onizawa,” Effect of Reflected Ray from Outdoor Building on Propagation Loss in High Frequency Band,” *IEICE General Conference*, March.2016
8. Minoru Inomata, Wataru Yamada, Motoharu Sasaki, Takeshi Onizawa, Koshiro Kitao, Tetsuro Imai, “Building Entry Loss Model in 0.8 to 37 GHz Bands,” *IEICE Tech. Rep.*, vol. 116, no. 142, AP2016-38, pp. 7-12, July 2016.
9. Minoru Inomata Motoharu Sasaki Takeshi Onizawa Koshiro Kitao Tetsuro Imai, “Building entry loss model from microwave band to millimeter-wave band,” *IEICE Society Conference*, Sep.2016
10. Minoru Inomata, Motoharu Sasaki, Yasushi Takatori, Koshiro Kitao, Tetsuro Imai,“Effects of Building Shapes at an Intersection on Path Loss Characteristics for Millimeter WaveBand in Street Microcell Environments,” *IEICE Tech. Rep.*, vol. 116, no. 397, AP2016-142, pp. 73-78, Jan. 2017.
11. Minoru Inomata, Motoharu Sasaki, Yasushi Takatori, “Simulating Diffuse Scatter Based on Rough Surface for High Frequency Bands in Indoor Office Environment,” *IEICE Tech. Rep.*, vol. 117, no. 2, AP2017-4, pp. 19-24, April 2017.
12. Minoru Inomata, Motoharu Sasaki, Yasushi Takatori, “Radio Propagation Prediction Method with Point Cloud Data in Indoor Office Environments for 26 to 66 GHz Bands,” *IEICE Tech. Rep.*, vol. 117, no. 150, AP2017-66, pp. 117-122, July 2017.
13. Minoru Inomata Motoharu Sasaki Yasushi Takatori, “Radio Propagation Prediction with Point Cloud Data in Indoor Environments for 26 to 66 GHz Bands,” *IEICE Society Conference*, Sep.2017
14. Minoru Inomata, Imai Tetsuro, Kitao Koshiro, Yukihiko Okumura, Motoharu Sasaki, Yasushi Takatori, “Radio Propagation Prediction Method Using Point Cloud Data in NLOS Urban Environments for high frequency bands,” *IEICE Tech. Rep.*, vol. 117, no. 382, AP2017-173, pp. 125-130, Jan. 2018.
15. Minoru Inomata, Imai Tetsuro, Kitao Koshiro, Yukihiko Okumura, “Effects of Vehicles on Dynamic Channel Property for High Frequency Bands in Urban NLOS Environments,” *IEICE Tech. Rep.*, vol. 117, no. 436, AP2017-185, pp. 51-56, Feb. 2018.
16. Minoru Inomata, Imai Tetsuro, Kitao Koshiro, Yukihiko Okumura, “Propagation Prediction Method based on Scattering from Vehicles for High Frequency Bands in Urban NLOS Environments,” *IEICE Tech. Rep.*, vol. 117, no. 490, AP2017-198, pp. 33-37, March 2018.
17. Minoru Inomata, Tetsuro Imai, Koshiro Kitao, Yukihiko Okumura, Motoharu Sasaki, Yasushi

Takatori, “Prediction accuracy of Radio Propagation Prediction Method using Point Cloud Data in NLOS Urban Environments for High Frequency Bands,” *IEICE General Conference*, March.2018

18. Minoru Inomata, Tetsuro Imai, Koshiro Kitao, Yukihiko Okumura, “Investigation of Doppler Characteristics for 28 GHz Band in Urban Street Microcell Environments,” *IEICE Society Conference*, Sep.2018
19. Minoru Inomata, Imai Tetsuro, Kitao Koshiro, Takahiro Asai, “Investigation of Channel Characteristics using ITU-R Models for 28 GHz Band in Urban Environment,” *IEICE Tech. Rep.*, vol. 118, no. 246, AP2018-90, pp. 7-12, Oct. 2018.
20. Minoru Inomata, Imai Tetsuro, Kitao Koshiro, Takahiro Asai,” Path Loss Characteristics for 3.7GHz and 28 GHz Band in Densely Populated Areas, ” *IEICE General Conference*, March.2019

International Standardization Conference

1. Minoru Inomata, “PROPOSED REVISION TO RECOMMENDATION ITU-R P.1411-8 -Extension of prediction method up to 40 GHz within NLOS urban street canyon-,“ ITU-R SG3
2. Minoru Inomata, “PROPOSED REVISION TO RECOMMENDATION ITU-R P.[BEL] Proposed building entry loss model up to 40 GHz in urban environment,” ITU-R SG3
3. Minoru Inomata, “SUPPORT DOCUMENT FOR THE WORKING DOCUMENT TOWARDS A REVISION OF RECOMMENDATION ITU-R P.1411,” ITU-R SG3

Acknowledgements

During my study in Tokyo Institute of Technology, I wish to express my sincere gratitude to Professor Jun-ichi Takada for their continuous guidance and encouragement.

I am grateful to Associate Professor Yukihiko Yamashita, Associate Professor Takahiro Aoyagi, Associate Professor Daisuke Akita, Assistant Professor Kentaro Saito and Professor Kei Sakaguchi for their useful suggestions.

I would also like to express my appreciation to Dr. Takeshi Onizawa of Project Manager, Dr. Yasushi Takatori of Project Manager of NTT Access Network Service Systems Laboratories, Dr. Yukihiko Okumura of Senior Manager, Dr. Takahiro Asai of Senior Manager of 5G Laboratories of NTT DOCOMO, INC. for giving me the chance to complete this dissertation.

I would also like to express my appreciation to Dr. Naoki Kita of Group Leader, Dr. Wataru Yamada, Dr. Motoharu Sasaki of NTT Access Network Service Systems Laboratories, Dr. Koshiro Kitao of 5G Laboratories of NTT DOCOMO, INC. for their useful technical suggestions and for their constant encouragement.

I would like to express my appreciation to Professor Tetsuro Imai of Tokyo Denki University and Associate Professor Kentaro Nishimori of Niigata University for his fruitful discussions.

I wish to express my devout thanks to Mr. Daisuke Mori of NTT Advanced Technology Corporation, Mr. Motoki Imanishi, Mr. Shinya Suzuki of NTT-AT Techno Communications Corporation for their help on measurements data processing.

I would like to thank the staff and colleagues of Takada Laboratories in Tokyo Institute of Technology.

I would like to express my special thanks to my father, mother, father-in-low and mother-in-low for their support and continuous encouragements.

Finally, I am most thankful to my wife Chigusa and my son Yutaka for genuine love, encouragement, and patience through the long hours to complete this dissertation.

December 2019
Minoru INOMATA